NASA SP-225

MARINER-MARS 1969
A PRELIMINARY REPORT

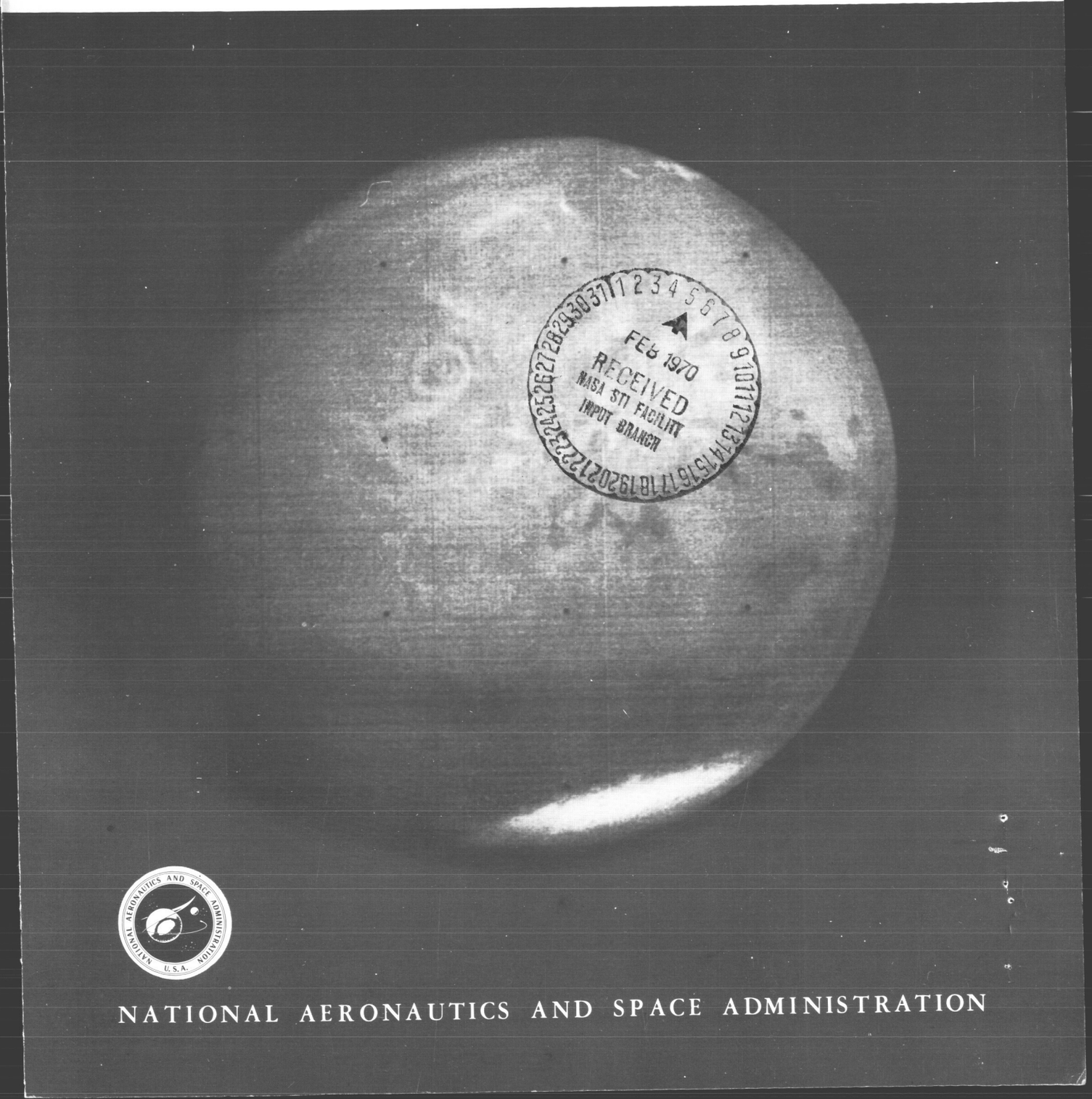

NATIONAL AERONAUTICS AND SPACE ADMINISTRATION

NASA SP-225

MARINER-MARS 1969
A PRELIMINARY REPORT

Scientific and Technical Information Division
OFFICE OF TECHNOLOGY UTILIZATION 1969
NATIONAL AERONAUTICS AND SPACE ADMINISTRATION
Washington, D.C.

NATIONAL AERONAUTICS AND SPACE ADMINISTRATION

For sale by the Clearinghouse for Federal Scientific and Technical Information
Springfield, Virginia 22151 – Price $3.00

Foreword

MARINER-MARS 1969 was the most ambitious and successful planetary reconnaissance yet mounted by the National Aeronautics and Space Administration. Two spacecraft, carrying improved sensors and telemetry, were dispatched February 24 and March 27, near the beginning and end of the 1969 Mars launch window. Their arrivals at the distant planet were timed so that the findings of the first could be used to reprogram the second for maximum scientific return. As the following pages attest, the mission proved highly rewarding; both spacecraft transmitted a wealth of scientific data 60 million miles to Earth.

One way to gauge the pace and excitement of our times is to look back a few years at the tantalizingly equivocal images of Mars that were then the best that Earth telescopes could give us, and to contrast these with the scientifically rewarding television imagery of Mars reproduced here. Another indication of our rapid rate of advance is to compare the pictures that we received in 1965 from Mariner 4 — historic though they were — with the quality and amount of information about Mars received by the big Goldstone antenna during this encounter.

We are learning about the solar system, the neighborhood of man, at an increasing pace. In 1971 two automated spacecraft placed in orbit about Mars will send back detailed photos of the entire globe from which the first authoritative maps of the red planet will be prepared. And it will be only two years from then when the first precursor machines descend to the surface of Mars and begin transmitting back information on what their biological and other sensors perceive about surface conditions. Our schedules are necessarily imprecise for the years that follow, in part because each new advance must derive from the technology and science that preceded it. But the language of the President's Space Task Group is explicit: ". . . we will plan and move forward as a Nation toward the objective of a manned Mars landing before the end of this century." The record of progress in the space age, when achievements like those summarized in this volume have come only a few years after our first planetary venture, point clearly to the day when man will set forth from his home planet in new odysseys to explore the vast reaches of the solar system.

THOMAS O. PAINE, *Administrator*
National Aeronautics and Space Administration

November 3, 1969

Contents

Introduction

N. W. Cunningham and H. M. Schurmeier

The Mariner-Mars 1969 mission was undertaken to enhance man's knowledge of the surface and atmosphere of Mars and to provide a firm basis for an imaginative, long-range program of Martian exploration. The two flights were authorized after the successful 1964–1965 flight of Mariner 4 and the cancellation of the Voyager Mars Landing Program.

Despite the many recent impressive additions to human capabilities, the origins of the universe, the solar system, and life will continue to intrigue and mystify many more generations of men. The findings from Mariner 4 surprised most of the world's astronomers and indicated that much more could be learned about the origin of the universe by further study of the red planet. Mariners 6 and 7 obtained the information needed to determine the most effective strategy to pursue in the future, and helped to develop the technology needed for further explorations.

The instruments for the scientific experiments aboard Mariners 6 and 7 included two television cameras, an infrared spectrometer, an ultraviolet spectrometer, and an infrared radiometer. A celestial mechanics experiment and an S-band occultation experiment, which required no instruments, were also conducted. A summary of results from these experiments is presented as chapter 1 of this preliminary report. Chapters 2, 3, and 4 describe the spacecraft, the flights, and the instruments; the final six chapters give the preliminary results from each experiment.

SPACECRAFT DESIGN

To meet the requirements for these experiments in a way that would maximize the scientific returns from the missions was one of the most challenging tasks ever undertaken by a team responsible for an unmanned vehicle. The mission profile was, in some ways, similar to the profiles of previous planetary missions; however, it differed drastically in design, philosophy, and implementation during the encounter operations. Numerous major innovations were needed.

The entirely planet-oriented scientific payload, selected by Dr. Homer Newell in 1966, called not only for an ambitious advance in scientific knowledge, but also for major advances in the design, fabrication, and operation of the hard-

ware used. Problems encountered and solved during the spacecraft-development period resulted in the following changes:

(1) A redesigned scan platform with two degrees of freedom, capable of accommodating both of the television cameras, both of the infrared instruments, the ultraviolet spectrometer, and two planet sensors.

(2) A data storage subsystem to meet requirements 35 times greater than those on Mariner 4. Two tape recorders were especially designed for this program: an analog recorder with an equivalent digital capacity of 1.57×10^8 bits, and a digital recorder with a capacity of 2.3×10^7 bits.

(3) A telemetry subsystem with three channels (Mariner 4 had only one), and a telemetry data rate increased from $8\frac{1}{3}$ to 16 200 bps.

(4) A central computer and sequencer subsystem, which, because of its capability of being reprogramed in flight, proved to be the heart of the science effort. Mariner 7 was reprogramed almost at the last minute to benefit from the knowledge and experience of Mariner 6.

MISSION OPERATIONS

Compared with earlier flights, the Mariner-Mars 1969 mission was both novel and bold. For example, it was required that

(1) Both spacecraft encounter the planet within a 5-day period.

(2) Both spacecraft start television operations from 2 to 3 days before reaching the planet and continue to tape and transmit pictures to Earth up to a minimum of $4\frac{1}{2}$ hr before the start of encounter operations.

(3) All science data from both spacecraft be returned to Earth in real time during the near-encounter operations at the 16 200-bps data rate.

(4) Television data from Mariner 6, especially during the encounter, be processed and sufficiently analyzed to permit reprograming of Mariner 7.

These and related requirements were more than met—almost all data returns far exceeded the original expectations. A comparison of the requirements with the actual data return from four of the experiments on the spacecraft follows:

For the television experiment, 16 far-encounter and 48 near-encounter pictures were originally planned. The actual returns were 147 analog and 2414 digital far-encounter pictures and 67 analog and 510 digital near-encounter pictures.

For the infrared spectroscopy experiment, the requirement of 288 near-encounter spectral pairs was more than met with 600 spectral pairs.

For the infrared radiometry experiment, 350 000 far-encounter measure-

ments of the planet were obtained, although only 270 000 had been planned. During the near-encounter 3000 measurements of the planet were sought and obtained.

For the ultraviolet spectrometer experiment, 81 000 far-encounter measurements (Lyman-alpha) were required, and 93 000 were obtained; 920 near-encounter spectra were required, and 1000 obtained.

The S-band occultation experiment yielded data as planned; however, because of nongravitational effects, the planetary portion of the celestial mechanics experiment was limited by much unusable data.

The scientific findings from the Mariner-Mars 1969 flights already have been acclaimed as a historic addition to man's knowledge of the Martian atmosphere and surface properties. Two more programs are scheduled: Mariner-Mars 1971, in which two spacecraft are to be placed in orbit around Mars for periods up to 9 days, and Viking 1973, which will be NASA's first attempt to land on another planet a survivable payload that will include life-detection instrumentation.

Late in the 1970's, Jupiter, Saturn, Uranus, Neptune, and Pluto will be alined in a manner favorable for a "grand tour," which would permit information regarding those distant planets to be obtained in much the same way as it was obtained during the encounters of Mariners 6 and 7.

CHAPTER 1

*Summary of Results**

Scientific experiments on Mariners 6 and 7 provided data for a far more detailed and comprehensive understanding of Mars than had been obtained from Mariner 4, the only previous mission to that planet.

During the approach and encounter sequences of the flights, 200 pictures of Mars were taken by the Mariner 6 and 7 television cameras; 1100 digital pictures also were obtained. The track of the 24 wide-angle and narrow-angle pictures taken during the Mariner 6 encounter crossed equatorial zones of the planet, including many known light and dark features of its surface. The track of the Mariner 7 cameras, which took 33 encounter pictures, swept down a roughly north-south course, intersecting that of Mariner 6 and continuing across the Martian south polar cap. The two tracks were designed to cross the dark area of Meridiani Sinus at different times of day, thus obtaining a range of lighting conditions from near noon to late afternoon for taking pictures of the same area.

The infrared spectroscopy experiment obtained spectra during the encounters of both Mariners 6 and 7, although the long-wavelength channel on Mariner 6 did not operate. Spectral information was obtained in the region from 1.9 to 14.3μ in a 10-sec scanning interval. The ultraviolet spectroscopy experiment provided measurements of emission features in the Martian upper atmosphere. The wavelength band from 1100 to 4300 Å was scanned in a 3-sec interval. The motion of the spacecraft, relative to Mars, caused the fields of view of the spectrometers to sweep down through the atmosphere toward the surface of Mars, across the bright side of the disk, and then past the dark side of the planet. The scanning intervals of the two spectrometers provided samples of the Martian atmosphere at altitude increments of 60 km for the infrared spectrometer and 20 km for the ultraviolet spectrometer. The projected size of the ultraviolet spectrometer field of view in the vertical direction varied from 20 to 30 km, depending on range. The instrument pointing capability of the Mariner spacecraft allowed the Martian atmosphere to be swept through by the ultraviolet spectrometer a total of four times in this manner before being carried finally across the disk to complete the lower-atmosphere phase of the experiment.

* Results from these experiments are covered in more detail in chapters 5 through 10.

The infrared radiometer was boresighted with the television cameras to insure surface temperature measurements of those areas photographed at high resolution. Like the spectrometers, the radiometer continued to take data across the dark side of the planet.

In the S-band occultation experiment, profiles of the Martian temperature and pressure were obtained at four locations above the surface. Mariner 6 entered the occultation zone at a point corresponding to a surface location of 4° N latitude and 356° E longitude near Meridiani Sinus. The spacecraft emerged from behind the planet at about 79° N latitude and 84° E longitude near the north pole. Mariner 7 entered the occultation zone at 58° S latitude and 30° E longitude near the south polar cap in the region of Hellespontus. The spacecraft emerged at about 38° N latitude and 212° E longitude near the crater Nix Olympica between the classical light areas of Amazonis and Arcadia.

The celestial mechanics experiment made use of ranging and tracking data from Mariners 6 and 7 to determine astronomical constants. Computations of ratios of the mass of the Earth to that of the Moon and the mass of Mars to that of the Earth have been completed. On this mission, the value of the near-Mars data was degraded by spacecraft accelerations introduced by blowdown of the gas bottles on the infrared spectrometer. In the case of Mariner 7, the data were further degraded by the unfortunate spacecraft anomaly that occurred several days before encounter.

ASTRONOMICAL CONSTANTS

On the basis of analysis of 3 months of ranging and tracking data from Mariners 6 and 7, it was determined by the celestial mechanics experiment that the ratio of the mass of the Earth to that of the Moon is 81.3000, with an uncertainty of 0.0015; and the ratio of the mass of Mars to that of the Earth is 0.1074469 ± 0.0000035.

The radius of Mars, as determined by the S-band occultation experiment, is 3394 km (2108 miles) around the equator at the entry point of Mariner 6 (4° N), and 3374 km (2096 miles) at the exit point (79° N). This difference of 20 km (12 miles) indicates that the shape of the surface conforms more closely to the value obtained from dynamic measurements than to that obtained from optical measurements.

THE MARTIAN ATMOSPHERE

As expected, the infrared spectroscopy and ultraviolet spectroscopy experiments returned a wealth of data on atmospheric composition; temperature/pres-

sure profiles were deduced from the S-band occultation experiment data. The television experiment also yielded significant information about the Martian atmosphere.

Initial analyses of the data from the ultraviolet spectroscopy experiment are consistent with a Martian atmosphere consisting of CO_2 as the major constituent and CO_2^+ as the dominant ion in the ionosphere. The relative distribution with altitude of the emission features associated with CO_2 indicates that the scale height of the neutral atmosphere above 130 km is about 23 km. Comparison of the ultraviolet spectra of Mars with similar spectra taken on Earth indicates the absence of the emissions from atomic, molecular, and ionized molecular nitrogen. The absence of these emissions indicates that molecular nitrogen comprises less than 1 percent of the total Martian atmosphere. The 1304-Å emissions from atomic oxygen indicate that a small amount exists in the upper atmosphere. Mars is observed to have a hydrogen exosphere or corona. Notably absent from the Mars spectra were emissions from the gamma bands of nitric oxide.

Preliminary analysis of the data on the Martian disk from the ultraviolet spectroscopy experiment indicates that the reflected ultraviolet signal tends to be dominated more by atmospheric scattering as one approaches shorter wavelengths in the ultraviolet. Optically thin atmospheric scattering is observed down to 1950 Å, where the absorption due to CO_2 becomes apparent. The magnitude of the intensities, as well as the wavelength dependence of the intensity, indicates the existence of small particulate matter in the Martian atmosphere. The amount of particulate matter necessary to account for the scattered light intensity is small and would not cause appreciable obscuration at visible wavelengths. The optically thin nature of the ultraviolet intensity down to 1950 Å indicates that any loosely bound molecular species such as ozone, nitrogen dioxide, ammonia, nitrous oxide, and sulfur dioxide would be shortlived in this radiation environment. In the small percentage of the planetary disk observed by the ultraviolet spectrometer, the characteristic absorption feature of ozone, centered at 2600 Å, has not been found.

The television cameras found no trace of cloudiness in the atmosphere of Mars, except for a few ill-defined regions detected in the polar-cap area, which could consist of clouds or fog. There is evidence, however, of a deep, but extremely thin, layer of haze in the final far-encounter sequence of Mariner 7 pictures and tangential views of the illuminated limb of the planet at the start of the near-encounter picture sequence. The apparent haze is somewhat brighter when viewed through the blue filter than through the red and green, suggesting that it consists of small particles of aerosol. It is estimated that the thickness of the haze layer

ranges from 8 to 16 km (5 to 10 miles) and that its height above the surface varies from 16 to 50 km (10 to 30 miles). Results from the infrared spectroscopy experiment provide a probable identification of the haze. An infrared reflection peak, recorded three times in the atmosphere off the bright limb of Mars at intermediate altitudes, shows the presence of solid CO_2 at high altitudes. Profiles derived from S-band occultation data show that the temperature and pressure conditions at high altitudes are favorable for the formation of solid CO_2. Because vertical television views of the planet were not affected by the thin haze layer, even when taken through the filter, the premission hypothesis of an obscuring "blue haze" above Mars is considered disproved. Surface features seen as albedo variations lost their contrast when viewed in blue light, as in Earth-based observations; this is considered a surface effect and not a result of any atmospheric constituent.

In reducing the data from the S-band occultation experiment to obtain pressure and temperature profiles, the composition of the atmosphere was assumed to be 90 percent CO_2. None of the results from the other experiments contradicted this assumption, as no other constituents were indicated in quantities large enough to affect greatly the findings of the S-band occultation experiment.

Three out of four of the pressure measurements taken were consistent, in the range between 6 and 7 mb (0.09 and 0.10 psi), equivalent to the atmospheric pressure at an altitude of 30 500 to 35 000 m (100 000 to 115 000 ft) above the Earth. The sole exception was the measurement in the region of Hellespontus, which was only 3.8 mb (0.06 psi), suggesting that Hellespontus is raised considerably above the mean gravitational potential surface of Mars. Because no high peaks, as such, were identifiable in the television pictures of Hellespontus (which did not include the occultation point), it is thought that the area at 58° S is possibly a large plateau, around 100 km (60 miles) across and standing 4 to 5 km (2 to 3 miles) higher than the surrounding surface.

Temperatures deduced from the S-band occultation experiment were in agreement with measurements from the infrared radiometry and infrared spectroscopy experiments, but the shapes of the temperature profiles, essential in determination of the circulation processes in the Martian atmosphere, are not yet certain. At present, the temperature profiles are not consistent with either radiative balance or convective balance.

Ionospheric electron density at an altitude of 130 km (80 miles), in the afternoon, was about 1.5×10^5 electrons/cm^3, and the plasma temperature about 450° K.

Several preliminary results from the infrared spectroscopy experiment, in

addition to the detection of high-altitude solid CO_2, are of interest relative to the Martian atmosphere.

(1) Infrared spectral features near 3μ were first ascribed to methane and ammonia, but subsequently have been shown to be absorptions of solid CO_2 previously undiscovered.

(2) Broad absorption attributable to solid H_2O (as a fog) or, perhaps, to surface hydrates, and sharp absorptions of carbon monoxide were detected at all latitudes.

(3) Broad absorptions near 12μ were recorded near the dark limb. These are as yet unassigned and may or may not relate to the atmosphere.

(4) Over most of the polar cap, the spectra give positive identification of solid CO_2, requiring either that the polar cap is composed of solid CO_2 covering part of the surface or that the polar cap is shrouded by a thin fog or cloud of solid CO_2.

THE MARTIAN SURFACE

Pictures taken by the Mariner 4 camera revealed that the surface of Mars was heavily cratered and resembled that of the Moon. Pictures taken by the Mariner 6 and 7 television cameras, which covered approximately 20 times more of the Martian surface, confirm that discovery, but reveal distinct differences between Mars and the Moon. In preliminary studies of the pictures, three types of Martian terrain are distinguished.

(1) *Cratered terrain* is prevalent; it includes many craters 50 to 75 km (30 to 45 miles) in diameter, and at least one (Nix Olympica) as large as 500 km (300 miles) in diameter. It includes the south polar cap and its boundary area, as well as the equatorial regions of Mars. The craters can be classified by size, depth, slope, and characteristics, and can be plotted, but the Martian plot varies distinctly from that of the lunar surface, implying differences in modifying processes or materials.

(2) *Featureless terrain,* exemplified by the bright desert of Hellas, appears in resolutions as high as 300 m (1000 ft) to be a flat floor, unlike any part of the Moon, but as smooth as terrestrial dry lake beds. The featureless terrain observed in Hellas covers at least 1900 km (1200 miles) of surface. No craters appear on Hellas. Because there is no way in which Hellas could have been sheltered from impacts by meteorites, it is estimated that, by some process, the effects of meteoroid impacts have been erased more rapidly in that area. Pictures of higher resolution than those obtained by the cameras on Mariners 6 and 7, however, could reveal

small craters in the surface of Hellas, but there should be large ones in evidence. It is hypothesized that the material comprising the floor of Hellas responds more readily than other Martian materials to whatever processes of erosion exist on Mars. An observation made by the infrared spectrometer is of interest relative to this problem. The 2μ absorption of gaseous CO_2 gave a topographic map along the track of the field of view with altitude sensitivity of about ± 0.3 km. As the field of view passed from Hellespontus into Hellas, a substantial drop in surface elevation was observed.

(3) *Chaotic terrain,* discovered in two Mariner 6 narrow-angle pictures, is described as irregular, jumbled topography, reminiscent of the slumped aspect of a terrestrial landslide. It is estimated that, in a specific Martian area of about 2 million km^2 (772 000 sq miles), as much as 10^6 km^2 (386 000 sq miles) may consist of chaotic terrain. As recorded by the infrared radiometer, the only fluctuation not correlated to albedo variation was found over the area observed by the television cameras to have chaotic terrain.

These three types of terrain show that the evolutionary history of Mars has been different from that of the Moon, and may possibly be unique in the solar system.

In a narrow-angle television view of one boundary of the south polar cap, many craters are visible, and it is evident that "snow" has been removed, by the process of absorbing solar radiation, from the slopes better illuminated by the Sun, and retained on the relatively shaded slopes of the craters. It is believed that the white polar cover consists of a very thin substance, though certain observed features, if interpreted as being due to drifts of material, could be a few meters in thickness. Preliminary studies of the pictures have not provided evidence of the dark polar collar noted by Earth-based observers. However, the south polar cap is observed by means of the ultraviolet spectroscopy experiment to have a polar collar at ultraviolet wavelengths. The polar cap itself is bright in the ultraviolet even at wavelengths as short as 1950 Å.

The primary purpose of the infrared radiometry experiment was to determine the composition of the south polar cap from its temperature. As Mariner 7 crossed the boundary of the polar cap, the temperature readings of the infrared radiometer dropped abruptly and leveled off at about 150° K (−193° F). These values are higher than the frost temperature of pure carbon dioxide at the pressure (around 6 mb, or 0.09 psi) generally admitted for the Martian atmosphere. The infrared spectrometer also made temperature measurements over the polar cap, indicating that average temperatures recorded between 61° S and 75° S

latitude are above those at which CO_2 could cover the ground completely at 6 mb. After correcting for stray light collected outside the field of view of the infrared spectrometer, the lowest temperature was about 150° K, in agreement with the value recorded by the radiometer. This value is still too high for CO_2 condensation over the entire surface, but a tentative statement regarding the constitution of the polar cap can be made. The instrument readings represent average temperatures over a considerable area, and if outcrops of solid material occur within the polar cap, the higher temperatures at those points could raise the average temperature readings for the area above the frost point of pure carbon dioxide. The low temperatures measured thus provide evidence for the composition of the polar cap as predominantly CO_2.

Elsewhere on the planet, the infrared radiometry experiment provided measurements of temperatures in the daytime hemisphere close to those expected from Earth-based work, i.e., about 290° K (62° F) at noon at the equator and 230° K (−45° F) at the polar-cap edge. In the nightside at the equator, unobservable from Earth, temperatures as low as 200° K (−100° F) were measured. The temperature fluctuations detected in daytime correspond to the large-scale variations in the ability of the surface to absorb solar radiation. As previously mentioned, the only fluctuation not correlated to albedo variation was found over chaotic terrain. The infrared spectroscopy experiment also shows an anticorrelation of temperature with the albedo it measured at 2.5μ.

The infrared spectrometer recorded close to the bright limb a broad absorption near 9μ. This has been ascribed to solid silica or silicate material, providing a possible clue regarding the composition of the surface in that area.

Sharply defined areas of light and dark, long delineated on maps based on telescopic observations of Mars, are diffused and splotchy in the near-encounter television pictures. Although it is not possible at this time to determine the colors, evidences of color variations in surface features have been found in comparing pictures taken with different filters.

There is no evidence of seasonal darkening in the television pictures; no distinctive topographic or physiographic character has been revealed by the pictures in the regions where the observed "wave of darkening" takes place.

In only a few instances are surficial structures identified with classical "canals." Some of these are considered to be the result of quasi-linear alinements of what appear to be impact craters with dark floors; the others seem to be linear alinements of diffuse dark patches, which may have some physical significance yet undetermined.

THE QUESTION OF LIFE ON MARS

Nothing in the data from Mariners 6 and 7 encourages the belief that life exists on Mars, although the results do not exclude that possibility. If it exists, it is almost certainly microbial. Limiting factors for Martian life in any form known on Earth include the evident lack of atmospheric nitrogen and the observed hard ultraviolet penetration to the surface. The scarcity of water also remains a very serious limiting factor for life on Mars. As determined from Earth-based experiments and possibly confirmed by the findings of the infrared spectroscopy experiment, there is water vapor in the Martian atmosphere; however, there is not a sufficient amount to make liquid water stable on the surface of the planet. The only stable states of water on Mars are vapor or ice, and no known terrestrial species could exist in that very dry environment. It is theoretically possible, however, to make evolutionary extensions of terrestrial life that could utilize water in the form of vapor or ice.

CHAPTER 2

The Program and Its Spacecraft

Authorization for Mariner-Mars 1969 as a project was given by NASA on December 22, 1965, in a teletype message from H. E. Newell, then Associate Administrator for Space Science and Applications, to W. H. Pickering, Director of the Jet Propulsion Laboratory (JPL), California Institute of Technology.

The objectives of the program were

(1) To conduct flyby missions to make exploratory investigations of Mars that will set the basis for future experiments, particularly those relevant to the search for extraterrestrial life

(2) To develop the technology needed for succeeding Mars missions

The scientific experiments selected to achieve the primary objective were

(1) Television
(2) Infrared spectroscopy
(3) Infrared radiometry
(4) Ultraviolet spectroscopy
(5) S-band occultation
(6) Celestial mechanics

The first four investigations required onboard instruments that viewed the planet; the last two required no instruments, but used radio tracking data acquired by the tracking and data system equipment.

To achieve the mission objectives, functional capability, instrument performance, and power capacity superior to those of any previous Mariner were required. For the first time, one spacecraft of a dual-spacecraft mission would gather Mars data and experience that would be used to benefit the second spacecraft's planetary encounter just 5 days later.

Responsibility for project management and for the design, fabrication, testing, and mission operations of the two identical spacecraft was assigned to JPL.

Tracking and communications would be accomplished by the Deep Space Network (DSN), which is the network for two-way communication with unmanned space vehicles traveling 10 000 miles from Earth, and beyond, to interplanetary distances.

The main elements of the DSN are the Tracking Stations; the Ground Communications Facility, which connects all parts of the DSN by telephone, teletype, and high-speed data lines; and the Space Flight Operations Facility, in Pasadena, Calif., which is the command and control center. Mission control switches to the SFOF immediately after the Unmanned Launch Operations of the Kennedy Space Center successfully launches the spacecraft, and remains there for the duration of the flights.

The spacecraft built for Mariner-Mars 1969 were attitude stabilized on three axes, solar-powered, capable of providing continuous telemetry transmission, and fully automatic in operation; the spacecraft could be commanded from Earth, when necessary.

Mariners 6 and 7 weighed about 380 kg (840 lb) each, considerably more than their predecessors (table 2–I). The two-axis scan platform provided considerably more capability and flexibility for the scientific payload than that of Mariner 4, and the solar panels and antennas were larger. (See figs. 2–1 and 2–2.)

Despite the increased functional capabilities of Mariners 6 and 7, the eight electronics bays in the base of each spacecraft were no larger than those of Mariner 4, owing to improved packaging and wide use of integrated circuitry. Although there were 40 percent fewer electronic parts in Mariners 6 and 7, integrated circuitry more than doubled the number of equivalent discrete parts flown on Mariner 4.

The primary power source for Mariners 6 and 7 was a total of 17 472 photovoltaic cells, covering an area of 7.7 m^2 (83 ft^2). The cells, which faced the Sun during most of the flight to Mars, provided 800 W near Earth and 450 W at the distance of Mars. The latter provided a margin above the maximum power requirement of 380 W at encounter to allow for solar cell degradation resulting from solar flares (table 2–I). The 14-kg (31-lb) rechargeable silver-zinc storage

Table 2–I.—Comparison of Mariner spacecraft parameters

Parameter	Mariner 2 (Venus, 1962)	Mariner 4 (Mars, 1964–1965)	Mariner 5 (Venus, 1967)	Mariners 6 and 7 (Mars, 1969)
Spacecraft separated weight, kg	204	261	245	380
Electric power supplied at planet, W	180	194	198	450
Instrument weight, kg	19	23	14	59
Science support equipment, kg	4	16	15	58
Mars encounter data return, bits	—	5.2×10^6	—	8×10^8

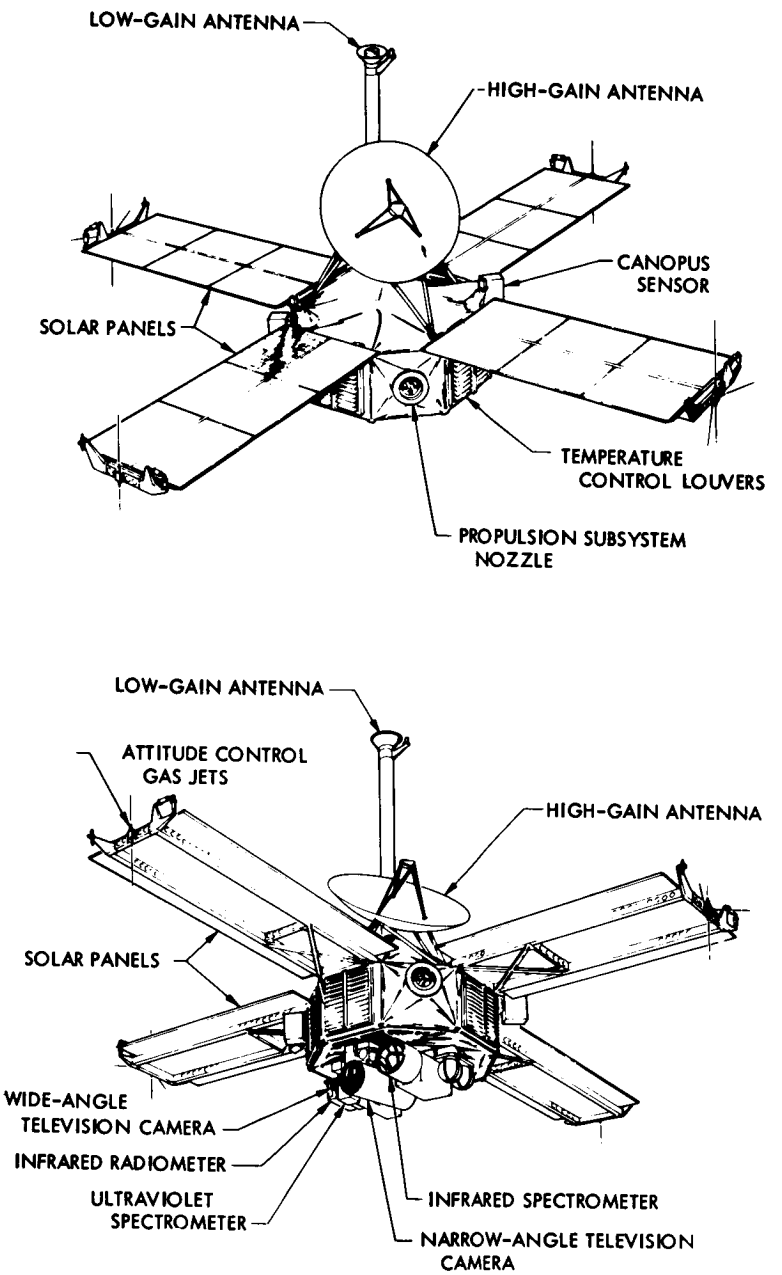

Figure 2–1. – Spacecraft configuration for Mariners 6 and 7.

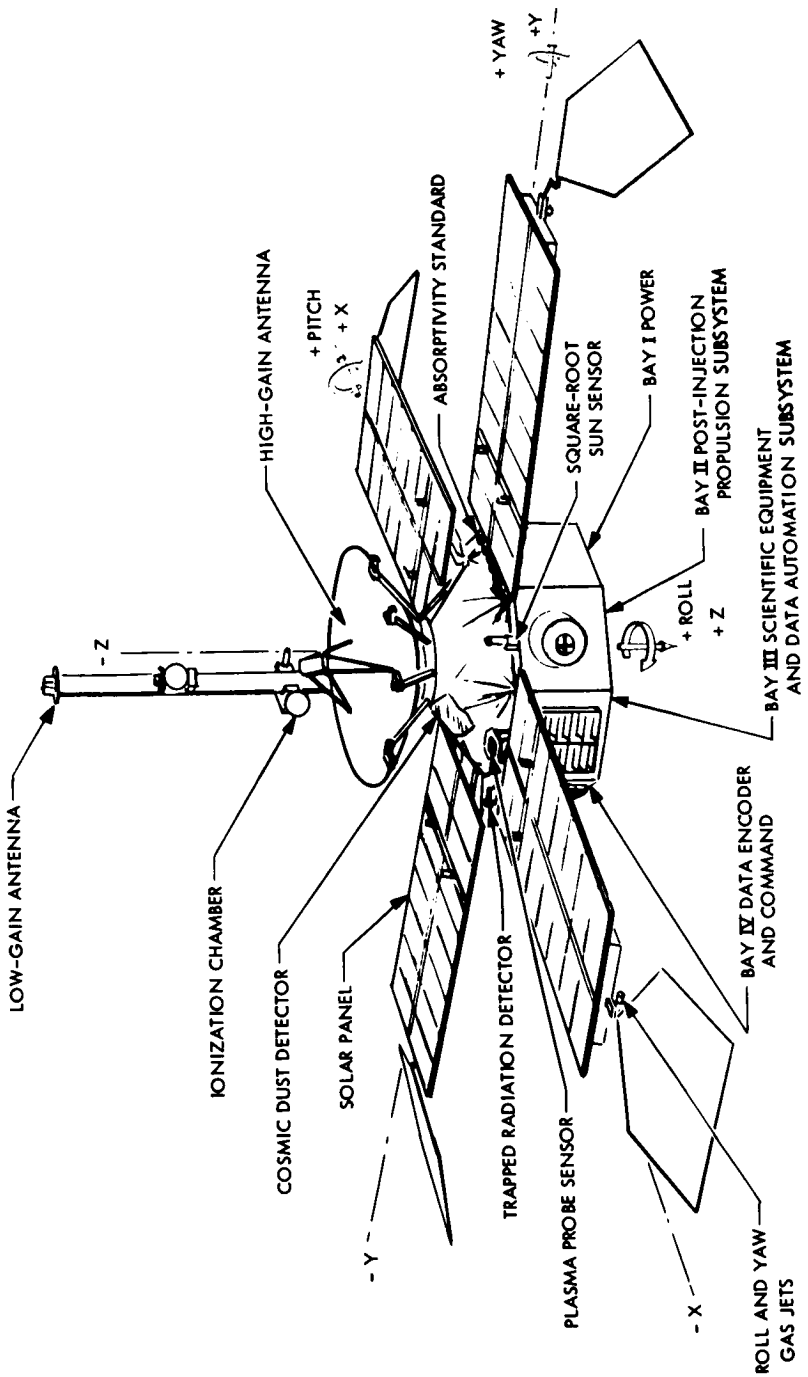

FIGURE 2-2. — Mariner 4 spacecraft configuration.

battery on each spacecraft provided power during launch, midcourse maneuver, and whenever the solar panels were turned away from the Sun. The battery was intended to be kept at full charge throughout the mission and to be available as a backup source of emergency power during encounter. This proved true of the Mariner 6 battery, but not of the one on Mariner 7, which failed a few days before encounter.

Where Mariner 4 had only one telemetry channel, used alternately for scientific and engineering data at 8⅓ or 33⅓ bps, three telemetry channels were incorporated on Mariners 6 and 7. A maximum transmission rate of 16 200 bps was used for the first time. Channel A carried engineering data at either 8⅓ or 33⅓ bps; channel B carried scientific data at either 66⅔ or 270 bps; channel C carried scientific data at 16 200 bps. Because only two of these channels could be used at one time, the workable combinations for simultaneous telemetry were channels A and B or channels A and C, which were used for real-time transmission of scientific and engineering data during the encounter phases of the missions.

The high-rate telemetry (HRT) system developed for Mariners 6 and 7 resulted in a large increase in data return over that of the previous Mars mission (see table 2–I), and an improvement in the capability of the telemetry by a factor of 2000 (33 dB) over that of Mariner 4. Development of the system involved designing, developing, and operating equipment that could receive transmissions from the Mariner spacecraft at the rate of 16 200 bps.

Engineering data from each spacecraft consisted of about 90 different measurements obtained continuously by transducers and transmitted over the engineering data telemetry channel.

Mariners 6 and 7 carried dual traveling-wave-tube amplifiers, capable of operating at an output of 10 or 20 W. These amplifiers provided redundancy and gave mission operators the option of selecting the transmitting power most suitable to the circumstances. The signal could be transmitted through the 1-m (40-in.) circular high-gain antenna or the omnidirectional low-gain antenna.

When the high bit rate was used, data from the analog tape recorder, which stored television data only, was fed to the telemetry subsystem through an analog-to-digital converter. The top telemetry rate could be used, however, only when the ground receiver was the 64-m (210-ft) antenna (fig. 2–3) at Goldstone, Calif., the largest antenna in the DSN. Use of the 16 200-bps rate depended, too, on a complex array of digital computers on the ground to provide bit synchronization and reconstruction of the data that had been block-encoded on the spacecraft,

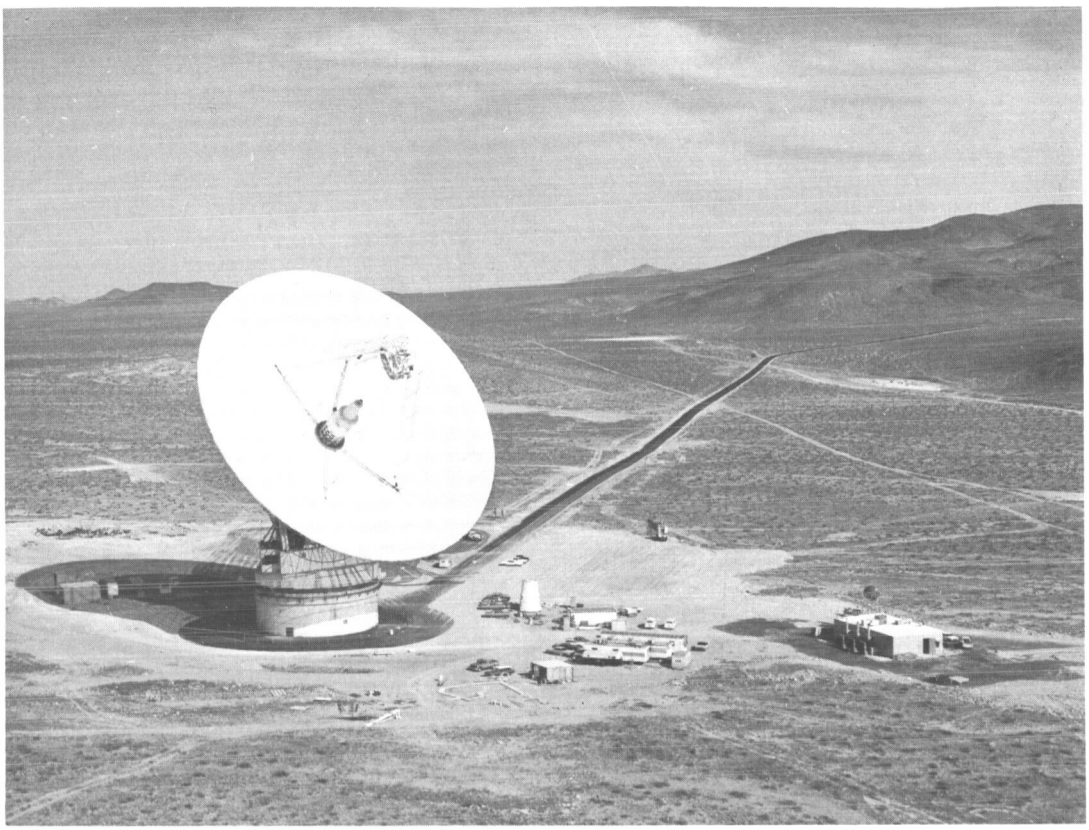

FIGURE 2–3. — The 64-m (210-ft) antenna at the Goldstone, Calif., tracking station. This is the most sensitive communications antenna in the world and has the capability of communicating with a spacecraft at the edge of the solar system.

converting it back to a serial bit stream of 16 200 bps and recording it on magnetic tapes.

The HRT prototype system was designed, tested, and performance verified by late January 1968. The first of two field sets was installed at Cape Kennedy in November 1968. After the Mariner 7 launch, both field sets were moved to the Goldstone tracking station to support operations at encounter, for together the field sets provided a complete, redundant ground system.

A new central computer and sequencer (CC&S), which for the first time could be reprogramed in flight, was added to Mariners 6 and 7. The primary purpose of this first-generation piece of equipment was to actuate specific events at precise

times fixed before launch and stored in its memory. The CC&S could be commanded in flight to actuate any event in real time if mission controllers considered this action desirable, and could have its memory changed at the discretion of the mission controllers, who were thus able to program, during flight, major sequences not planned before launch.

The CC&S enabled mission controllers to reschedule the Mariner 7 far-encounter picture sequence to try to gain time lost when problems developed during the flight.

The CC&S capability and flexibility were used to enhance the mission by modifying the encounter sequences after launch and to correct for several inflight difficulties.

The spacecraft system design philosophy was that there should be no state in which the spacecraft could be placed, by ground command or CC&S command, from which it could not retreat by the same means—with a few exceptions, such as power turn-on and solar panel deployment. This made it impossible for the spacecraft to become stuck in any one mode. The flexibility of the design also gave mission controllers the option of making a dry run of any programed mission event before it was timed to occur.

The new CC&S was programed at launch with both a standard and a conservative mission. The standard mission would transmit its scientific findings at the high bit rate and would provide extensive photographic coverage during the far-encounter sequence. The conservative backup mission would provide only eight approach pictures from each spacecraft, and would play back the data at 270 bps. Both missions would be automatic once initiated, but the standard mission would be executed only if commanded from Earth; the conservative mission needed no starting signal other than that supplied by the CC&S. Choice of mission depended on the condition of each spacecraft at the beginning of far encounter and on the availability of the 64-m (210-ft) antenna, which had not been completed at the time of the Mariner 4 mission.

The CC&S contained a fixed sequencer and a programable computer, which, under normal circumstances, worked in tandem, providing redundancy. If a problem with either occurred during any step of the midcourse maneuver, with the exception of the command to terminate rocket firing, the maneuver would automatically have aborted and the spacecraft would have returned to cruise condition. Either the computer or the sequencer alone could have commanded the midcourse maneuver.

CHAPTER 3

The Flights

At 01:29:02 G.m.t. on February 24, 1969, Mariner 6 was launched from Launch Complex 36B at Cape Kennedy, Fla., using as a launch vehicle the Atlas/Centaur, a 2½-stage vehicle that consists of a 1½-stage Atlas SLV-3C booster and a liquid oxygen/liquid hydrogen-fueled restartable Centaur stage. The launch azimuth was 108° east of north. The main booster was jettisoned 4 min and 38 sec after launch; the Centaur stage then burned for 7½ min before engine cutoff. At the time of spacecraft separation, the Centaur had achieved a velocity of about 8400 m/sec (25 000 mph) about 14 min after launch. The solar panels were deployed, and Sun acquisition occurred less than 2 min after the spacecraft emerged from the Earth's shadow. Four hours after launch the spacecraft began a programed search for the star Canopus to achieve attitude stabilization of its cruise mode. Canopus was acquired in 17 min.

Mariner 6 was initially injected into a trajectory biased away from the desired final aiming point. The bias was precautionary to insure that neither the Centaur stage nor the unsterilized spacecraft could be captured by the planet during encounter, thereby violating the biological quarantine imposed by NASA. The direction of bias was dictated by the desire to keep the midcourse correction maneuver well within the 220-N (50-lb)-thrust capacity of the spacecraft's small hydrazine-fueled rocket motor.

Each spacecraft could make two trajectory corrections, if necessary, to achieve the required accuracy. Precise tracking data identify the spacecraft's orbit. A trajectory correction involves gyro-controlled precision turns from the Sun-Canopus reference cruise attitude, followed by the firing of the spacecraft's hydrazine rocket motor to gain the necessary velocity increment. On March 1, Mariner 6 was instructed to pitch −23.44 deg, to roll 78.72 deg, and to fire its rocket motor for 5.35 sec. During the motor burn, the Canopus sensor indicated it apparently "saw" sunlit dust particles. (At a distance of 1.2 m (4 ft) from the sensor, a shiny particle only 0.003 cm (0.001 in.) in diameter would appear as bright as Canopus.)

The midcourse correction put Mariner 6 on a trajectory that would place it within about 440 km (about 260 miles) of the preferred location from Mars.

A few days later, when explosive valves were actuated to unlatch the scan platform on which the scientific instruments were mounted, the Canopus sensor again was distracted by bright particles, and the spacecraft lost roll-control lock on Canopus; the star was reacquired 26 min later. Because this situation could not be tolerated when the explosive valves were actuated to initiate cooling of one channel of the infrared spectrometer about 35 min before encounter, a plan was devised to place both spacecraft on inertial guidance for the Mars flyby. This mode was used during the platform unlatch on Mariner 7.

In late May, Mariner 6 developed what was believed to be a sticking relay in its Canopus tracker, and it was feared that the tracker would be unable to follow the star as it moved in cone angle. However, several ground commands to the spacecraft conquered the difficulty.

At 22:22:01 G.m.t. on March 27, 1969, Mariner 7 was launched from Launch Complex 36A at Cape Kennedy. The Atlas/Centaur again delivered the spacecraft to injection with high accuracy. On April 8, Mariner 7 was instructed to give up lock on the star Canopus and roll to acquire a new star, Sirius, before the midcourse maneuver. Starting the maneuver from Sirius orientation reduced the magnitude of the pitch and roll turns necessary to the maneuver, thus avoiding certain problems posed by the maneuver geometry. The spacecraft was commanded to pitch $-35.6°$ from Sun orientation, to roll $-12.8°$, and to fire its rocket engine for 7.6 sec. This increased the velocity of the spacecraft about 4 m/sec (14 ft/sec) and corrected its flyby point to within about 190 km (about 120 miles) of the desired location. At the distance of the trajectory arc, this represented an accuracy of better than one part in 3 million.

To avoid problems with the Canopus sensor when explosive squibs unlatched the scan platform, Mariner 7 was placed on gyro control on May 8. Several bright transients were observed during the unlatching of the scan platform, but the spacecraft was under gyro control; its attitude was not disturbed. Mariner 7 soon returned to normal cruise mode. The following day, coded commands, which already had been sent to Mariner 6, were sent to the central computer and sequencer (CC&S), modifying and updating the control parameters for cruise and encounter and setting up the automatic gyro-controlled encounter mode.

On July 29, 50 hr before closest approach, the Mariner 6 CC&S commanded the scan platform to point at Mars, enabling the far-encounter planet sensor to view the planet and to track the center of brightness, thus keeping the high-resolution (narrow-angle) television camera pointed accurately at Mars. The

CC&S then activated all scientific instruments except the drive motor and cryogenic cooling of the infrared spectrometer.

Beginning 2 hr later, and continuing for 20 hr thereafter, the Mariner 6 narrow-angle camera took 33 pictures of the planet, all of which was visible except for a small area near its northern pole. These 33 pictures, taken at 37-min intervals from distances ranging downward from 1 240 800 km (771 000 miles) to 724 990 km (451 000 miles), were recorded on the spacecraft's analog tape recorder, which takes television information only. After the last picture had been obtained, the data were played back to the 64-m (210-ft) antenna at Goldstone at the high bit rate. The tape was then erased, in preparation for receiving a subsequent series of 16 complete pictures and a fractional 17th that the narrow-angle camera began to take 22 hr before encounter, at distances ranging from 561 000 km (349 000 miles) to 175 000 km (108 000 miles). The seventh and eighth frames of this second series of approach pictures had been programed to be taken 2 min apart in an attempt to record the rising of Phobos, one of the two Martian satellites, on the eastern limb of the planet.

The best resolution of the second series of approach pictures was about 24 km (15 miles), in contrast to the best resolution of Earth-based telescopic photographs of about 160 km (100 miles). After the last picture of this series was recorded, about 7 hr before encounter, the analog tape recorder played the picture back to Goldstone, and the tape was again erased. During this period, the spacecraft's CC&S had commanded the scan platform to slue to its proper orientation for the near-encounter phase of the mission. This maneuver also pointed the radiator plate of the infrared spectrometer at deep space to facilitate its cooling before near encounter.

Thirty-five minutes before closest approach, one of the two planet sensors viewed the bright limb of Mars, thus triggering the start of the motor and initiating cryogenic cooling of channel 1 on the infrared spectrometer. Because of cooling system failure, however, channel 1 did not cool sufficiently to permit measurements in the 6-to-14μ spectral range. The other scientific instruments aboard had been taking data and transmitting selected portions since earlier in the far-encounter phase.

Twenty minutes later, the second narrow-angle Mars gate viewed the planet's limb, initiating the near-encounter sequence at 05:03 G.m.t. on July 31 by starting both the analog and the digital tape recorders; the former recorded television data, the latter recorded in digital form all other scientific data, plus every

seventh picture element. The digital data were transmitted in real time by means of the high-rate telemetry before, during, and after the time of digital recording. This high-rate telemetry mode was the primary method of return of the digital data. The wide- and narrow-angle cameras shuttered alternately, with the wide-angle pictures overlapping and the narrow-angle pictures centered successively in each region of overlap. The two cameras took 24 pictures of the Martian surface. The scan platform on which the two cameras were mounted moved from one angle to another, according to the computer-program sequence, to cover areas that would not have been within camera range if the instruments had maintained a fixed angle during the swath across the planet. At nearest approach, 05:19:07 G.m.t., Mariner 6 passed within 3431 km (2131 miles) of Mars.

The analog tape recorder was stopped as the spacecraft crossed the terminator to the nightside of Mars, but the digital tape recorder continued to acquire spectral data for 6 or 7 min afterward, to obtain measurements on the dark side of the planet. These data also were transmitted in real time on the high-rate telemetry channel. Eleven minutes after encounter, Mariner 6 passed behind Mars, and radio contact with Earth was lost for 25 min. The S-band occultation experiment was conducted as the spacecraft entered and exited from the occultation zone.

After exit from occultation, the digital tape recorder data were played back to the Goldstone, Woomera, and Madrid tracking stations at a 270-bps rate. The next day, the television data on the analog tape recorder were transmitted to the 64-m (210-ft) antenna of the Goldstone station at 16 200 bps. After the analog tape recorder had concluded two complete playbacks, which lasted almost 6 hr, the digital tape recorder resumed its playback at the 270-bps rate. As soon as the spacecraft was once again in view of the Goldstone station, however, the digital tape recorder was interrupted and another complete analog playback was made at the high bit rate to insure the successful recovery of the television data.

Only a few hours before Mariner 6 began its near-encounter sequence, the tracking station in South Africa reported the sudden loss of telemetry on Mariner 7. The spacecraft performance and command (SPAC) team then was involved in the final updating of the CC&S memory on Mariner 6 and in rechecking all subsystems for the approaching near-encounter sequence. Because it was believed that the most logical explanation for the signal loss was that either the high-gain transmitter had failed or the spacecraft had lost Canopus lock, a command was sent to Mariner 7 to switch from the high-gain to the low-gain antenna. The first

command brought a response within 10 min, the round-trip transmission time to Mariner 7 at that distance.

It was found that the telemetry was partially garbled and that 15 channels were missing entirely. The spacecraft signal was lost and acquired twice before Canopus was reacquired and the transmitter switched to the high-gain antenna. Although the cause of the anomaly was unknown, initial speculation was that either a micrometeorite had struck the spacecraft or that some part of Mariner, such as the battery or the infrared spectrometer cooling gas system, had failed, leaking gases and producing erroneous electrical signals. This conjecture at first seemed to be verified by the discovery that Mariner 7 had decreased slightly in radial velocity with respect to Earth (the only velocity increment directly measurable by Doppler tracking) during the silent 7 hr. After the spacecraft had been recovered, the change in velocity slowly increased over the next 24 hr to at least 8 cm/sec and possibly as much as 50 cm/sec (the measurements are necessarily approximate) before leveling off.

When the scientific instruments were turned on, it was discovered that they were in acceptable working order. The device for pointing them at the desired Martian regions, which had been upset in the anomaly, was quickly recalibrated using television pictures of Mars (at extreme range) as a substitute for the lost telemetry.

At 09:32:33 G.m.t. on August 2, Mariner 7 began its first far-encounter sequence of approach photography. The narrow-angle camera took 33 pictures during each of two subsequent 20-hr periods, and a third series of 25 pictures during a 17-hr period ending 5 hr before closest approach. The first series of pictures was taken at distances ranging downward from 1 716 000 km (1 065 000 miles to 1 340 000 km (840 000 miles); the second from ranges of 1 196 000 km (742 000 miles) to 707 000 km (439 000 miles); the third from ranges of 532 000 km (330 000 miles) to 127 000 km (78 600 miles). Each series was played back to the Goldstone station at the high bit rate as soon as it was completed.

Analysis of the Mariner 6 far-encounter pictures showed that an attempt should be made to obtain additional pictures of the polar cap. Shortly after the Mariner 6 near-encounter sequence, operators reprogramed the Mariner 7 CC&S to order additional near-encounter pictures and additional scientific data on the lighted side of Mars. Nine more near-encounter pictures were obtained during the Mariner 7 flyby than during that of Mariner 6. Because the digital tape recorder would now be full before complete passage over the dark side, the dark

side science data would have to be received by the high-rate telemetry mode without tape recorder redundancy. Reprograming of the Mariner 7 near-encounter strategy also involved changes in scan-platform sluing angles to compensate for the more southerly instrument track that resulted from the perturbation of the spacecraft orbit.

Thus, in the Mariner 7 encounter, as it actually occurred, all of the scanning instruments received more data than originally planned. The spectrometers and the radiometer shared in the increased polar coverage, and obtained additional atmospheric data. The cryogenic equipment on the infrared spectrometer operated correctly on this encounter, permitting acquisition of valuable spectra in the 6-to-14μ spectral range.

The change in velocity resulting from the anomaly altered the Mariner 7 trajectory so that the flyby point was moved about 130 km (about 80 miles) southeast. The spacecraft altitude at closest approach was slightly increased, and the time of arrival at that point was delayed a few seconds beyond the estimate made just before the anomaly. At closest approach, Mariner 7 flew within 3430 km (2130 miles) of the Martian surface.

Immediately following each encounter, after six complete high-rate playbacks of analog recorder near-encounter data from both spacecraft, one track of the analog information was transferred to the digital tape recorder aboard each Mariner and played back in digital form at 270 bps.

The spacecraft then were returned to the cruise mode for additional engineering tests, communications performance tests, and scientific operations while in orbit around the Sun. The scientific operations included a star-photography test of the television cameras and scans by the ultraviolet spectrometer of the Milky Way and of an area containing a comet called 1969–B.

Periodic tracking is planned as the spacecraft travel around the Sun through the point of opposition with Earth in an attempt to make a check on Einstein's theory of general relativity.

CHAPTER 4

Scientific Payload

The Mariner 4 flyby on July 15, 1965, the first successful space flight to Mars, revealed that the planet's surface is heavily cratered and that its atmosphere is extremely thin, with a surface pressure less than 0.01 that of the Earth. Mariner 4 was not designed to provide answers to such questions as

(1) Has Mars been in its present state throughout geological ages, or is it in a later stage of an evolution that may once have included a denser atmosphere and perhaps liquid surface water?

(2) What is the significance of the light and dark areas of the planet, some of which show seasonal changes in albedo and possibly in color?

(3) Does life of any kind exist on Mars, or did it ever exist there?

The basic objectives of the missions to Mars in 1969 were (1) to explore further the surface and atmosphere of the planet with the intent of establishing the basis for future experiments, particularly those that could determine whether or not the past or present environment of Mars would permit life forms to exist and (2) to develop the technology necessary to conduct those experiments for succeeding missions to Mars.

Of the six scientific experiments selected to achieve the first objective, five were designed to yield data on the physical, chemical, and thermal properties of the planet. The purpose of the sixth experiment was to refine astronomical data.

Different aiming points were selected for Mariners 6 and 7. An equatorial aiming point ($-10° < \theta < 0°$) with arrival date of July 31 was chosen for Mariner 6 to provide good coverage of the many light and dark surface features available in that region. A southerly aiming point ($-30° < \theta < -20°$) with arrival date of August 5 was chosen for Mariner 7 to permit coverage of the south polar cap; the thaw regions on its edge; Hellespontus, which was particularly interesting because it appears to darken immediately after the polar cap starts to recede; and Hellas, which is a classic bright surface feature.[1] A nominal altitude of 3000 km (1860 miles) was chosen as the closest approach to Mars for both spacecraft,

[1] The spring season had just begun in the southern hemisphere of Mars, and the south polar cap had settled into its normal recession cycle.

in contrast to the Mariner 4 altitude of 9844 km (6118 miles) at closest approach. Thus, the spacecraft could investigate about 20 percent of the surface of the planet from near-encounter altitudes, in contrast to the little more than 1 percent coverage by Mariner 4, and could obtain data on the Martian geography and climate.

Both spacecraft carried identical scientific instruments (fig. 4–1): two television cameras, one of medium resolution (wide angle), and the other of high resolution (narrow angle); an infrared spectrometer; an ultraviolet spectrometer; and an infrared radiometer. The instruments were mounted on a single scan platform, which could be driven through 215° of clock angle and 69° in cone angle. The combined weight of instruments and platform was about 75 kg (165 lb). These instruments are discussed in more detail in the following paragraphs.

The subsequent chapters, which were prepared by the investigator teams,

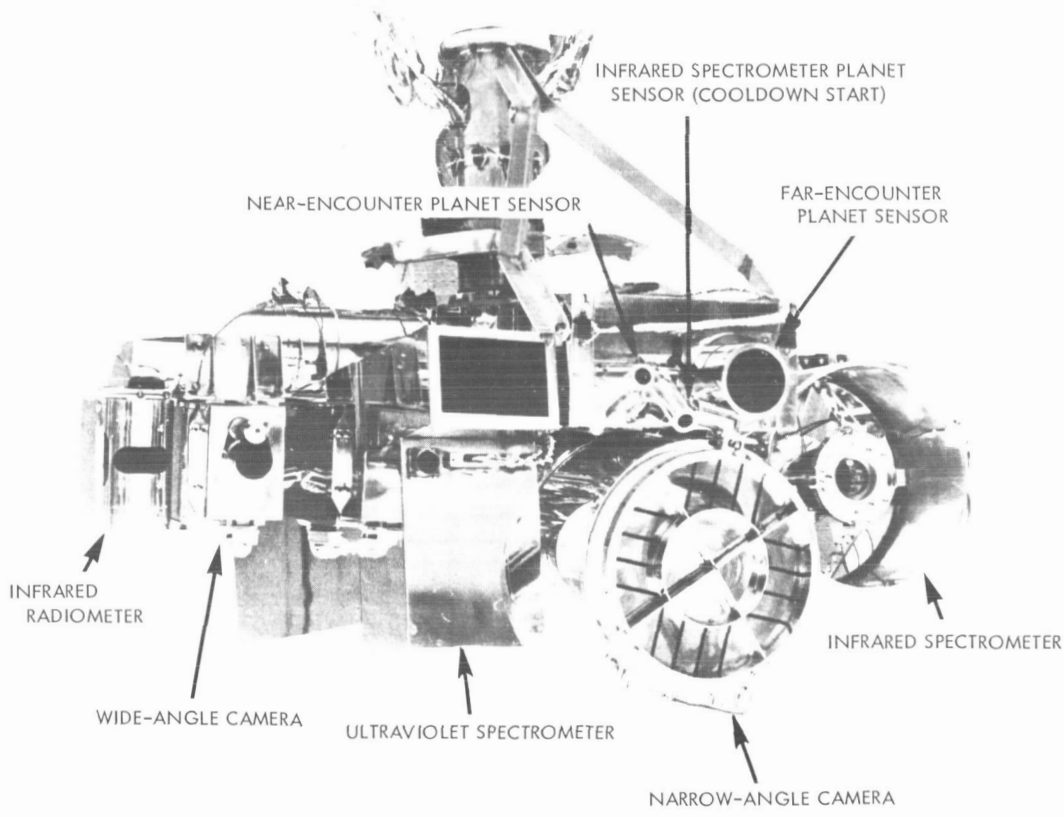

FIGURE 4–1.—Relative positions of scientific instruments carried on Mariners 6 and 7.

contain the preliminary scientific results from the experiments. The chapters were written independently of one another; therefore, some differences in interpretation may exist among them. The interpretations given are those of the appropriate investigator team.

TELEVISION CAMERAS

The wide-angle camera covered an area 12 to 15 times larger than the Mariner 4 camera, but had approximately the same surface resolution. The field of view of the wide-angle camera was 11° by 14°, encompassing 100 times more surface area in each picture than did the narrow-angle camera. The iris setting was $f/3.0$; the focal length was 50 mm. Automatic aperture control, actuated by gain circuitry, provided a fast shutter speed of 90 msec and a slow shutter speed of 180 msec. The camera was equipped with red, green, and blue filters to delineate color differences. The filters were automatically rotated in a green, red, green, blue sequence.

The narrow-angle camera, used alone for the far-encounter pictures, was boresighted with the wide-angle camera; a modified Schmidt-Cassegrain telescope provided a linear resolution 10 times higher than that of the wide-angle camera. At closest approach, the camera covered an area of about 70 by 90 km (44 by 56 miles); its resolution was about 300 m (1000 ft). The iris setting was $f/2.5$; the focal length was 508 mm. Automatic aperture control provided a fast shutter speed of 6 msec and a slow shutter speed of 12 msec. The camera was equipped with a yellow filter to reduce haze effects.

The cameras shuttered alternately. They were timed to provide overlapping of the wide-angle pictures, with the narrow-angle pictures falling inside the overlapped portions to aid in interpretation. Each camera took one picture each 84.48 sec, with continual shuttering throughout the far- and near-encounter phases of each flight.

The vidicon tube in each camera had a surface sensitive to light, and lost an electrical charge in proportion to the intensity of the light striking the surface of the tube. An electron beam scanned 665 280 points on the target in 42.24 sec, and generated an electrical current proportional to the charge loss at each point and, therefore, in proportion to the light value for each point. This converted the image to intensity information, which was stored in the spacecraft tape recorders. Because transmission from spacecraft to Earth was in binary form, the analog data were converted to digital data before transmission. When received on Earth, the binary coding was reconverted to electrical impulses, which repre-

sented the pattern of light and dark elements of the original image on the vidicon tube. They were used to modify the intensity of a beam of light that swept across a 70-mm negative to expose it and thus re-create the original image.

INFRARED SPECTROMETER

The objectives of the infrared spectroscopy experiment were (1) to determine the atmospheric composition, including polyatomic molecules such as the possible life-related molecules H_2O, CH_4, NH_4, CO ethylene, acetylene, nitric oxide, ozone, and nitrogen dioxide; (2) to determine the surface temperature along the track of the field of view, including the dark side of the planet; (3) to search for evidence concerning surface composition; (4) to provide topographical information through the intensity of the carbon dioxide spectral absorptions; (5) to provide evidence on the composition of the polar cap; and (6) to examine infrared emission from the bright limb.

To accomplish these objectives, an infrared spectrometer, designed and built at the University of California, Berkeley, was carried as part of the scientific payload.

To help determine the composition of the visible Martian light and dark surface areas, the spectrometer covered about the same areas as did the television cameras. Data from the experiment were also compared with some of the results from the ultraviolet spectroscopy experiment to obtain a detailed analysis of the Martian atmosphere from upper limits to near surface.

Light from Mars entered the instrument (fig. 4–2) through a telescope, and was focused, split into two beams, and directed to two detectors, both of which were cooled for maximum efficiency. The cooling system for the channel 1 detector (mercury-doped germanium) employed two 380-atm (5500-psi) gas bottles storing gaseous hydrogen and nitrogen. Shortly before encounter, on command from the spacecraft CC&S and a Mars sensor, explosive devices opened valves that started the gas flow to the cooling unit. The same command started the spectrometer filter-wheel motor. The channel 1 detector was intended to be cooled to about 22° K (−420° F). The cooling worked as designed on Mariner 7, but failed on Mariner 6. The channel 2 detector (lead selenide) was cooled to about 165° K (−163° F) by a radiator plate exposed to deep space.

Wavelengths reaching the detectors were selected by continuously variable filters, rotating each 10 sec to complete one scan of the wavelength region being examined. At closest approach, the geographical resolution of the field of view was about 120 km by 3 km, and during a single scan 120 km by 120 km.

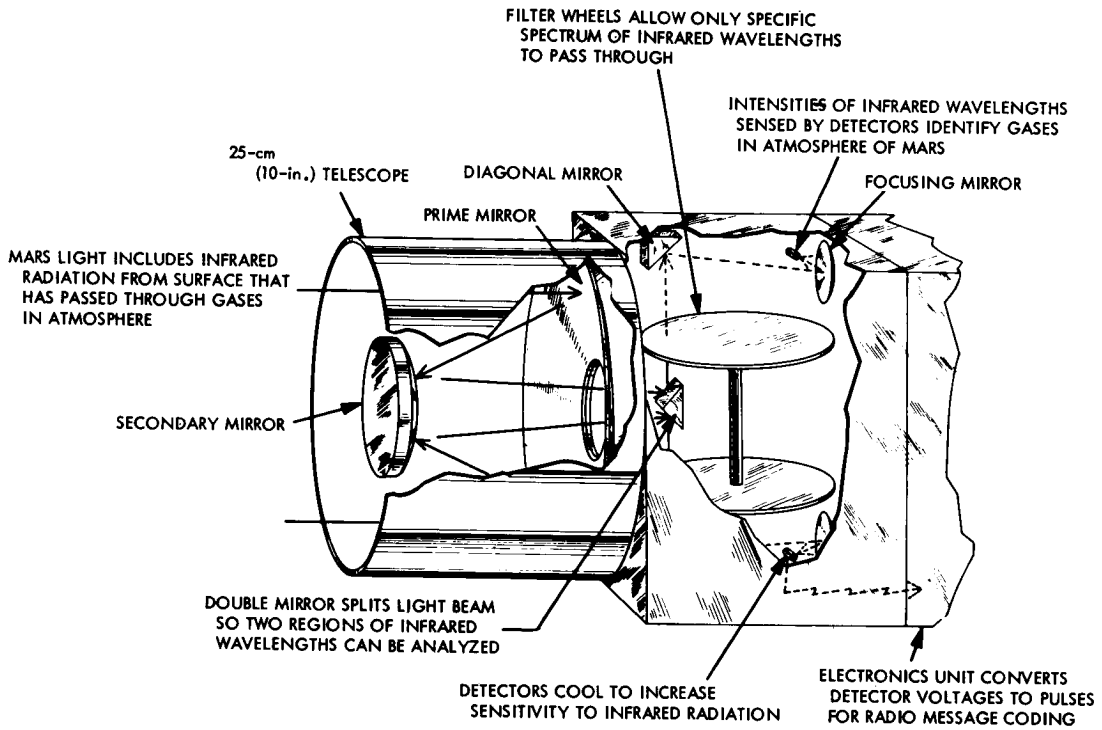

FIGURE 4–2.—Diagram of infrared spectrometer.

The energy of the light registered as a voltage change across the detectors. This analog signal was processed and converted to two pulses, which were separated in time proportional to the analog signal. The pulses were converted to binary values by the spacecraft data automation subsystem and stored in the digital tape recorder for transmission after the flyby. Engineering measurements on the experiment (critical voltages, temperatures, and gas pressures), important in analyzing the experimental data, were transmitted in real time, each 42 sec.

The infrared spectrometer, which weighed 16.2 kg (35.8 lb), used 4 W of power for heaters during cruise and approximately 8 W of power during the encounter sequence.

ULTRAVIOLET SPECTROMETER

The ultraviolet spectroscopy experiment was designed to identify gases in the upper atmosphere of Mars by detecting various molecules, atoms, and ions (molecules or atoms that have gained or lost electrons), and to determine their amounts. The ultraviolet spectrometer identifies these species by the wave-

lengths of light that they absorb or emit. Data on the composition of the Martian atmosphere not only provide knowledge of how the atmosphere itself originated and evolved, but, in turn, is a source of information regarding the age and evolution of the planet. It also is essential in an understanding of whether or not life could exist there.

It has not been possible to make ultraviolet studies of Mars from the surface of the Earth because the relevant wavelengths of radiation cannot penetrate the Earth's atmosphere, and only brief samplings have been taken by ultraviolet spectrometers carried on Earth satellites and high-altitude balloons.

The ultraviolet spectrometer carried on Mariners 6 and 7 focused and collimated Martian light (made its rays parallel) by means of mirror elements in the instrument (fig. 4–3) and directed the light onto a grating that diffracted it into its separate wavelengths. The diffracted light was again focused by a mirror element through slits and onto two detectors, which were photomultiplier tubes, each sensitive to different regions of the wavelength spectrum. One tube responded in the region from 1100 to 1900 Å, the other in the region from 1600 to 4350 Å.

The spectrometer's grating was ruled, or grooved, with 2160 rules/mm and mechanized to rotate. Because each wavelength was diffracted at a different angle, the rotation of the grating directed the separated wavelengths to the detectors

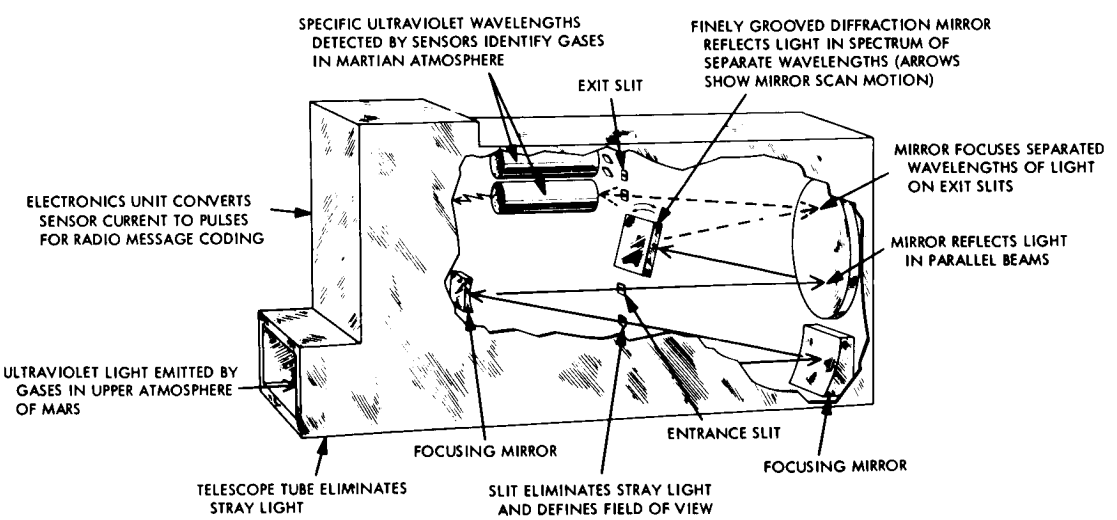

FIGURE 4–3.—Diagram of ultraviolet spectrometer.

sequentially. The known position of the grating in time made it possible to determine the wavelengths striking the detectors. The light that reached them was converted to a voltage proportionate to the amount. The voltage was then processed and stored for transmission to Earth after the flyby, though some of the data were transmitted in near real time while each spacecraft was passing Mars.

The atmospheric species primarily sought in the ultraviolet spectroscopy experiment were H (1216 Å), O (1304 Å), N (1200 Å), N_2^+ (3914 Å), CO^+ (4264 Å), N_2 (1354 Å, 3371 Å), NO (2150 Å), CO (2160 Å), and CN (3876 Å). Although it was felt that there may not be sufficient solar energy at Mars to excite other atmospheric species, a secondary objective of the experiment was to seek species such as Kr (1235 Å), Xe (1470 Å), metallic ions, and other molecules in the spectral range examined.

INFRARED RADIOMETER

The objectives of the infrared radiometery experiment on Mariners 6 and 7 were to measure the infrared emission from those areas of Mars scanned by the television cameras to obtain a temperature map that could be correlated exactly with topographic or cloud features shown in the imagery; to obtain a curve of surface cooling by a scan trace across the terminator; and to obtain absolute temperature measurements of the south polar cap to determine whether the frost that covers it is formed from carbon dioxide, water, or a combination of both.

The two-channel radiometer (fig. 4–4), which weighed 3.4 kg (7.5 lb), was boresighted with the narrow-angle television camera. The instrument looked through the atmosphere of Mars in two different wavelength regions: 8.5 to 12.4μ in channel 1 and 18 to 25μ in channel 2. Filters in the radiometer determined the wavelengths reaching the two antimony-bismuth thermopile detectors. Of the 60 readings provided by the detectors every 63 sec, 54 were planetary temperatures, 4 were calibration readings, and 2 were engineering measurements in the instrument (temperature or voltage). The calibration readings were made from an internal source of known temperature and from deep space, the latter representing a zero reference point.

The thermal radiation from the Martian surface was focused and filtered by optical elements in the radiometer onto the two detectors, producing a voltage proportional to surface temperature. This analog voltage was converted to two pulses whose separation in time was proportional to the voltage. The information

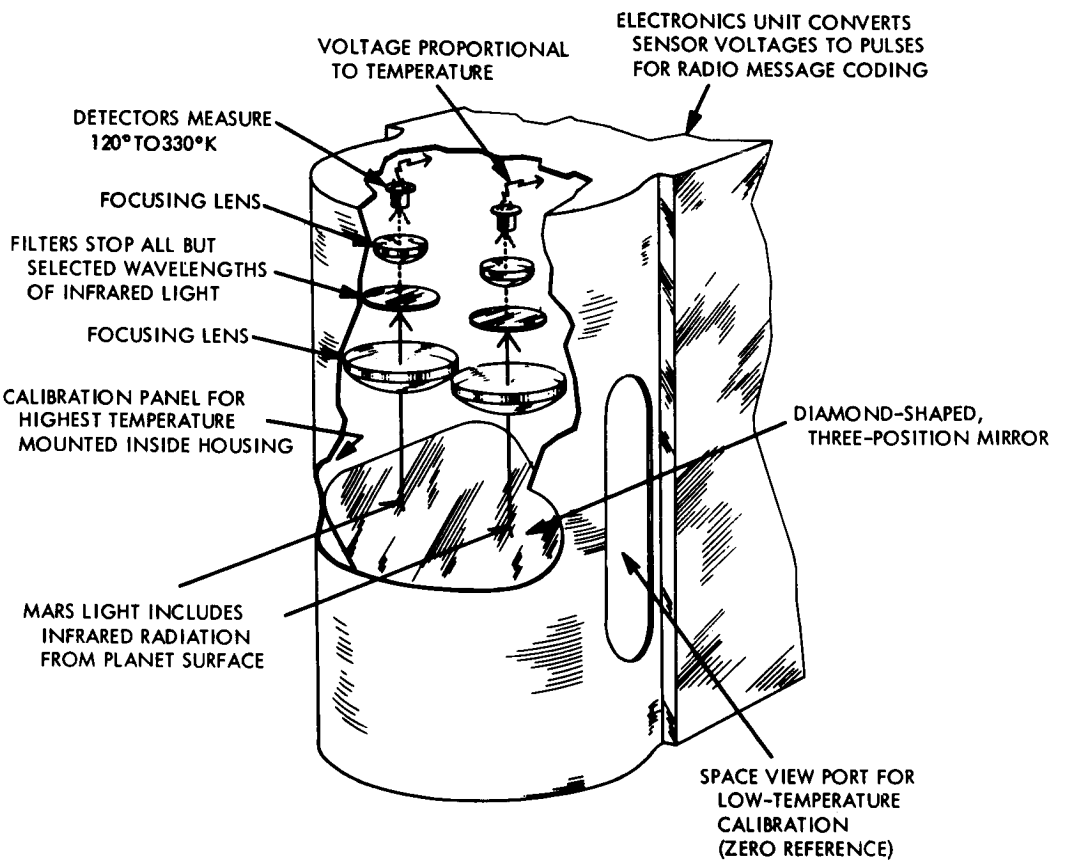

FIGURE 4-4.—Diagram of infrared radiometer.

was encoded in binary form by the spacecraft data automation subsystem for transmission. Data from the experiment were stored in the digital tape recorder and also transmitted in real time.

S-BAND OCCULTATION

The first S-band occultation experiment was performed by Mariner 4. The data returned provided new values for the pressure, density, and electron density of the Martian atmosphere, and significantly changed scientific views of the planet. The objectives of the experiment on Mariners 6 and 7 were to refine these data, to obtain measurements of the figure of Mars, and to attempt to measure radio signals reflected from the planet's surface. Data from this last part of

the experiment could be correlated with data from other experiments on the spacecraft to make estimates of the electrical characteristics of the Martian surface.

The experiment utilized the radio signals transmitted from the spacecraft and did not require a separate onboard instrument. It did, however, require a trajectory that passed behind Mars, as seen from Earth, thus occulting the spacecraft from the view of tracking stations. As the spacecraft curved behind Mars, its radio signal passed through the Martian atmosphere and was cut off at the surface. The signal reappeared as the spacecraft emerged from behind the planet, and again the radio signal passed through the planet's atmosphere. The atmosphere refracted the radio waves, changing the frequency and strength of the signal received on Earth. Measurements of the changes yielded the desired data on the density and pressure of the Martian atmosphere. Similar changes are caused by electrons in the ionosphere of Mars; these also were measured in this experiment.

To enhance the results, the trajectories of Mariners 6 and 7 were selected to provide four occultation points separated in latitude. It was expected that the data also would yield accurate values for the radius and oblateness of Mars, thus providing an estimate of its density and aiding in the understanding of its internal structure.

Determination of the atmospheric density of Mars is vital to the design of future landing missions and is a critical factor in the resolution of important scientific questions regarding the nature of the planet.

CELESTIAL MECHANICS

The primary purposes of the celestial mechanics experiment on Mariners 6 and 7 were to determine the mass of Mars, the ratio of the masses of the Earth and the Moon, and the distance from Earth to Mars at encounter. Additional purposes of the experiment were to refine the ephemeris of Mars, as part of an existing project to improve the ephemerides of all the inner planets, and to attempt to measure general relativistic effects on Mariners 6 and 7 while in solar orbit, as part of the extended mission plan.

Because the experiment was based on determining the mass of celestial bodies by measuring their effects on the flightpaths of the two spacecraft, data were obtained exclusively by ground tracking equipment. To achieve maximum precision, the results were correlated with radar-bounce data and optical telescopic findings, as during the Mariner 5 flyby of Venus in October 1967.

The celestial mechanics experiment on Mariner 6 was conducted as planned. For Mariner 7, the necessity to determine the nongravitational forces acting on the spacecraft during the period of the anomaly and recovery from that event has delayed any thorough analysis of the data.

CHAPTER 5

*Television Observations From Mariners 6 and 7**

R. B. LEIGHTON *(Principal Investigator)*, N. H. HOROWITZ, B. C. MURRAY,
R. P. SHARP, A. G. HERRIMAN, A. T. YOUNG, B. A. SMITH,
M. E. DAVIES, AND C. B. LEOVY

In July 1965, a new era in the closeup study of planetary surfaces by using imaging techniques began with the successful flyby of Mariner 4 past Mars. In spite of its limited data return, Mariner 4 established the basic workability of one imaging technique that utilized a vidicon image tube, onboard digitization of the video signal, storage of the data on magnetic tape, transmission to Earth at reduced bit rate via a directional antenna, and reconstruction into a picture under computer control. Although the pictures covered an area of only about 1 percent of Mars, they contributed significantly to our knowledge of that planet's surface and history (refs. 5–1 and 5–2).

The objectives of the television experiment on Mariners 6 and 7 were (1) to apply the successful techniques of Mariner 4 to explore further the surface and atmosphere of Mars, both at long range and at close range, in order to determine the basic character of features familiar from ground-based telescopic studies; (2) to discover possible further clues as to the internal state and past history of the planet; and (3) to provide information germane to the search for extraterrestrial life.

Mariners 6 and 7 flew past Mars on July 31 and August 5, 1969, respectively; first results of the television experiment, based upon qualitative study of the uncalibrated pictures, have been reported (refs. 5–3 and 5–4). This chapter draws together the preliminary results from the experiment; presents tentative data concerning crater size distributions, wall slopes, and geographic distributions; discusses evidences of haze or clouds; describes new distinctive types of topography seen in the pictures; and discusses the implications of the results with respect to the present state, past history, and possible biological status of Mars.

Data presented in this report were obtained by inspecting and measuring a sample of pictures in various stages of processing. The results, therefore, must

* The results described in this chapter have been published in *Science*, vol. 166, 1969, pp. 49–67.

be regarded as preliminary, subject to considerable expansion and possible modification as more complete sets and better quality versions of the pictures become available, and as more quantitative measurements become possible.

EXPERIMENT DESIGN AND CAMERA OPERATION

Television Subsystem Design

The experience and results of Mariner 4 strongly influenced the basic design of the Mariner 6 and 7 television experiment. The earlier pictures showed that Mars was heavily cratered but had rather low surface relief, and therefore low local photographic contrast, and that there was a possible hazy atmosphere. It also was discovered that a vidicon-type camera tube exhibits a most important property: the "target noise," analogous to photographic grain, is less than that of a photographic emulsion by perhaps a factor of 10 (ref. 5–2) and is the same from picture to picture. Thus, the 64-level (6-bit) encoding scheme of Mariner 4 could cope with the extremely low contrast conditions because intensity calibration and contrast enhancement using computer techniques could be applied effectively to the data to produce pictures of useful quality.

Early design studies for Mariners 6 and 7 centered on 256-level (8-bit) encoding (at least a tenfold increase in data return over Mariner 4); overlapping two-color coverage along the picture track (similar to that of Mariner 4); use of two cameras of different focal lengths to provide high-resolution views of areas nested within overlapping, wide-angle frames; and use of the longer focal-length camera to obtain some full-disk pictures showing all sides of Mars as the spacecraft approached the planet. To study atmospheric effects, a blue filter was added to the red and green filters carried on Mariner 4.

The Mariner 6 and 7 television experiment employed two cameras with identical picture formats and electronic circuits (for economy and for efficient use of the tape recorders), a digital tape recorder to store the six lowest order bits of an 8-bit encoded word for every seventh picture element (pixel) along each television picture line (referred to as 1/7 digital data),[1] and a second, similar tape recorder to store analog data for all pixels (ref. 5–5). The instrumental characteristics of the Mariner 6 and 7 television cameras are outlined in table 5–I; those of Mariner 4 are included for comparison.

[1] The 1/7 digital television data for the central 20 percent of each line were replaced by encoded data from other onboard experiments. In this region, coarser 1/28 digital data (6-bit coded for every 28th pixel), stored on the analog tape recorder, were available. (See fig. 5–2.)

Table 5–I. — Characteristics of television cameras and data systems for Mariners 4, 6, and 7

Item	Mariner 4	Mariner 6 and 7 cameras	
		Wide-angle	Narrow-angle
Optics:			
Aperture, mm	60	10	200
Focal length, mm	305	52	508
T-number	8	6.5	3.6, 3.84
Type	Simple Cassegrain	Lens	Equal-radii Schmidt-Cassegrain
Shutter	4-position rotary	4-position rotary	2-blade, right-left
Exposure (fast, slow), msec	85; 200	90; 180	6; 12
Filters: effective wavelength, nm	600 (red)	573 (red)	—
	—	526 (green)	560
	540 (green)	469 (blue)	—
Picture:			
Absolute size, mm	5.5×5.5	9.6×12.3	9.6×12.3
Angular field, deg	1.1×1.1	11×14	1.1×1.4
Resolution elements (pixels)	200×200	704×935	704×935
Frame readout time, sec	24	42.25	42.25
Picture interval, sec	48	84.5	84.5
Encoding levels, $N=2^n$	$n=6$	$n=8$	$n=8$
		Digital	Analog
Tape recorders:			
Number	1	1	1
Tracks	4	4	4
Tape length, m	100	110	110
Stored bits (effective)	5×10^6	1.3×10^7	1.2×10^8
Tape speed, cm/sec:			
Record	32.5	30	30
Playback	0.025	4.3	4.3
Data transmission rates:			
As used, bps	8⅓	16.2×10^3	16.2×10^3
Backup, bps	—	270	270

To reduce the noise introduced by analog recording, the average signal level was held nearly constant and the modulation index was increased by automatic gain control (AGC) and a cube-law contrast-enhancement circuit. This signal processing increased the data return by a factor of about 5; it also made necessary an elaborate program of computer restoration of the pictorial data after receipt on Earth.

The wide-angle camera (camera A) has an 11° by 14° field of view and a rotary shutter that consists of four colored filters in the sequence red, green, blue, green, etc. Alternating exposures with the wide-angle camera is the narrow-angle camera (camera B), which has a focal length 10 times longer and a 1.1° by 1.4° field of view, but carries only a minus-blue haze filter. Figure 5–1 shows the cam-

eras mounted on the spacecraft, and the relative positions of the other scientific instruments. Figure 5–2 shows the effect of AGC on the analog signal, an effect similar to that of a high-pass filter in that it diminishes the amplitude of long spatial wavelength (low-frequency) signals. Spectral sensitivity curves, with and without filters, are shown in figure 5–3. The approximately 6-msec response time of the AGC corresponds to about one-tenth of a picture line, and its characteristic effects are apparent in all near-encounter pictures, especially those with high contrast (e.g., the polar-cap boundary, the planet limb, and the terminator).

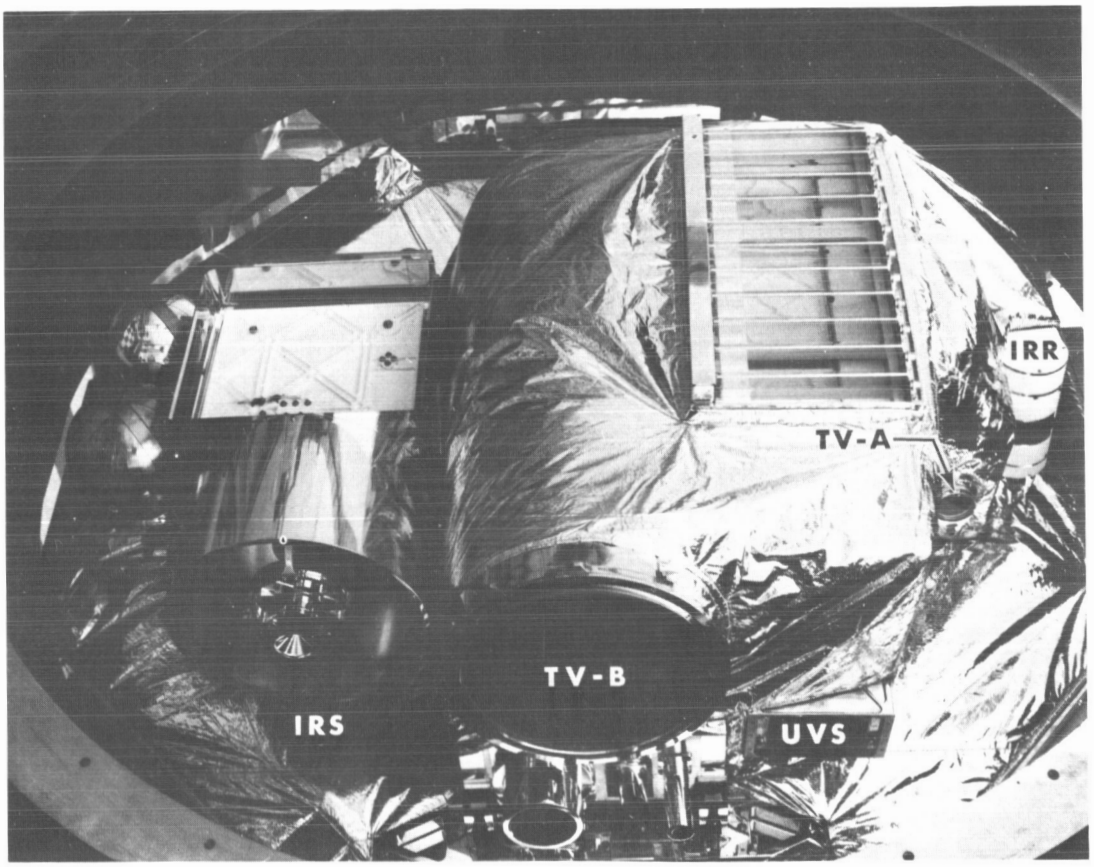

FIGURE 5–1. — Scientific instruments mounted on the scan platform of Mariner 6. The five principal instruments are: infrared spectrometer (IRS), ultraviolet spectrometer (UVS), infrared radiometer (IRR), wide-angle television camera (TV-A), and narrow-angle television camera (TV-B).

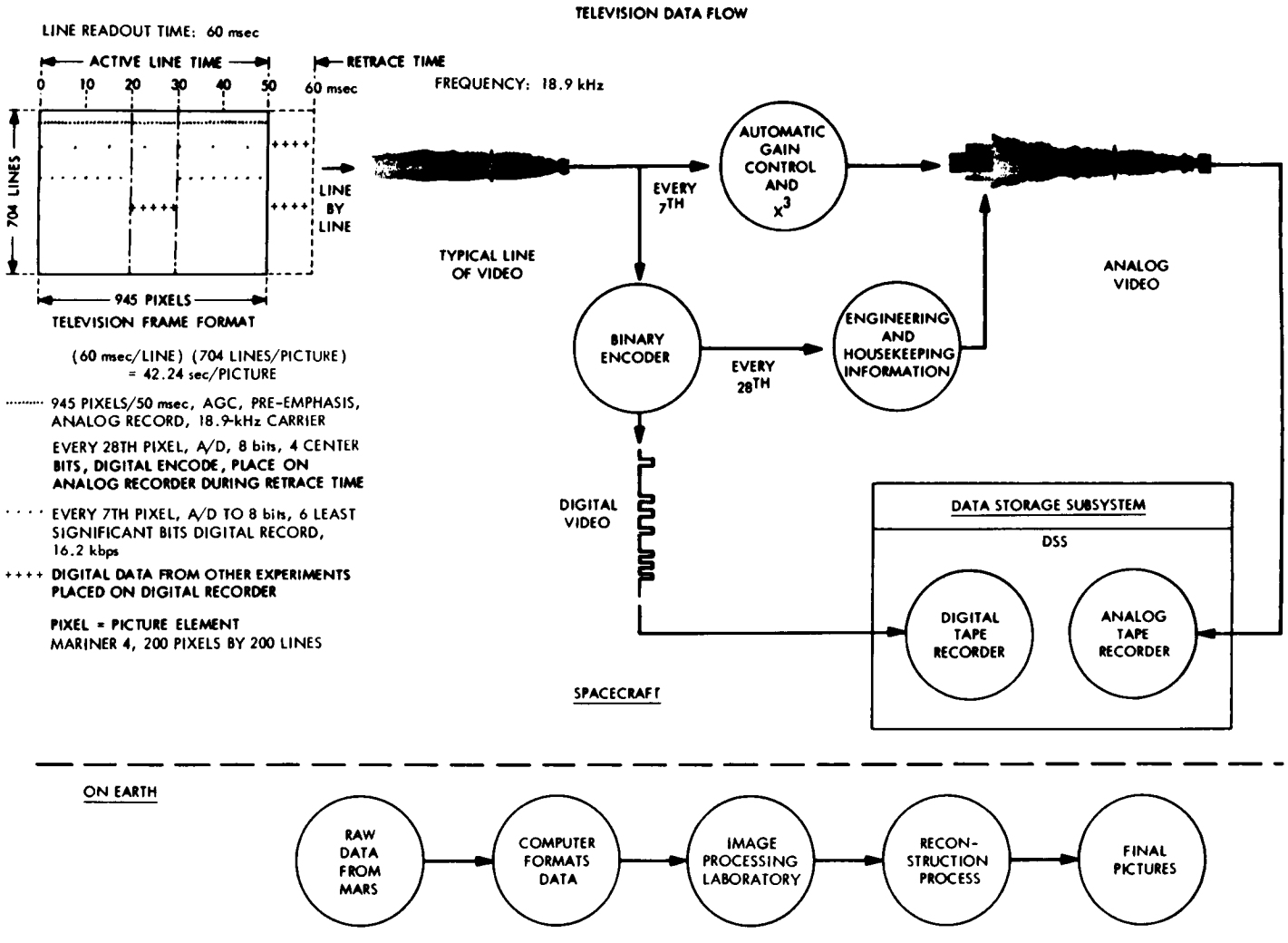

FIGURE 5–2. – Diagram showing video signal processing.

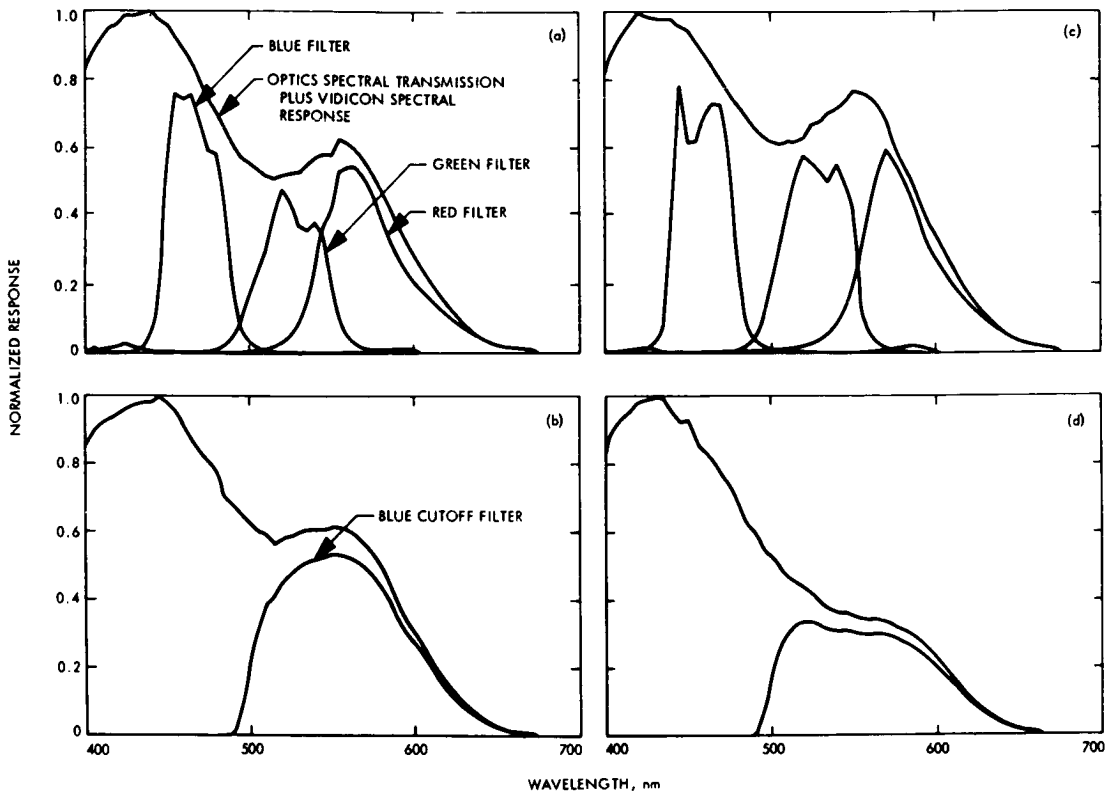

FIGURE 5-3. — Spectral sensitivity curves for television cameras, with and without filters. (a) Mariner 6 wide-angle camera. (b) Mariner 6 narrow-angle camera. (c) Mariner 7 wide-angle camera. (d) Mariner 7 narrow-angle camera.

To show the nature of the picture restoration process, some of the steps in the computer reduction are listed: restore the two highest order bits to the digital data, remove effects of AGC and "cuber" in the analog data,[2] combine digital and analog data, measure and remove electronic "pickup" noise,[2] measure pixel locations of reseau marks on flight and calibration pictures (ref. 5-6), shift pictorial calibration and flight data by interpolation so as to agree with the known reseau pattern, measure and correct for optical distortions, measure and remove effects of residual image from calibration and flight data, evaluate the sensitometric response of each pixel from calibration data and deduce the true photo-

[2] This procedure is semiautomatic, subject to hand correction by the computer operator, as necessary.

metric exposure for each flight pixel,[3] correct for the effects of shutter-speed variations and light leakage (narrow-angle camera), and evaluate and correct for the modulation transfer function of the camera subsystem. Some of these steps have been applied to a few of the flight pictures on an experimental ad hoc basis, pending receipt of complete, corrected telemetry data from the six playbacks of the recorded closeup pictures.

Mission Design and Television Data Return

The planetary encounter period for each spacecraft was divided into two parts: a far-encounter (FE) period starting 2 or 3 days before, and extending to within a few hours of, closest approach; and a near-encounter (NE) period bracketing the time of closest approach. (See ref. 5–3.)

As the Mariner 6 and 7 missions were originally conceived, the analog data for 8 FE narrow-angle pictures and 25 NE pictures, and the 1/7 digital NE picture data (and other NE science data) were to be recorded and later transmitted to Earth at 270 bps over a 5-day period for each spacecraft. However, a sixtyfold increase in bit transmission was realized during the development of the spacecraft, so that real-time transmission of the 1/7 digital data stream, or of the digitized analog data during picture playback, became possible. Thus, this capability led to the extended FE picture sequences actually used, in which the analog tape recorder was filled and played back several times. In addition, several hundred 1/7 digital pictures were transmitted directly to Earth in real time. Some of these digital pictures, taken during the very late FE period of Mariner 7, contain valuable three-color wide-angle photometric data for large areas of Mars at a resolution greatly superior to that attainable from Earth. Fifty FE pictures, 26 NE pictures, and 428 useful[4] real-time 1/7 digital pictures were returned from Mariner 6; 93 FE pictures, 33 NE pictures, and 749 useful real-time digital pictures were returned from Mariner 7. This ninefold increase in the number of FE pictures and 18 percent increase in the number of NE pictures over the original plan represents a total data return 200 times that of Mariner 4, not including the real-time digital frames.

Pictures are designated by spacecraft, camera mode, and frame number. Thus, 6N17 means Mariner 6 near-encounter frame 17, 7F77 means Mariner 7

[3] For each spacecraft, this must be done for each filter of each camera and for all calibration temperatures, and the results corrected to the observed flight temperature.

[4] Most of the real-time FE wide-angle pictures were valueless because little or none of the image projected outside the central 20 percent blank area.

far-encounter frame 77, etc. The first NE picture from each spacecraft was taken with a blue filter by the wide-angle camera. Thus, in near encounter, all odd-numbered frames are wide-angle, low-resolution pictures.

During each day of the FE period, the narrow-angle camera was used to record a series of up to 33 full-disk analog pictures of Mars with the AGC clamped. These pictures were transmitted to Earth during each daily period when the 16.2-kbps signal could be received by the 64-m (210-ft) antenna at the Goldstone, Calif., tracking station of the NASA Deep Space Network. These pictures showed all sides of the planet as it rotated each day, and within the total 5-day series, each face of Mars was recorded at many different scales and viewing conditions. The phase angle was nearly constant and was the same for both spacecraft (25°, morning terminator visible).

Approximate NE picture locations for the two spacecraft are shown in figure 5–4; relevant data are presented in tables 5–II and 5–III. The picture tracks were

Table 5-II. — Mariner 6 NE picture data at center of frame

Picture	Slant range, km	View angle from vertical, deg	Solar zenith angle, deg	Latitude, °S	Longitude, °E	Area, height×width, km²
1	Center of picture does not intercept planet					Limb
2	7401	70.2	18.8	4.3	292.3	157.2×556.4
3	6614	57.3	6.8	−2.0	303.2	Limb
4	6130	49.8	4.9	−5.2	310.3	125.6×229.1
5	5682	41.8	11.1	−8.6	317.3	Limb
6	5348	36.2	17.1	−10.6	323.0	109.1×158.7
7	5028	29.7	23.5	−12.9	329.1	1112×1597
8	4777	25.2	28.9	−14.1	334.4	97.4×125.7
9	4920	40.5	41.3	−0.1	346.0	1679×1861
10	4737	39.4	45.8	−1.2	350.7	119.1×122.1
11	4558	38.1	50.8	−2.7	355.8	1309×1378
12	4439	38.8	55.6	−3.0	0.6	113.9×108.4
13	4333	39.6	60.9	−3.7	5.8	1191×1243
14	4832	59.5	20.5	−13.0	324.8	99.8×231.4
15	4382	49.3	30.6	−15.9	334.7	Limb
16	4103	42.1	38.2	−17.3	342.3	83.7×132.8
17	3868	34.6	45.7	−18.5	349.9	858×1289
18	3738	30.3	52.1	−16.6	356.6	77.1×102.5
19	3613	24.4	58.5	−16.9	3.1	773×1036
20	3543	20.4	64.2	−16.6	8.9	73.1×88.8
21	3498	16.3	70.3	−16.2	15.1	723×929
22	3497	14.9	75.8	−15.2	20.5	72.3×84.4
23	3522	15.0	81.7	−14.2	26.4	718×921
24	3584	17.6	87.2	−12.7	31.7	74.8×87.0
25	3622	19.1	90.0	−12.1	34.4	765×973
26	3680	21.3	93.0	−11.0	37.3	77.4×91.1

Table 5-III. — Mariner 7 NE picture data at center of frame

Picture	Slant range, km	View angle from vertical, deg	Solar zenith angle, deg	Latitude, °S	Longitude, °E	Area, height×width, km²
1						Limb
2		Center of picture does not intercept planet				Limb
3	9243	69.6	25.8	14.4	350.3	Limb
4	8533	59.7	15.6	5.3	354.9	175.3×412.5
5	7993	52.3	8.2	−1.4	357.7	Limb
6	7533	46.1	2.5	−7.0	1.3	152.9×262.0
7	7129	40.6	4.7	−12.0	3.8	Limb
8	6771	35.8	10.2	−16.4	7.3	137.7×200.4
9	6443	31.4	15.1	−20.5	10.0	1503×2233
10	6654	47.5	50.5	−53.1	328.3	197.0×165.7
11	6377	45.6	52.1	−57.1	332.4	2282×1672
12	6084	42.9	53.4	−60.6	338.9	166.6×147.5
13	5864	42.4	55.9	−64.2	344.1	2049×1912
14	5631	41.1	58.2	−67.4	352.3	148.8×139.4
15	5462	41.9	61.4	−70.7	0.1	2098×2058
16	5285	42.1	64.5	−73.2	12.5	137.4×138.9
17	5167	44.2	68.3	−75.9	26.6	1368×1561
18	5049	45.8	72.1	−76.8	46.3	131.69×147.2
19	4994	49.2	76.7	−77.3	68.6	1343×1862
20	4949	52.4	81.4	−75.4	89.4	133.5×171.7
21	5314	65.7	14.0	−20.6	6.1	Limb
22	4776	55.0	24.9	−28.5	14.2	97.9×201.3
23	4405	46.8	33.3	−34.3	21.2	1383×2488
24	4130	39.9	40.7	−38.3	28.8	84.5×128.9
25	3917	33.7	47.3	−41.7	36.2	874×1291
26	3759	28.4	53.6	−43.7	44.2	77.2×101.4
27	3638	23.6	59.5	−45.3	52.0	775×1035
28	3664	28.1	65.6	−40.4	62.1	80.7×92.2
29	3619	26.6	71.1	−40.4	69.3	823×995
30	3621	27.3	76.7	−39.1	76.3	81.5×87.7
31	3646	28.4	82.1	−37.7	83.1	831×987
32	3722	31.6	87.7	−35.0	89.5	87.1×90.8
33	3822	34.9	93.4	−32.2	95.5	996×1116

chosen, in cooperation with investigators for other onboard experiments, on the basis of several considerations and constraints. First, the choice of possible arrival dates was limited by engineering considerations to the interval of July 31 to August 15, 1969. Second, on any given arrival date, the time of closest approach was limited to an interval of about 1 hr by the requirement that the spacecraft be in radio view of the Goldstone tracking station during a several-hour period bracketing the time of closest approach. These two constraints and the approximate 24-hr rotation period of Mars limited the possible Martian longitudes that could be viewed effectively; in particular, the most prominent dark area, Syrtis

Major, could not be seen under optimal conditions. Fortunately, Meridiani Sinus, a prominent dark area almost as strong and permanent as Syrtis Major, and a variety of other important features well known from Earth observations were easily accessible.

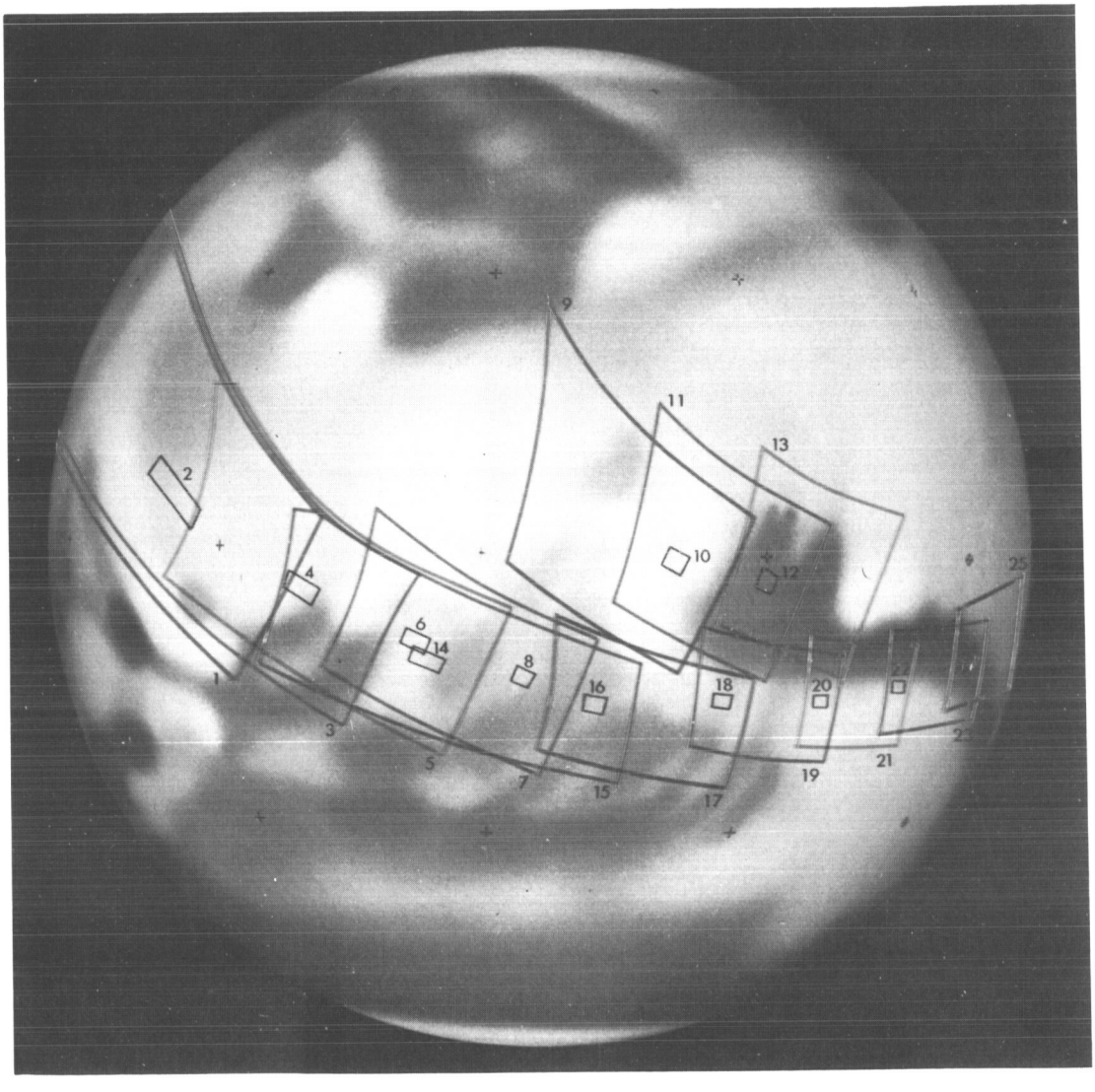

(a)

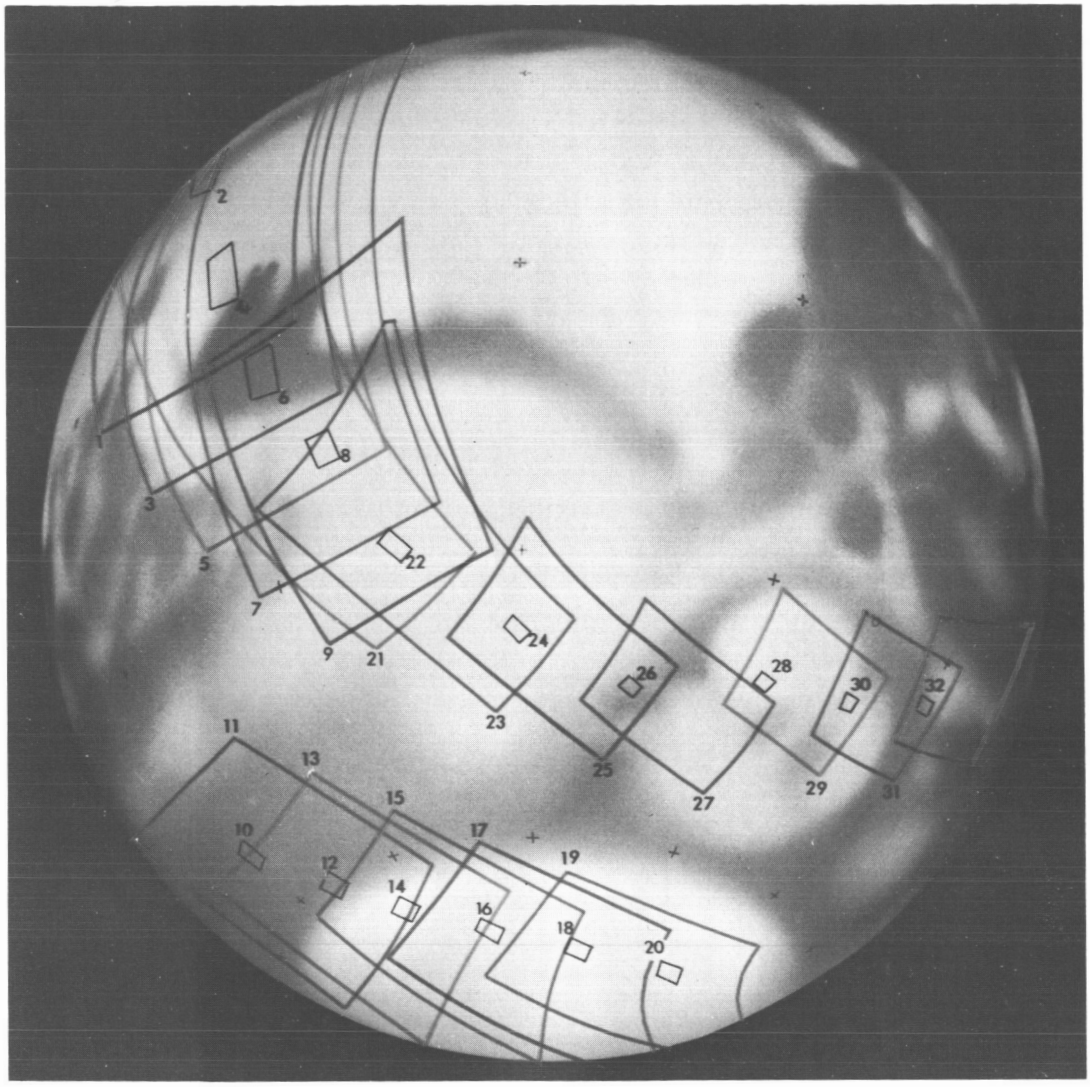

(b)

FIGURE 5–4. – Mariner NE picture tracks, plotted on a painted globe of Mars. The wide-angle camera filter sequence is blue-green-red-green, etc. The first picture is taken using the blue filter. Wide-angle and narrow-angle pictures alternate. (a) Mariner 6 picture locations. (b) Mariner 7 picture locations.

The cameras and other instruments were mounted on a two-axis scan platform, which could be programed to point the instruments in as many as five successive directions during near encounter. (See fig. 5-1.) The orbit and platform pointing strategy adopted for each spacecraft was designed to optimize the total scientific data return within a context of substantial commonality, but with some divergence of needs of the various experiments. Emphasis was placed on viewing a wide variety of classical features, including the polar cap; continuity of picture coverage; substantial two-color overlap and some three-color overlap, if possible; stereoscopic overlap; viewing the planet limb in blue light; viewing the same area under two different phase angles; and seeing the same area under different viewing conditions at almost the same phase angle.

The picture track for Mariner 6 was chosen to cover a broad longitude range at low latitudes to bring into view some well studied transitional zones between light and dark areas, two "oases" (Juventae Fons and Oxia Palus), and a variable light region (Deucalionis Regio). The Mariner 7 picture track was selected to cross that of Mariner 6 on the dark area, Meridiani Sinus, thus providing views of that important region under different lighting conditions. The track also was arranged to include the south polar cap and cap edge; to intersect the "wave-of-darkening" feature, Hellespontus; and to cross Hellas — the classical, bright, circular "desert."

Camera Operation and General Observations

Both television cameras operated well within expected ranges of the ambient parameters. The contrast of the Mariner 6 FE pictures, however, was lower than expected because of an unaccountably low signal level; the electronic pickup noise from the square-wave power system was somewhat greater than anticipated for both spacecraft; the first track of the Mariner 6 analog tape recorder showed a 50 percent drop in amplifier gain between FE and NE playbacks; and the fourth track of the Mariner 7 analog tape recorder showed greater than normal "dropout" noise. These exceptions not only affected subjective appearance of the pictures, but also necessitate more elaborate processing of the data before accurate, high-resolution photometric measurements can be made.

As observed by the Mariner 6 and 7 television cameras, the Martian surface is generally visible; with the possible exception of the polar regions and a few areas marked by the appearance of afternoon "clouds," it is not obscured by clouds or haze. The classical Martian features stand out clearly in the FE pictures; in closer views, these features are transformed into areas with recognizable rela-

tionships to the numerous craters that mark the surface. The NE pictures seem to show a moonlike surface. (It should be remembered, however, that the cameras were designed to enhance the contrast of local brightness fluctuations by a factor of 3 and that the pictures are often further contrast enhanced in printing.) Actually, although the surface is generally visible, under similar lighting conditions its contrast is much less than that of the Moon. Fewer shadows are visible near the terminator.

The determination of true surface contrast depends critically upon the amount of haze or veiling glare in the picture field. The pictures appear to be free of such effects; however, more refined photometric measurements may reveal the presence of veiling glare or a general atmospheric haze. Definite conclusions cannot be drawn until the photometric reduction of the pictures is completed, including corrections for vidicon dark current, residual images, shutter light leaks, and possible instrumental scattering.

ATMOSPHERIC FEATURES

Aerosol Scattering

The Mariner 7 northeastern limb pictures provide clear evidence for scattering layers in the atmosphere. The limb appears in frames 7N1, 2, 3, 5, and 7, and in a few real-time 1/7 digital wide-angle frames received immediately before picture 7N1. The limb appears again in frame 7N21 after the platform slue, which began the track across Hellas. Thus, the limb coverage includes pictures taken with each of the filters on the wide-angle camera and one narrow-angle picture.

Several characteristics of the scattering layer shown in figure 5–5 are evident thus far:

(1) The scattering is distinctly stratified in horizontal layers, just as is scattering from aerosol layers in the Earth's atmosphere.

(2) The intensity of the scattering varies substantially over distances of a few hundred kilometers and is more intense toward the west or toward earlier local times of day.

(3) The thickness of the scattering layer is about 10 km.

(4) The height of the layer is difficult to determine because of the difficulty of locating the true planetary limb; however, it is estimated to be between 15 and 25 km in the region covered by frames 7N1 through 7N7 and up to 40 km in frame 7N21.

(5) The layer is about 50 percent brighter in the pictures taken with a blue filter than in pictures taken with red or green filters. This is not as much difference in intensity as would be expected for Rayleigh scattering; it corresponds more closely to λ^{-2} wavelength dependence.

The relationship between this scattering layer and the Martian tropopause will be studied carefully as more refined data become available.

The normal-incidence optical depth, assuming isotropic scattering, is estimated as 0.01 in the red and about 0.03 in the blue. A λ^{-2} dependence suggests that scattering should be predominantly forward, so that these very small values should be underestimates.

Near the south polar cap and over the regions of Mare Hadriaticum and

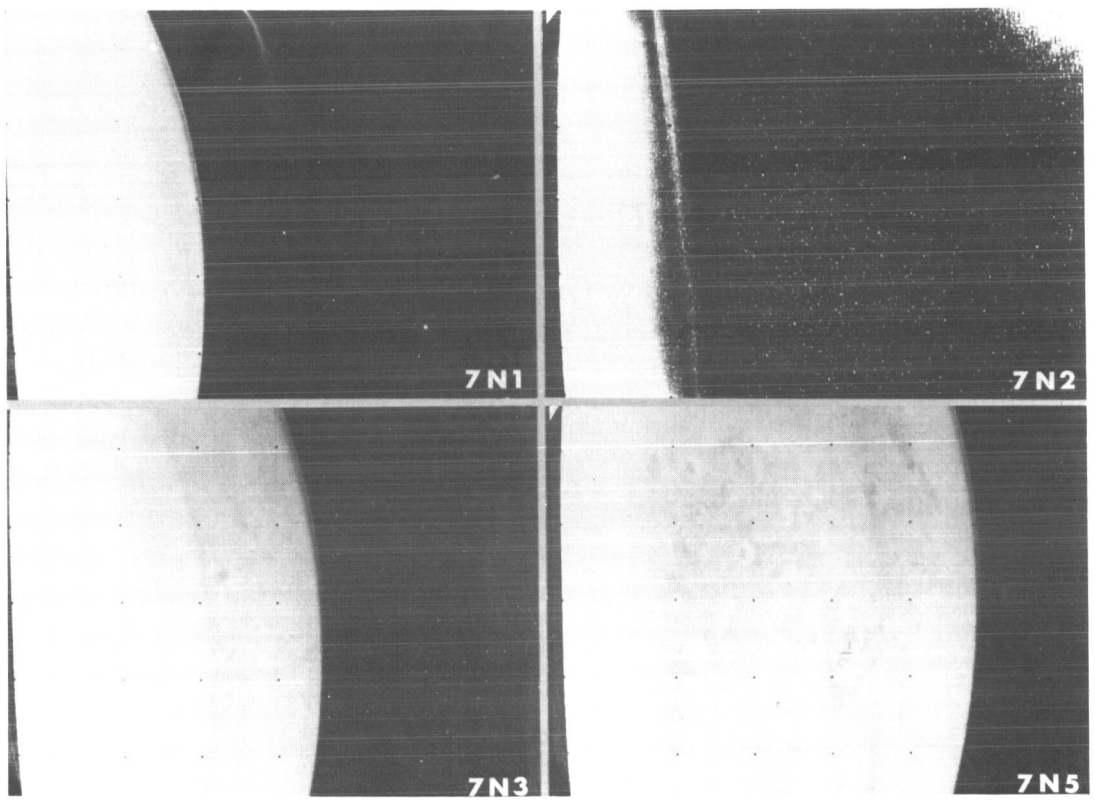

FIGURE 5–5. – Mariner 7 limb pictures. Note the sharp layer of haze next to the limb in frames 7N1, 3, and 5, and the magnified view in frame 7N2. The prominent, cratered dark feature in frame 7N5 is Meridiani Sinus. North is approximately toward the right.

Ausonia just east of Hellas, the real-time digital data reveal an apparent limb haze. The haze over these regions is not as bright as the haze discussed previously, so that it is unlikely to be dense enough to obscure surface features observed at NE viewing angles. A faint limb haze also may be present in the Mariner 6 pictures of the limb.

Blue Haze

Despite these evidences of very thin aerosol hazes, visible tangentially on the limb, there is no obscuring blue haze sufficient to account for the normally poor visibility of dark surface features observed or photographed in blue light or for their occasional better visibility (the so-called "blue clearing" phenomenon; see refs. 5–7 and 5–8).

The suitability of the pictures taken with a blue filter for blue haze observations was tested by photographing Mars through one of the blue filters on Eastman III–G plates, which have a response in this spectral region similar to that of the vidicons used in the Mariner cameras. Conventional blue photographs on unsensitized emulsions and green photographs were taken for comparison. A typical result is shown in figure 5–6; the simulated blue photograph is similar to the conventional blue photographs. The effective wavelength of the actual blue television pictures should be even shorter, owing to a lower ambient temperature and to the absence of reddening due to the Earth's atmosphere.

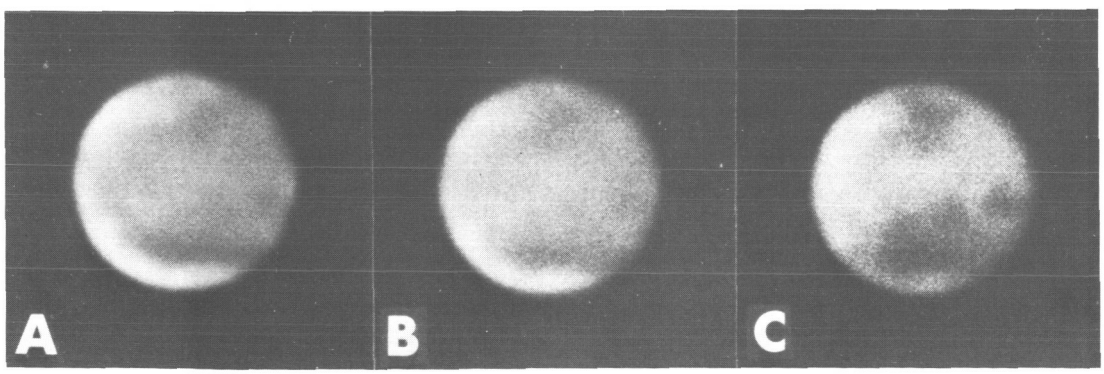

FIGURE 5–6. — Photographs of Mars from Earth, taken to compare Mariner-type pictures taken with a blue filter with "standard" green and blue photographs of Mars. These photographs were taken on May 24, 1969, at New Mexico State University Observatory. North is at the top. A. Standard blue (09:15 G.m.t.). B. Mariner blue (09:05 G.m.t.). C. Standard green (08:44 G.m.t.).

The blue pictures taken by Mariners 6 and 7 clearly show craters and other surface features, even near the limb and terminator where atmospheric obscuration is strong. Frame 7N17 (polar cap) shows sharp surface detail near the terminator. The blue frame 6N1 (limb) shows surface detail corresponding to that seen in the subsequent overlapping green frame 6N3. Figure 5–7 includes blue, green, and red pictures in the region of Meridiani Sinus. Although craters are distinct in all three colors, albedo variations, associated both with craters and with large-scale features, are more pronounced in green and red than in blue. Earth-based blue photographs obtained during the Mariner encounters show the normal obscured appearance of Mars.

Shading of South Polar Cap

Another possible indication of atmospheric haze is the remarkable darkening of the south polar cap near both limb and terminator in the FE pictures (fig. 5–8). Because, during near encounter, surface features are clearly visible everywhere over the polar cap, the darkening is obviously *not* due to clouds or thick haze. It may be related to darkening observed in Mariner 7 NE pictures near the polar-cap terminator (fig. 5–9(a)), and to the decrease in contrast with increasing viewing angle between the cap and the adjacent mare area observed in frame 7N11 (fig. 5–9(b)). The darkening may be caused by optically thin aerosol scattering over the polar cap, or possibly by unusual photometric behavior of the cap itself. In either case, it may be complicated by systematic diurnal or latitudinal effects.

North Polar Phenomena

There are marked changes between Mariners 6 and 7 in the appearance of high northern latitudes; some of these changes are revealed by a comparison between frames 6F34 and 7F73, which correspond to approximately the same central meridian and distance from Mars (fig. 5–8). Despite the generally higher contrast of Mariner 7 FE pictures, a large, bright "tongue" (point 1 in frame 7F73) and a larger bright region near the limb (point 2) appear smaller and fainter in the Mariner 7 picture. Much of the brightening near point 2 has disappeared completely between the two flybys; in fact, it was not visible on pictures taken by Mariner 7 during the previous Mars rotation, although it was clearly visible in several Mariner 6 pictures taken over the same range of distances. The bright tongue (point 1) increases in size and brightness during the Martian day, as seen clearly by comparing its appearance in frames 7F73 and 7F76 (fig. 5–8).

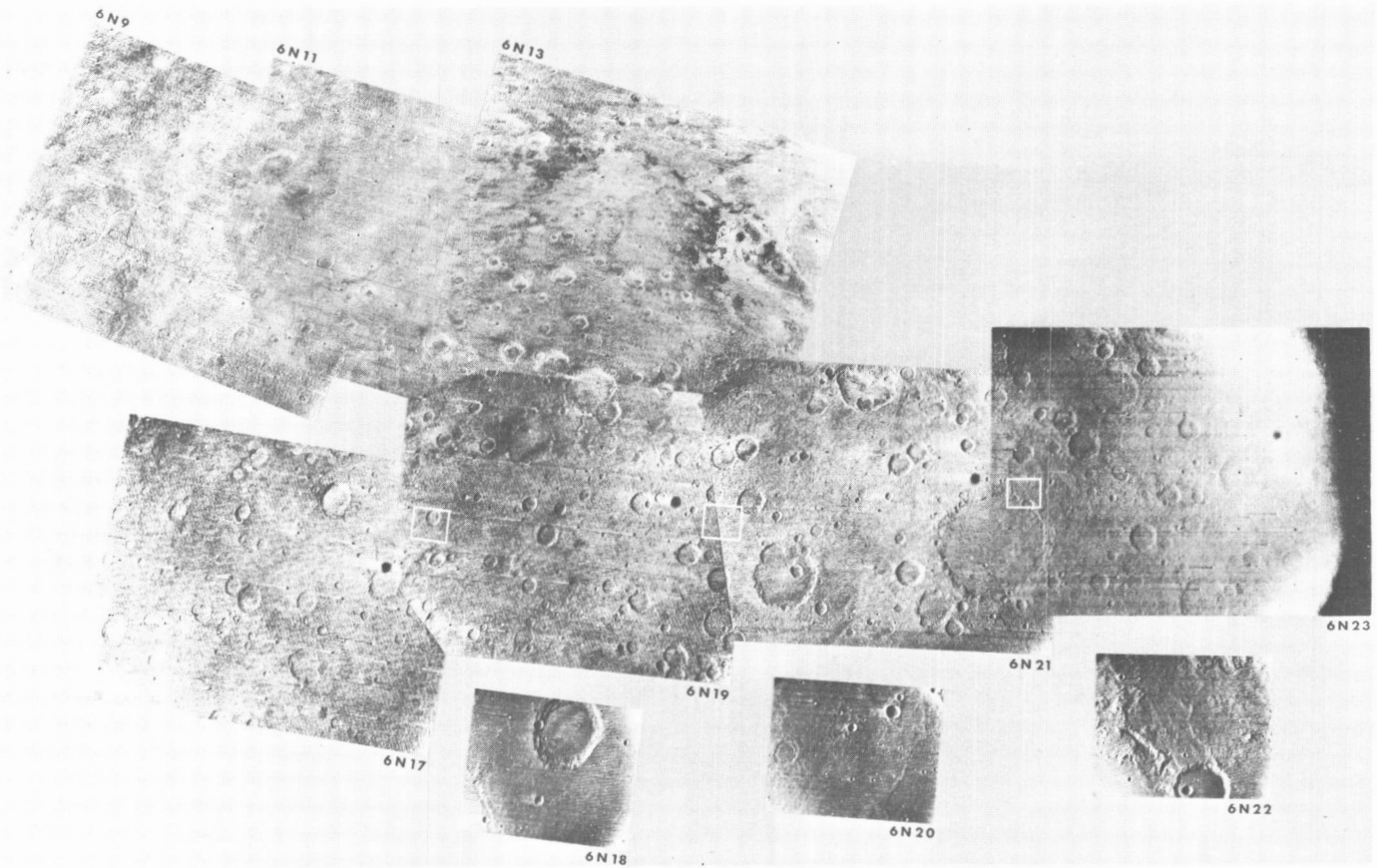

FIGURE 5–7. — Mosaic of 10 Mariner 6 pictures showing cratered terrain in the areas of Margaritifer Sinus (top left), Meridiani Sinus (top center), and Deucalionis Regio (lower strip). Large-scale contrasts are suppressed by automatic gain control, and small-scale contrast is enhanced. Craters are clearly visible in blue frames 6N9 and 6N17, but albedo variations are subdued. Locations of three narrow-angle pictures are marked by rectangles. North is approximately toward the top, and the sunset terminator lies near the right edge of frame 6N23.

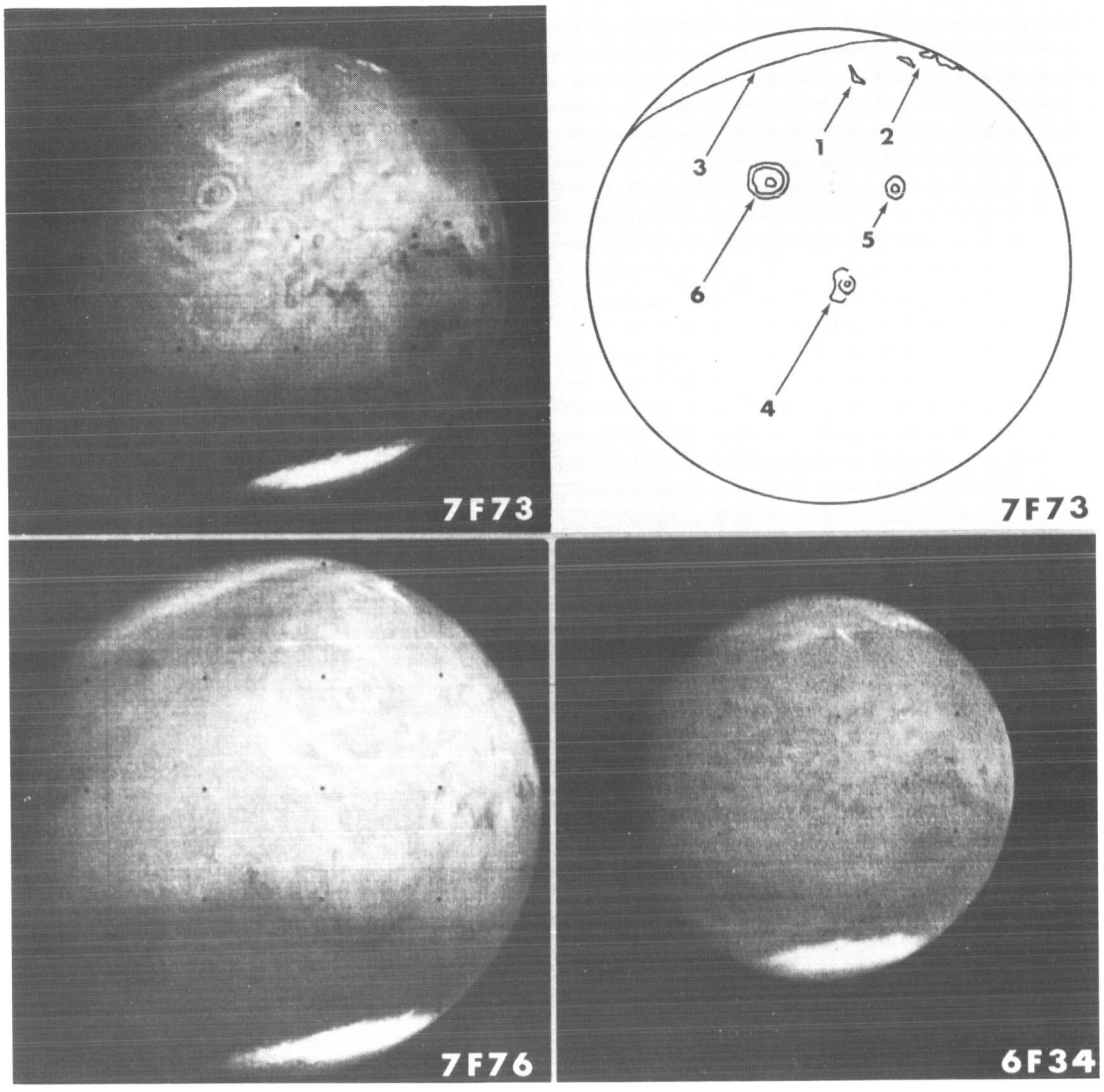

FIGURE 5–8. — FE pictures showing atmospheric and atmosphere/surface effects. Picture times were: 6F34, July 30, 07:32 G.m.t.; 7F73, August 4, 11:15 G.m.t.; and 7F76, August 4, 13:36 G.m.t.

The widespread, diffuse brightening that covers much of the region of the north polar cap (point 3) apparently corresponds to the polar hood which has been observed from the Earth at this Martian season (northern early autumn). This hood is smaller in Mariner 7 pictures than in those of Mariner 6; the region

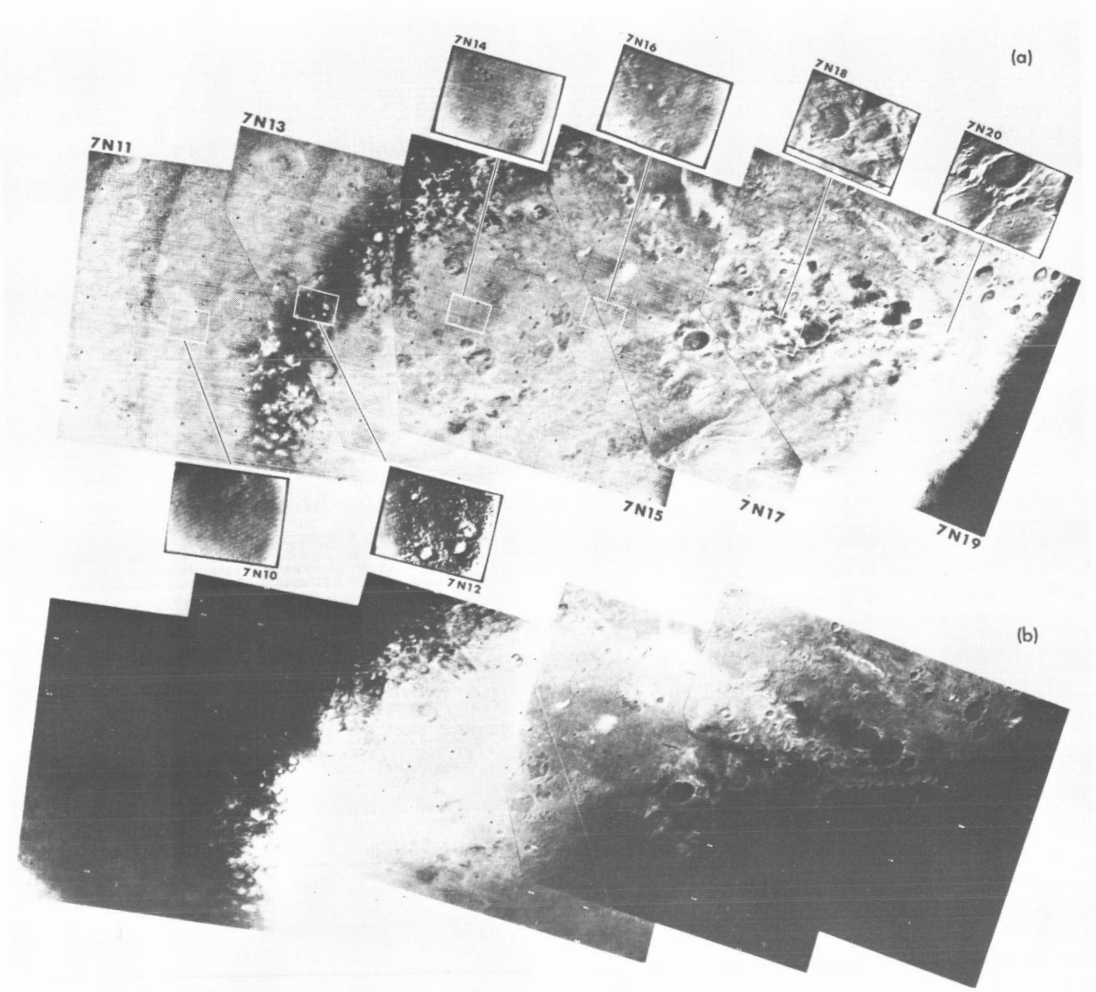

FIGURE 5–9. — Mosaic of polar cap pictures. (a) Frames 7N10 through 7N20. Effects of automatic gain control are clearly evident near the terminator (right) and at the edge of the polar cap. (b) Frames 7N11 through 7N19, taken with the wide-angle camera. The effects of automatic gain control have been corrected partially, but the contrast is enhanced. The south pole lies near the parallel streaks in the lower-right corner of frame 7N17.

between, and just north of, points 1 and 2 appears to be covered by the hood in the Mariner 6 pictures, but shows no brightening in the Mariner 7 pictures.

The different behaviors of the discrete bright regions and the hood suggest different origins for these features, although both are apparently atmospheric

phenomena or result from atmosphere and surface interactions. The discrete bright regions have fixed locations that suggest surface frost or orographically fixed clouds. The fluctuation in the areal extent of the diffuse hood suggests clouds or haze. An extensive cloud or haze composed of either CO_2 or CO_2 and H_2O ice would be consistent with the atmospheric temperature structure revealed by the S-band occultation experiment on Mariner 6. (See ch. 9 of this report.)

Diurnal Brightening

Other variable bright features that may be indicative of atmospheric processes appear throughout the Tharsis, Candor, Tractus Albus, and Nix Olympica regions. (See frame 7F73 in fig. 5–8; also see ref. 5–3.) The brightness of these areas is observed, in the Mariner pictures and in Earth-based photographs, to develop during the forenoon and increase during the Martian afternoon. The structure and locations of these features in the FE pictures do not show any variations over the 6 Martian days during which the region was observed; the features appear to be topographically fixed. Particularly striking are several long, light streaks near Nix Olympica (point 6 in 7F73) and many circular features that resemble craters with bright centers and dark edges. Several of these circular features exhibit one or more concentric circles similar to, but less striking than, those near Nix Olympica. Two features of this type form two of the westernmost points of the classical W-cloud (points 4 and 5) . No morphology associated with clouds (waves, billows, or cirriform streaks) appears in this region; at the 30-km resolution of these pictures, however, such features would be visible in terrestrial clouds.

Search for Local Clouds and Fog

All NE pictures from both spacecraft were examined carefully for evidences of clouds or fog. There are no evidences of such atmospheric phenomena away from the south polar cap. Over the polar cap and near its edge, a number of bright features, possibly atmospheric in origin, can be seen. No detectable shadows are present, and no local height differences can be detected by stereoscopic viewing of overlapping regions whose stereo angles lie between 5° and 12°. There is little or no illumination evident near and beyond the polar-cap terminator. However, frames 7N11, 12, and 13 (figs. 5–9(a) and 5–9(b)) show several diffuse, bright patches suggestive of clouds near the polar-cap edge. On the cap itself, a few local diffuse, bright patches are present in frames 7N15 (green) and 7N17 (blue). Unlike most polar-cap craters, which appear sharp and clear, a few crater rims

and other topographic forms appear diffuse (frames 7N17, 18, and 19). In frames 7N17 (blue) and 7N19 (green), remarkable curved, quasi-parallel bright streaks are visible near the south pole. Although these suggest topographic form or control, including some craterlike shapes, their possible cloudlike nature is suggested by the lack of shading. Frames 7N17 and 7N19 show faint, but definite, streaks and mottles close to the terminator, superimposed on a sparsely cratered surface.

SURFACE FEATURES

A primary objective of the television experiment was to examine, at close range, the principal types of features on the Martian surface, as observed from Earth.

While confirming a cratered appearance similar to that of the Moon for much of the Martian surface, Mariners 6 and 7 also revealed significantly different terrains with the added implication of more active, and more recent, surface processes than were evident previously. Preliminary analyses indicate that at least three distinctive terrains are represented in the pictures, as well as a mixture of permanent and transitory surface features displayed at the edge of, and within, the south polar cap. These terrains do not exhibit any simple correlation with the light and dark markings observed from Earth.

Cratered Terrains

Pictures from Mariners 4, 6, and 7 suggest that craters are prevalent in the southern hemisphere; however, knowledge of cratered terrains[5] in the northern hemisphere is less complete. Cratered areas appear in some Mariner pictures as far as 20° N latitude. Nix Olympica, which in FE pictures appears to be an unusually large crater, lies at 18° N. Many craters can be seen in close-range FE pictures. These are almost exclusively visible in the dark areas of the southern hemisphere, with only a few visible in the northern hemisphere; the difference may result from an enhancement of crater visibility by reflectivity variations in dark areas. However, poor photographic coverage, highly oblique views, and unfavorable Sun angles limit knowledge of the northern part of Mars.

Preliminary measurements of the diameter-frequency distribution of Martian craters in the region Deucalionis Regio were made on frames 6N19 through 6N22 and are shown in figure 5–10. The curves are based upon 256 craters with

[5] Defined as the areas of the Martian surface in which craters are the dominant topographic form. (See fig. 5–7.)

diameters of more than 7 km (frames 6N19 and 21) and upon 104 craters with diameters of more than 0.7 km (frames 6N20 and 22). The most significant result is the existence of two different crater distributions, a dichotomy also apparent in morphology. The two morphological crater types are large and flat-bottomed, and small and bowl-shaped. Craters with flat bottoms are most evident on frames 6N19 and 6N21. Diameters range from a few kilometers to a few hundred kilometers, with estimated diameter-to-depth ratios on the order of 100 to 1. The small bowl-shaped craters, best observed in frames 6N20 and 6N22, resemble lunar primary impact craters. Some of them appear to have interior slopes steeper than 20°.

The diameter-frequency distribution of large craters with flat bottoms is compared in figure 5–11(a) with the crater distribution in the uplands on the far side of the Moon near Tsiolkovsky. This particular lunar region was chosen for comparison because it is evidently a primordial surface, devoid of large post-upland features that may have modified the original crater distribution. The

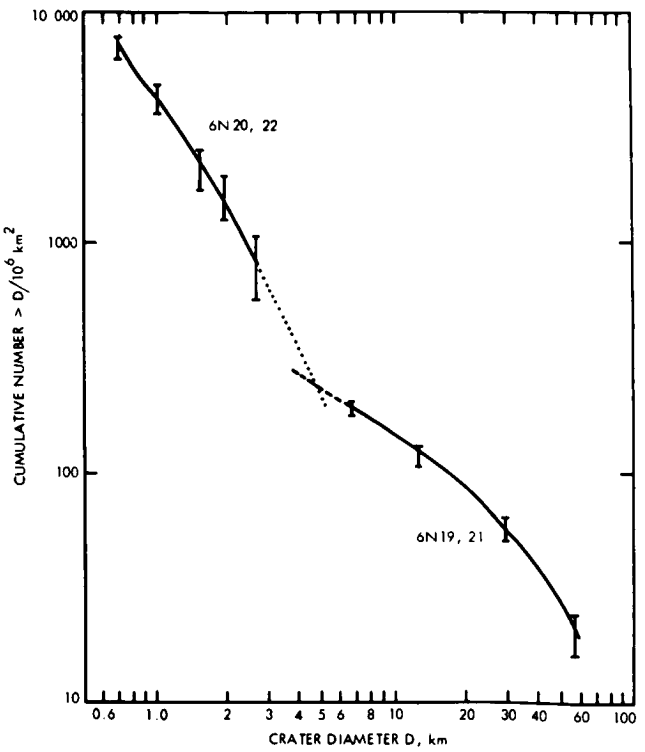

FIGURE 5–10. — Preliminary cumulative distribution of crater diameters. Solid curve at right is based on 256 counted craters in frames 6N19 and 6N21 with diameters more than 7 km. The solid curve at the left is based on 104 counted craters in frames 6N20 and 6N22 with diameters of more than 0.7 km. Error bars are from counting statistics only ($N^{1/2}$).

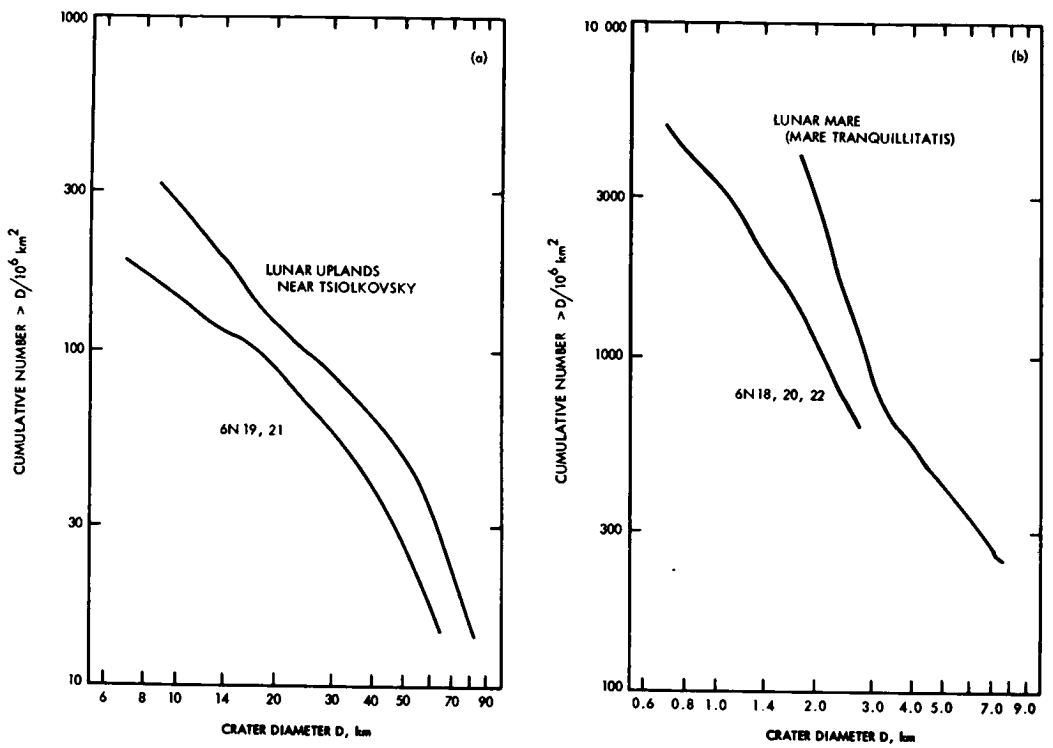

FIGURE 5–11. — Comparisons of Martian and lunar size distributions. (a) Comparison of large craters on Mars with those on the lunar uplands. (b) Comparison of small craters on Mars with those on the lunar maria.

distribution of the small bowl-shaped craters is compared in figure 5–11(b) with the distribution of craters on the lunar maria (ref. 5–9). The distribution curve of small craters larger than about 1 km in diameter on Mars has a slope of about −2, which is similar to the curve for primary craters larger than 3 km in diameter on the lunar maria.

There are large variations in crater morphology among different crater terrains. The craters of the dark area Meridiani Sinus (fig. 5–7) have more marked polygonal outlines and more central peaks than craters in some other Martian areas; the especially distinctive lighter marking in the northwest portions of the crater floors is also seen, but less clearly, in some FE pictures. Many of the primary and secondary features associated with large lunar impact craters can be found on the Martian terrain. (See, for example, frame 6N18.). Certain associated features, however, such as rays and secondary crater swarms, seem to

be absent; ejecta blankets appear much less well developed. The missing features are, generally, those most easily removed or hidden by erosion or blanketing, a pattern consistent with the observation that the craters on Mars are usually more shallow and smoother than the lunar craters.

On frame 6N20, there are low, irregular ridges similar to those observed on the lunar maria. However, no straight or sinuous rilles have been identified

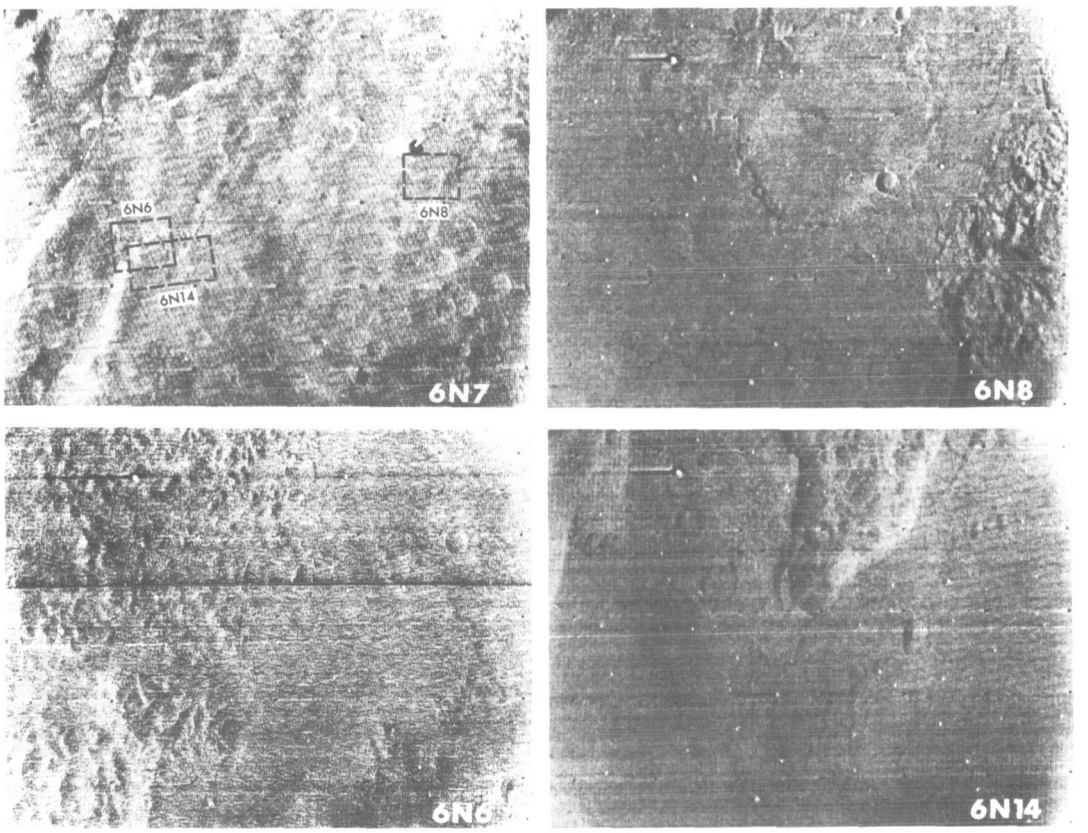

(a)

FIGURE 5-12. — (a) Examples of chaotic terrain. The approximate locations of the narrow-angle-camera views inside wide-angle-camera frame 6N7 are shown by the dashed rectangles. North is approximately at the top. (b) Possible chaotic terrain. The lighter color and the absence of craters suggest that large parts of the right-hand half of this view taken by the wide-angle camera may consist of chaotic terrain. (c) Example of chaotic terrain. The location of frame 6N14 inside frame 6N15 is shown by the solid rectangle.

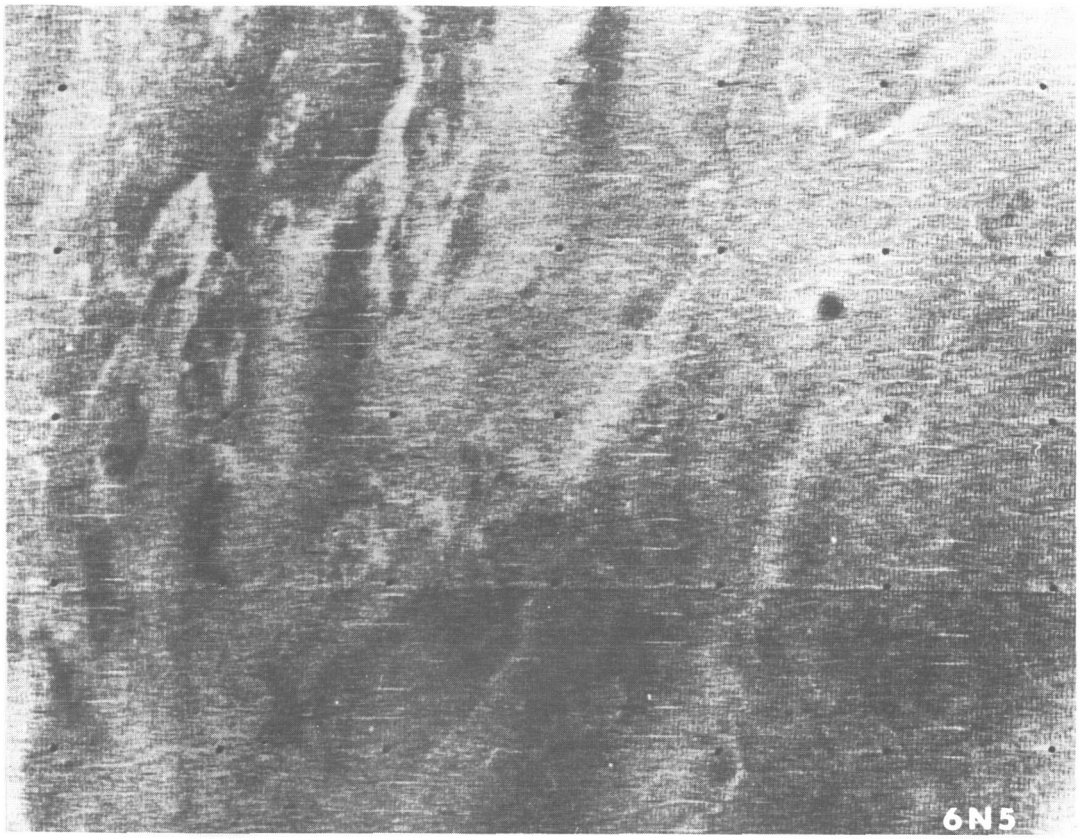

(b)

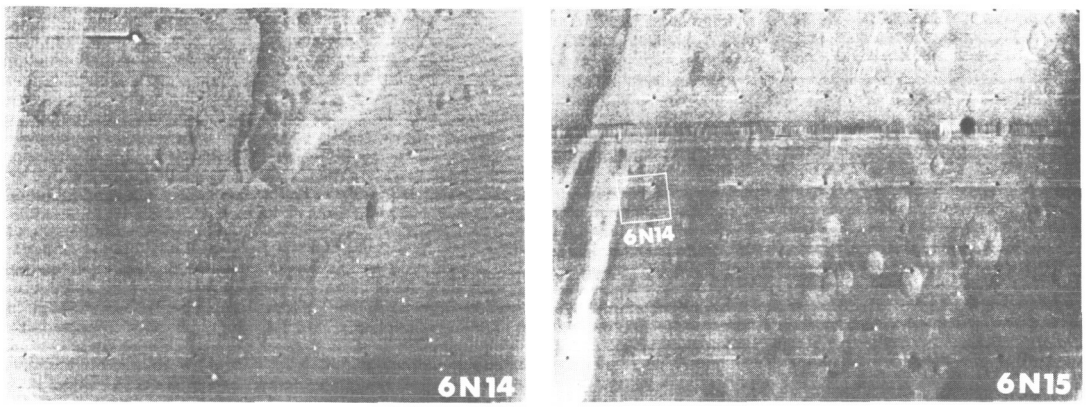

(c)

with confidence. Similarly, no earthlike tectonic forms possibly associated with mountain building, island-arc formation, or compressional deformation have been recognized.

Chaotic Terrains

Frames 6N6, 14, and 8 (fig. 5–12(a)) show a relatively smooth cratered surface giving way abruptly to apparently lower areas, irregular in shape, with chaotically jumbled ridges. This chaotic terrain characteristically seems to display higher albedo than its surroundings. On that basis, we infer that significant parts of overlapping frames 6N5, 7, and 15 may contain similar terrain, although the resolution of those frames is not great enough to reveal the general morphological characteristics. As shown in figure 5–12(a), frames 6N6, 14, and 8 lie within frame 6N7. An interpretive map of possible chaotic terrain extent for this frame has been prepared (fig. 5–13).

About 1 million sq km of chaotic terrain may lie within the 1000-km-wide and 2000-km-long strip covered by the Mariner 6 wide-angle pictures mentioned. Frames 6N9 and 10 contain faint suggestions of similar features. This belt lies at about 20° S latitude, primarily within the poorly defined, mixed light-and-dark area between the dark areas Aurorae Sinus and Margaritifer Sinus.

Chaotic terrain is composed of a highly irregular plexus of short ridges and depressions, 1 to 3 km wide and 2 to 10 km long, best displayed in frame 6N6 (fig. 5–12(a)). Although irregularly jumbled, this terrain is different in setting and pattern from crater ejecta sheets. Chaotic terrain is practically uncratered; only three faint possible craters are recognized in the 1-million-sq-km area. The patches of chaotic terrain are not all integrated, but they constitute an irregular pattern with an apparent N to N 30° E grain.

Featureless Terrains

The largest area of featureless terrain identified so far is the floor of Hellas, the bright, circular "desert," centered at about 40° S latitude. Under very low solar illumination, the area still appears devoid of craters, down to the resolution limit of about 300 m. Lunar surface areas of comparable size and smoothness are not known. It may be that all bright, circular deserts of Mars exhibit smooth featureless floors; in our present state of knowledge, however, it is not possible to define any significant geographic relationship for featureless terrains.

The Mariner 7 traverse shows that Hellespontus, the dark area that lies

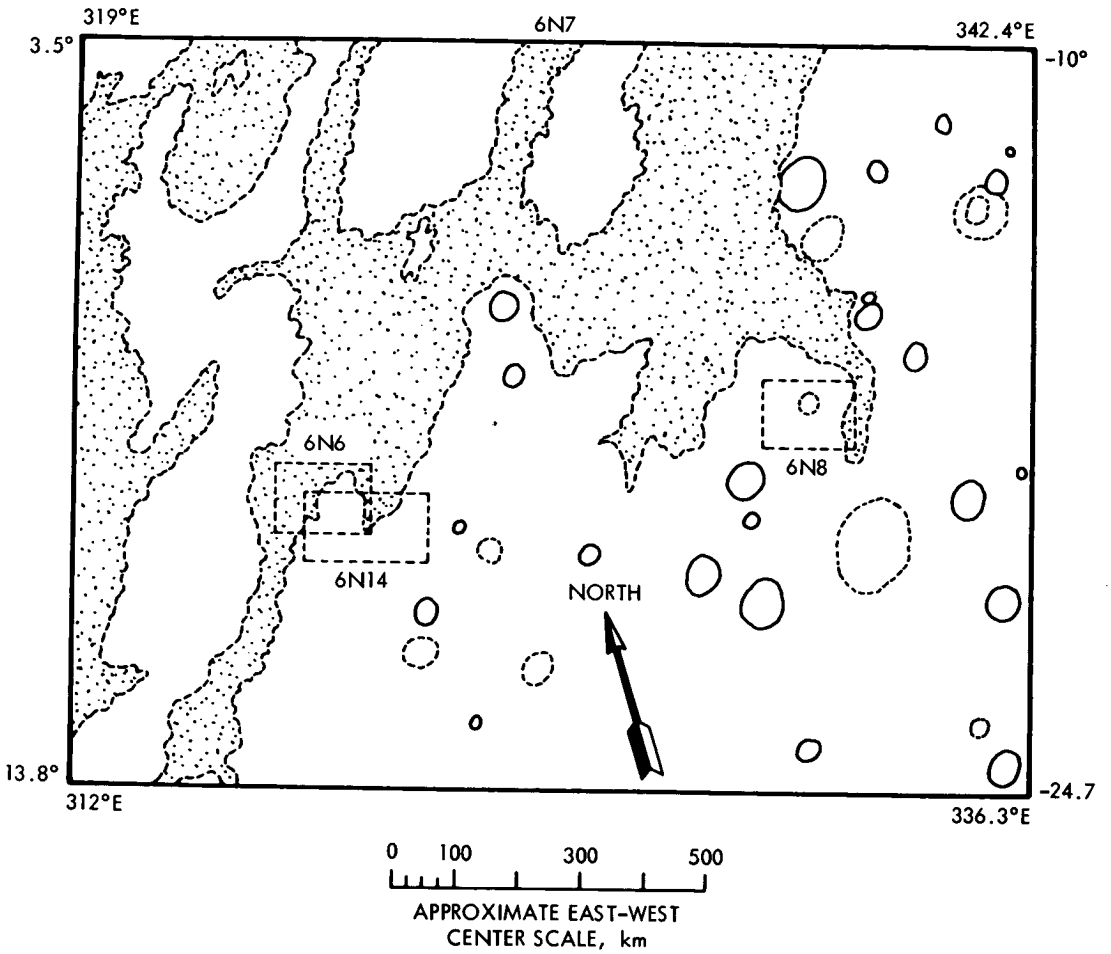

FIGURE 5–13. — Interpretive map showing the possible extent of chaotic terrain shown in frame 6N7.

west of Hellas, is heavily cratered. The 130- to 350-km-wide transitional zone also is heavily cratered and appears to slope gently downward to Hellas, interrupted by short, en echelon scarps and ridges (fig. 5–14). It gives way abruptly along an irregular foot to the flat floor of Hellas. Craters are observed within the transitional zone, but become obscured abruptly within the first 200 km toward the center of Hellas.

The possibility has been considered that a low haze or fog may be obscuring the surface of Hellas, and therefore that the featureless images are not relevant to the true surface. However, in frame 7N26, the ridges of the Hellas/Hellespon-

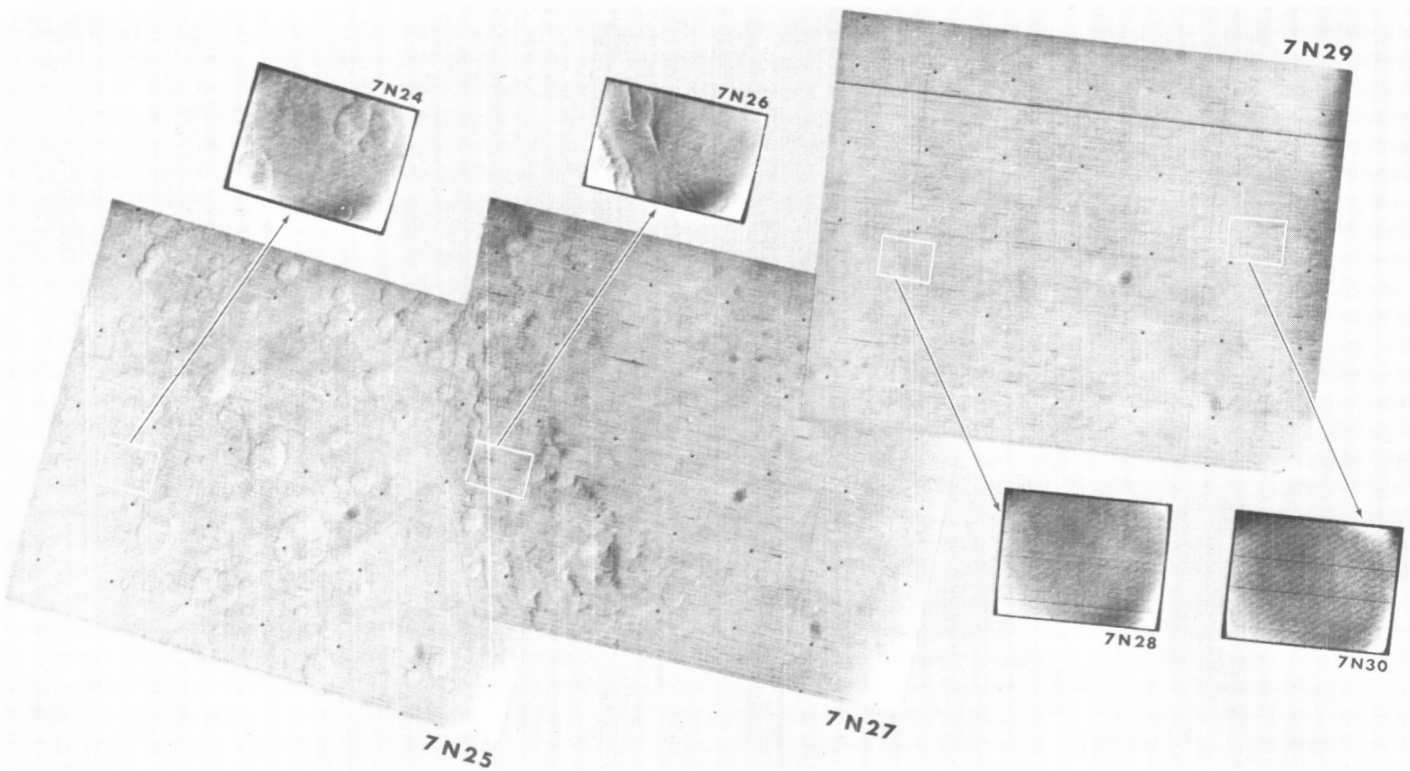

FIGURE 5–14. – Mosaic of seven pictures from Mariner 7 showing the cratered dark area, Hellespontus; the ridged, broken boundary between Hellespontus and Hellas; and the featureless terrain of the bright, circular "desert," Hellas. Large-scale contrast variations are suppressed by automatic gain control. Lighting conditions are similar to those of figure 5–7, frames 7N17 through 7N21. North is approximately at the top.

tus boundary are clearly visible, proving that the surface is seen; yet virtually no craters appear within that picture. Thus, the absence of well-defined craters appears to be a real effect.

South Polar-Cap Features

Over a 90° span of longitude, from 290° E to 20° E, the edge of the Martian south polar cap was visible at close range. The cap was observed over a latitude range from its edge at −60°, southward to and perhaps beyond the pole itself. Solar zenith angles ranged from 51° to 90° and more; the terminator is clearly visible in one picture. The phase angle for the picture centers was 35°. The superficial appearance is that of a clearly visible, moderately cratered surface covered with a varying thickness of snow. The viewing angle and the unfamiliar surface conditions make quantitative comparison with other areas of Mars difficult with respect to the number and size distributions of craters. This discussion is confined, therefore, to those qualitative aspects of the polar cap that seem distinctive to that region.

The edge of the cap was observed in the FE pictures to be very nearly at 60° S latitude, as predicted from Lowell Observatory measurements (ref. 5–10); this lends confidence to Earth-based observations concerning the past behavior of the polar caps.

The principal effect at the cap edge is a spectacular enhancement of crater visibility, with the subtle appearance of other topographic forms. In frames 7N11 to 7N13 where the local solar zenith angle was about 53°, craters are visible both on and off the cap. The population density of visible craters is several times greater in the transitional zone, about 2° of latitude in width, and may equal that observed thus far anywhere else on the planet. This enhancement of crater visibility results primarily from the tendency, noted in Mariner 4 pictures 14 and 15, for snow to lie preferentially on poleward-facing slopes.

Frame 7N12 shows the cap edge in finer detail. The tendency mentioned in the previous paragraph is so marked as to cause confusion regarding the direction of the illumination. In addition to several craters as small as 0.7 km in diameter, areas of fine mottling and sinuous lineations are visible near the larger craters. Near the center and on the west inner wall of the largest crater is an interesting grooved structure which appears similar to that in frame 6N18.

On the cap itself, the wide-angle views show many distinct reflectivity variations, for the most part related to moderately large craters, but not necessarily resulting from slope-illumination effects. Often, a crater appears to have a

darkened floor and a bright rim; in some craters with central peaks, the peaks seem unusually prominent. In frames 7N17 and 7N19, several large craters appear to have dark floors.

In contrast, high-resolution frames 7N14 through 7N20 of the polar cap suggest a more uniformly coated surface whose brightness variations are caused primarily by effects of illumination upon local relief. Several craters, some of them small in size, are visible in each picture. Unlike most other areas of Mars, regions of positive relief are also visible, especially in frames 7N14 and 7N16. Also distinctive in these frames are areas of fine, irregular, quasi-parallel bright boundaries and irregular, shallow depressed regions. Three such regions lie on the floor of a crater in frame 7N14. Other irregular, shallow depressions, apparently unrelated to craters, appear in frames 7N15 and 7N17. Some of these are tens of kilometers in diameter and have no known counterparts elsewhere in the picture series of either spacecraft.

In frame 7N19, a curved, scalloped escarpment is seen, forming a boundary between a heavily cratered area on its convex side and a relatively crater-free area on its concave side. This feature suggests the large circular structures associated with the mare basins on the Moon.

Relationship of the Terrain to Light and Dark Markings

The contrast of light and dark markings on Mars varies with wavelength, a fact long known from telescopic photography. In violet light, bright and dark areas are essentially indistinguishable because they have approximately the same reflectivity. With increasing wavelength, contrast is enhanced as redder areas become relatively brighter. Frame 6N13 (fig. 5–7) shows craters in a dark area that have partially bright rims and floors, while craters in bright areas have rim and floor reflectivities similar to the surroundings. These differences tend to increase the visibility of craters in dark areas, but only in pictures taken with red or green filters. West of Meridiani Sinus (frames 6N9 and 6N11), and in some other parts of the planet, there are dark-floored craters in bright areas; although otherwise relatively conspicuous, they are difficult to see in blue light. The floors of these craters exhibit the same general dependence of reflectivity on wavelength as do the larger dark areas.

The distinction between bright and dark areas on the Martian surface is generally more obvious in FE pictures. At higher resolution, the boundaries tend to become dispersed and indistinct. Exceptions are the sharp northeastern and

southern boundaries of Meridiani Sinus (frame 6N13) and the eastern edge of Hellespontus. The clearest structural relationship between a dark and a bright area is that of Hellespontus and Hellas (fig. 5–14).

Chaotic terrain appears to be lower and to have a somewhat higher reflectivity than adjacent cratered areas. Whether chaotic terrain is extensive enough to comprise any previously identified bright areas remains to be determined.

Some of the classical "oases" observed from Earth have now been identified with single large, dark-floored craters (such as Juventae Fons: fig. 5–5; also see ref. 5–4) or groups of such craters (Oxia Palus; frame 7N5). It has been found that at least two classical "canals" (Cantabras, Gehon) coincide with quasi-linear alinement of several dark-floored craters, also shown in frame 7N5. (See fig. 5–15.) As reported in reference 5–4, other canals are composed of irregular, dark patches. It is possible that upon closer inspection, it will be proved that most canals are associated with a variety of physiographic features and eventually will be considered less distinctive as a class.

Some early drawings and maps of Mars show a circular, bright area within the dark area south of Syrtis Major and east of Sabaeus Sinus, very nearly in the place occupied by a large crater[6] (fig. 3 of ref. 5–4). Additional comparisons of the Mariner pictures with early maps and photographs may reveal long-term aspects of topographic associations of dark-area boundaries.

A few rough comparisons can be made between the Mariner 6 and 7 pictures and estimates of Mars topographic elevations by Mariner occultations (see ch. 9 of this report), by Earth-based radar measurements,[7] or by CO_2 equivalent-width spectral measurements (ref. 5–11).

The long stretch of cratered terrain in Deucalionis Regio (fig. 5–7) is located on what Earth-based radar and CO_2 measurements both suggest is a very gradual slope rising westward. Here, at least, cratered terrain is not restricted to regionally high or to regionally low areas; like dark and light areas, it may not exhibit any particular correlation with planetary-scale relief.

The chaotic terrain viewed in Mariner 6 NE pictures appears in what seems to be the topographically lowest area surveyed by the spacecraft, if Earth-based CO_2 measurements are correct. Thus, it is possible that chaotic terrain is related in some consistent way to planetary-scale relief.

[6] E. Burgess, private communication.

[7] R. M. Goldstein, private communication; C. C. Councilman, private communication.

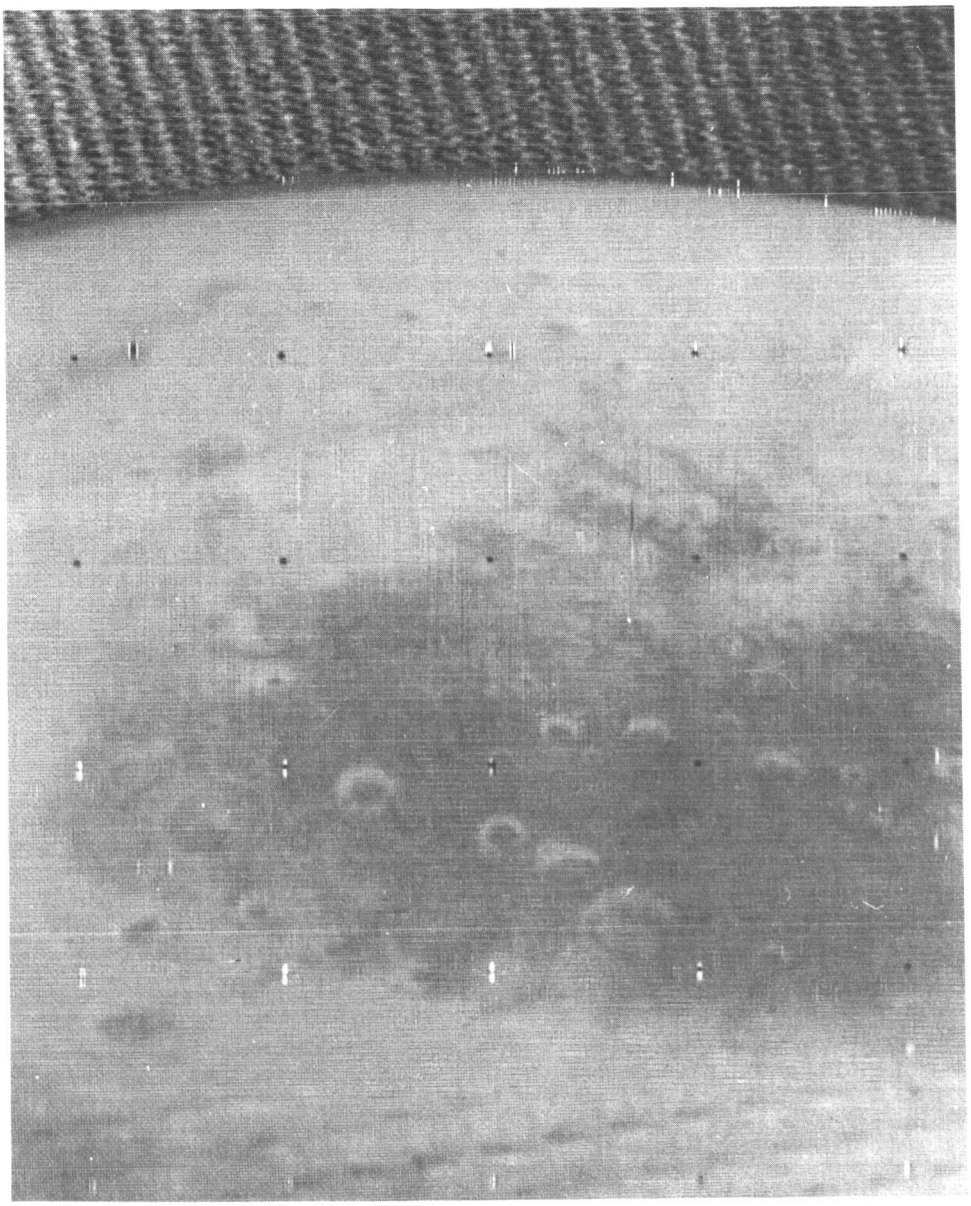

FIGURE 5–15. – Partially reconstructed frame 7N5 showing Meridiani Sinus in the foreground. The "oasis," Oxia Palus, projects into the picture from the left edge, near the limb. Note the asymmetric shading in several craters in Meridiani Sinus; the isolated, dark-floored craters in surrounding bright areas; and the crater complex in Oxia Palus. The view is approximately N 20° W. The banded appearance of the sky area is due to the picture processing.

The entry point of occultation of Mariner 7 occurred near Hellespontica Depressio, near 58° S latitude, 30° E longitude. A very low surface pressure was measured there, suggesting highly elevated terrain. If Hellespontica Depressio is elevated, Hellespontus also may be. This relationship would agree with the impression gained from the Mariner pictures that the floor of Hellas, with its featureless terrain, is a local basin rimmed by higher areas.

INFERENCES CONCERNING PROCESSES AND SURFACE HISTORY

Features observed in the Mariner 6 and 7 pictures are results of both present and past processes; therefore, they provide the basis of at least limited conjecture concerning those processes and their variations through time. In this part of this chapter, we consider the implications of (1) absence of earthlike tectonic features; (2) erosion, blanketing, and secondary modification evidenced in the three principal terrains; and (3) probable role of CO_2 solid/vapor equilibrium in formation of south polar-cap features. The possible role of equilibrium between H_2O solid and vapor also is considered as an explanation of the diurnal brightenings observed in the FE pictures and biological implications.

Significance of the Absence of Earthlike Forms

The absence of earthlike tectonic features on Mars indicates that, for the time period represented by the present large Martian topographic forms, the crust of Mars has not been subjected to the kinds of internal forces that have modified, and continue to modify, the Earth's surface.

It is inferred that, because the larger craters probably have survived from a very early time in the planet's history, the interior of Mars is, and probably always has been, much less active than that of the Earth (ref. 5–12). A view currently held (ref. 5–13) is that the Earth's dense, aqueous atmosphere may have formed early, in a singular event associated with planetary differentiation and the origin of the core. To the extent that surface tectonic features may be related in origin to the formation of a dense atmosphere, their absence on Mars independently suggests that Mars never had an atmosphere similar to that of Earth.

Age Implications of Cratered Terrains

At the present time, the ages of Martian topographic forms can be discussed only by comparison with those of the Moon. Both the Moon and Mars exhibit

heavily cratered and lightly cratered areas, which evidently reflect regional differences in the history of, or the response to, meteoroidal bombardment over the total lifespan of the surfaces. Compared with the Moon, where a significant atmosphere presumably has never existed, the presence of a thin atmosphere on Mars may have produced recognizable secondary effects in the form and size distribution of craters. To the extent that the relative fluxes of large objects impinging upon the two bodies can be determined, or a common episodic history established, a valid age comparison may be hoped for, except in the extreme case of a saturated cratered surface, where only a lower limit to an age can be found.

It is generally accepted that the present crater density on the lunar uplands cannot have been produced within the 4.5-billion-yr age of the solar system at the estimated present bombardment rate; that is, the inferred minimum age already is much older than is considered possible. Indeed, even the sparsely cratered mare areas on the Moon are found to require about a billion years to attain their present crater density. Unless this discrepancy is removed by direct measurements of the crystallization ages of returned samples of material from the lunar uplands and maria, the previously accepted implication of an early era of high bombardment followed by a long period of bombardment at a drastically reduced rate will presumably stand.

On Mars, a bombardment rate per unit area as much as 25 times that on the Moon has been estimated (ref. 5–14). However, even this would require at least several billion years to produce the density of large craters observed on Mars in the more heavily cratered areas (ref. 5–12). Thus, these areas *also could be primordial.* If these areas actually were bombarded at a constant rate for such a time, at least a few very recent, large craters should be visible, including secondary craters and other local effects. In contrast to this, the most heavily cratered areas seem relatively uniform in the degree of preservation of large craters, with no single major crater standing out from the rest as a Martian Tycho or Copernicus. This again suggests an early episodic history for cratered Martian terrain rather than a continuous one, and increases the likelihood that cratered terrain is primordial.

If areas of primordial terrain do exist on Mars, an important conclusion is that these areas have never been eroded by water. This, in turn, reduces the likelihood that a dense, earthlike atmosphere and large, open bodies of water were ever present on the planet, because these almost certainly would have produced high planetwide erosion rates. On Earth, no topographic form survives as long as 10^8 yr unless it is renewed by uplift or other tectonic activity.

Implications of Modification of Terrain

Although erosion and blanketing processes on Mars have not been strong enough to obliterate large craters within the cratered terrains, their effects are easily seen. On frames 6N19 and 6N21 (fig. 5–7), even craters as large as 20 to 50 km in diameter appear deficient by comparison with the lunar uplands (a feature originally noted by Hartmann (ref. 5–12) on the basis of the Mariner 4 data), and the scarcity of smaller craters is obvious. The small craters have a relatively fresh appearance, however, which suggests an episodic history of formation, modification, or both. Such a history is indicated particularly by the apparently bimodal crater frequency distribution of figures 5–10 and 5–11.

To account for the absence of even small craters in the areas of featureless and chaotic terrains, marked erosion, blanketing, and other surface processes must have been operating almost to the present time. These processes may not be the same as those on the cratered terrains, because large craters also have been erased. The cratered terrains obviously have *never been* affected by such processes, indicating an enduring geographic dependence of these extraordinary surface processes.

The chaotic terrain gives a general impression of collapse structures, suggesting the possibility of large-scale withdrawal of substances from the underlying layers. The possibility of kilometer-thick permafrost and its localized withdrawal may deserve further consideration. Magmatic withdrawal or other near-surface disturbance associated with regional volcanism may be another possibility; the apparent absence of extensive volcanic terrains on the surface, however, would seem to be a serious obstacle to such an interpretation. It also may be that chaotic terrain is the product of some unknown intense and localized erosion process, or of unsuspected local sensitivity to a widespread process.

CO_2 Solid/Vapor Process

The Mariner 7 NE pictures of the polar cap give no direct information concerning the material or the thickness of the polar snow deposit, since the observed brightness could be produced by a very few milligrams per square centimeter of any white powdery material. However, they do provide important indirect evidence regarding the thickness of the deposit and, along with other known factors, may help to establish its composition.

In the high-resolution pictures, the relatively normal appearance of craters on the polar cap and the existence of topographic relief unlike that so far recog-

nized elsewhere on the planet suggest that some of the apparent relief may be due to variable thicknesses of snow, perhaps drifted by wind. If so, local thicknesses of at least several meters are indicated.

The structure of the edge of the polar cap shows that evaporation of the snow is strongly influenced by local slopes; i.e., by insolation effects rather than by wind. One may estimate the daily evaporation loss from the polar cap on the assumption that the evaporation is determined entirely by the midday radiation balance, when the absorbed solar power exceeds the radiation loss at the appropriate frost-point temperature. We find the net daily loss to be about 0.8 g/cm^2 in the case of CO_2, although the loss is reduced by overnight recondensation. In the case of H_2O, the loss would be about 0.08 g/cm^2; because H_2O is a minor constituent whose deposition is limited by diffusion, the loss would be essentially irreversible.

As the complete evaporation of the cap at a given latitude requires many days, the above rates may be multiplied by a factor between 10 and 100 to obtain estimates of total cap thicknesses of tens of grams per square centimeter for CO_2 and several grams per square centimeter for H_2O, assuming that the cap is composed of one or the other of the materials. Such a thickness is acceptable for CO_2, but is unacceptable for H_2O because of the problem of transporting such quantities annually from one pole to the other at the observed vapor density (ref. 5–15).

We assume, for the remainder of this discussion, that the polar cap is composed of CO_2, with a few milligrams per square centimeter of H_2O deposited throughout the layer.

Several formations have been observed which suggest a tendency for snow to be preferentially removed from low elevations and deposited on high elevations, contrary to what may be expected under quiescent conditions (ref. 5–16). These formations include craters with dark floors and bright rims, enhanced central peaks in some craters, and irregular depressed areas (frames 7N14, 15, and 17). While such effects could result simply from wind transport of solid material, it also is possible that solid/vapor interchange plays a role.

The adiabatic lapse rate of the polar atmosphere is about 6° K/km, compared to a frost-point lapse rate of about 1° K/km. Therefore, adiabatic heating or cooling of Martian air blowing across sloping terrain may result in evaporation of low-lying solid and precipitation over high areas. The rate is determined by atmospheric density, latent heat, elevation difference, lateral scale of relief, wind

speed, turbulent-layer thickness, interfacial heat transfer, and net adiabatic gradient. As an example, a wind of 20 m/sec blowing across a crater 20 km in diameter and 0.5 km in depth, with a turbulent layer only 100 m in thickness, could differentially deposit about 0.1 g/cm^2 per day. Because this process would be effective during the entire time that snow is on the ground, several tens of grams per square centimeter could become systematically redistributed during an interval of a few hundred days. A speculative possibility is that such a process, or perhaps merely a sustained accumulation of snow in a particular topographic "trap," occasionally results in sufficient accumulation during the winter to survive summer evaporation. The increased albedo then could lead to a permanent accumulation of CO_2 snow within that topographic feature; i.e., to formation of a Martian glacier. The very prominent snow-covered central peaks of some of the small craters located at high latitude conceivably could be the sites of such permanent deposits of solid CO_2. Presumably, the permanent part of the north polar cap is such a structure (ref. 5–16).

H_2O: Processes Suggested by Brightening Phenomena

Several of the brightening and haze phenomena described previously could be related to formation of H_2O frost on the surface or to H_2O ice clouds in the atmosphere. However, the phenomena could be explained equally well in most of these instances by condensation of CO_2. This is true of the bright tongues and polar hood in the north polar region, of the cloudlike features observed over and near the south polar cap, and the limb hazes observed in tropical latitudes and over the regions of Mare Hadriaticum and Ausonia.

The brightenings in the regions of Nix Olympica, Tharsis, Candor, and Tractus Albus cannot be explained by CO_2 condensation because their complete topographic control requires that they be on or near the surfaces where temperatures are well above the CO_2 frost point. To explain these phenomena in terms of H_2O condensation processes also is difficult. Most of the region appears to brighten during the forenoon, when the surface is hotter than either the material below or the atmosphere above, so that water vapor could not diffuse toward the surface and condense on it, either from above or below. Thus, a surface ice frost is very unlikely. A few features in the area, parts of the W-cloud, for example, are observed to brighten markedly during the late afternoon, where H_2O frost could form on the surface if the air were sufficiently saturated. These features are not observed from Earth to be bright in the early morning, but a thin layer of H_2O

frost persisting through the night would evaporate almost immediately when illuminated by the early morning Sun, provided that the air were then sufficiently dry. The behavior of the W-cloud could, under these conditions, be due to frost.

The diurnal behavior of the bright regions throughout this part of Mars is consistent with convective H_2O ice clouds, but the absence of any cloudlike morphology and the clear topographic detail observed at the highest resolution available (frame 7F76) renders this explanation unlikely. Even very light winds of 5 m/sec would produce easily observable displacements on the order of 100 km during the more than one-fourth Martian day for which these regions were continuously observed by each spacecraft. Some observable distortion and streakiness due to these displacements should be seen in clouds, even if they are orographically produced, because condensation and evaporation processes are slow at Martian temperatures and pressures. No such distortions or streakiness have been observed.

Another difficulty in an explanation of these phenomena in terms of H_2O condensation lies in the relatively rapid removal of water from the local surface. Water vapor evolved from the surface during the daytime would be transported quickly upward through a deep atmospheric layer by thermal convection, and most of it would be removed from the source region. Local permafrost sources should be effectively exhausted by this mechanism within a few hundred years at most, unless replenished in some way. Because most of this region lies near the equator, where seasonal temperature variations are small, it is difficult to see how any significant seasonal replenishment from the atmosphere could occur. The possibility of replenishment from a subsurface source of liquid water is not considered in this report.

Biological Inferences

No direct evidence suggesting the presence of life on Mars has been found in the pictures. However, because Martian life, if any, probably would be microbial and undetectable at a resolution of 300 m, this is not surprising. Although inconclusive on the question of Martian life, the pictures are informative on at least three subjects of biological interest: the general nature of the Martian maria, the availability of water at present, and the availability of water in the past.

One of the most surprising results from the television experiment thus far is that nothing in the picture suggests that the dark regions, the sites of the seasonal darkening wave, are more favorable for life than other parts of the planet.

On the contrary, it now would appear that the large-scale surface processes implied by the chaotic and featureless terrains may be of greater biological interest than the classical wave of darkening. These are preliminary conclusions, however; it may be that subtle physiographic differences between dark and bright regions will become evident when photometrically corrected pictures are examined.

Regarding the availability of water, the pictures so far have not revealed any evidence of geothermal areas. These areas, which should be visible on the morning terminator, would be permanently covered with clouds and frost; no such areas have been observed. A classically described feature of the polar cap (the dark collar), which has been interpreted as wet ground, also has not been found. Other locales that have been considered sites of higher-than-average moisture content are those that show diurnal brightening. Many of these sites have been observed in the pictures; on close inspection, however, the brightening cannot be interpreted in terms of water frosts or clouds. Pending their definite identification, however, the brightenings should be considered as possible indications of water activity.

The results thus reinforce the conclusion, drawn from Mariner 4 and Earth-based observations, that scarcity of water is the most serious limiting factor for life on Mars. No terrestrial species known to us could live in the dry Martian environment. If there is a permafrost layer near the surface, or if the small amount of atmospheric water vapor condenses as frost in favorable sites, it is conceivable that, by evolutionary adaptation, life as we know it could use this water and survive on the planet. The continued search for regions of water condensation on Mars will be an important part of the missions to Mars in 1971.

The past history of water on Mars is a matter of much biological interest. According to current views, the chemical reactions that led to the origin of life on Earth were initiated in the reducing atmosphere of the primitive Earth. These reactions produced simple organic compounds which were precipitated into the ocean, where they underwent further reactions that eventually yielded living matter. The pictorial evidence raises the question of whether Mars ever had enough water to sustain an origin of life. If the proportion of water outgassed relative to CO_2 is the same for Mars as for the Earth, then, from the mass of CO_2 now in the Martian atmosphere, it can be estimated that Mars has produced sufficient water to cover the planet to a depth of a few meters. The question is whether anything approaching this quantity of water ever was present on Mars in the liquid state.

The existence of cratered terrains and the absence of earthlike tectonic forms on Mars clearly imply that the planet has not had oceans of terrestrial magnitude for a very long time, possibly never. However, we have only very rough ideas of how much ocean is required for an origin of life and how long such an ocean must last. An upper limit on the required time, based on terrestrial experience, can be derived from the $>3.2\times10^9$-yr age of the oldest fossils (refs. 5–17 and 5–18). Because these fossils are the remains of what apparently were highly evolved micro-organisms, the origin of life must have taken place at a much earlier time, probably during the first few hundred million years of the Earth's history. While one cannot exclude, on the basis of the television data, the possibility that a comparably brief, aqueous epoch occurred during the early history of the planet, the effect of the television results so far is to diminish the a priori likelihood of finding life on Mars. However, if Mars is to be a testing ground for ideas regarding the origin of life, we must avoid using these same ideas to disprove in advance the possibility of life on that planet.

DATA POTENTIALITIES

Computer restoration of the pictures, starting with data recovered from six sequential playbacks of the NE analog tapes, will be conducted over the next several months. This further processing will enhance the completeness, appearance, and quantitative usefulness of the pictures. There are reasonable grounds for thinking that much new information on physiography, meteorology, geography, and other aspects of Mars ultimately will be obtained from the pictures, although it is not yet certain whether the desired 8-bit relative photometric accuracy can be attained. Some of the planned uses of the processed data are discussed in the following paragraphs.

Stereoscopy

Most of the NE pictures taken with the wide-angle camera contain regions of two-picture overlap; some contain regions of three-picture overlap. These areas can be viewed in stereoscopic vision in the conventional manner of aerial photography. Preliminary tests using frames 7N17 and 7N19 of the south polar cap indicate that measurements of the crater depth, central-peak height, and crater-rim height are possible. No accuracy for determinations of elevation can be stated at this time.

Planetary Radii

Geometric correction of the FE pictures should make it possible to determine the radius of Mars as a function of latitude and possibly of longitude. Because of inconsistencies between the optical and dynamical oblateness, the geometric figure of Mars has been historically troublesome; the discrepancy amounts to about 18 km in the value for the difference of the equatorial and polar radii. It is possible that the polar limb darkening, as observed by Mariner, if it is a persistent phenomenon, systematically may have affected the earlier telescopic measurements of the polar diameter more than irradiation has, thus giving too large a value for the optical flattening. However, this cannot explain the large flattening obtained from surface-feature geodesy (ref. 5–19). Although a fairly reliable figure for the polar flattening may be obtained from the Mariner data, it is unlikely that the actual radii will be determined with an accuracy greater than several kilometers because of the relatively low pixel resolution in these frames and the difficulty in locating the limb.

Cartography

The large number of craters found on the Martian surface makes it feasible to establish a control network that uses topographic features as control points, instead of surface markings based on albedo differences. This network should provide the basic locations for compiling a new series of charts. The NE pictures, which cover 10 to 20 percent of the area of the planet, will constitute the basic material for detailed maps of these areas.

Satellites

It is hoped that Phobos, the larger of the Martian satellites, will be detected in two of the Mariner 6 FE pictures taken when Phobos was just beyond the limb of the planet. The satellite should have moved about 10 pixels between the two frames; it should appear as a "defect" that has moved this amount between the two pictures. If Phobos itself is not visible, its shadow (again detectable by its motion) should be. The shadow will be about 5 pixels across and will have a photometric depth of about 10 percent. If the photometric depth of the shadow can be measured accurately, the projected area (and hence the diameter) of the satellite can be determined. A similar method has been used to measure the diameter of Mercury during solar transits.

Photometric Studies

It is expected that the photometric function for each color, combining data from both spacecraft, will be derived. Observations were made near 25°, 35°, 45°, and 80° phase angles. Because data obtained from Earth can be used to establish the absolute calibration at the smaller phase angles, the 80° phase angle data also will be related to Earth-based observations, thus doubling the range over which the phase function is determined. This information should then permit the determination of crater slopes. Agreement for areas of overlap between different filters and between wide- and narrow-angle pictures can be used to check the validity of the results and possibly to measure and correct for atmospheric scattering.

The reciprocity principle may be useful in testing quantitatively for diurnal changes in the FE pictures. Such changes may include dissipation of frost or haze near the morning terminator and formation of afternoon clouds near the limb.

Overlap areas in NE pictures can be used to obtain approximate colors, even though these are observed at different phase angles in each color. Color-difference or color-ratio pictures also may be useful in identifying local areas of anomalous photometric or colorimetric behavior. Wide-angle digital pictures obtained by Mariner 7 in late far encounter will be useful for making color measurements.

Comparison of Pictures With Radar Scattering Anomalies and Height Data

The reflection coefficient of the Martian surface for radar waves of decimeter wavelength shows marked variations at a given latitude as a function of longitude. Even though few of the areas of Mars so far observed by radar are visible at close range, some correlation of topography with radar reflectivity may become apparent upon careful study. As more radar results and other height data become available, the Mariner pictures will become increasingly valuable in this connection.

SUMMARY AND CONCLUSIONS

Fundamental new insights concerning the Martian surface and atmosphere have been provided by the still relatively unprocessed television pictures from Mariners 6 and 7. Several unexpected results emphasize the importance of versatility in instrument design, flexibility in mission design, and use of an adaptive strategy in exploring planetary surfaces at high resolution.

(1) The surface is clearly visible in all wavelengths used, including the blue. No blue-absorbing haze has been found.

(2) Thin, patchy aerosol scattering layers are present in the atmosphere at heights of from 15 to 40 km, at several latitudes.

(3) Diurnal brightening in the W-cloud area is seen repeatedly and is associated with specific topographic features. No fully satisfactory explanation for the effect is known.

(4) Darkening of the polar cap in a band near the limb is seen clearly in FE pictures and is less distinctly visible in one or two NE pictures. Localized diffuse, bright patches are seen in several places on and near the polar cap; these may be small, low clouds.

(5) Widespread cratered terrain is observed, especially in dark areas of the southern hemisphere. Details of light/dark transitions are often related to local crater forms. Asymmetric markings are characteristic of craters in many dark areas; locally, these aysmmetries often appear related, as if defined by a prevailing wind direction.

(6) Two distinct populations of primary craters are present, distinguished on the basis of size, morphology, and age. An episodic surface history is indicated.

(7) In addition to the cratered terrain anticipated from Mariner 4 results, at least two new, distinctive topographic forms are seen: chaotic terrains and featureless terrains. The cratered terrain is indicative of extreme age; the two new terrains seem to require the present-day operation of especially active modifying processes in these areas. When observed at closer range, the very bright, streaked complex found in the region of Tharsis and Candor may reveal another distinctive topographic character. This area provides a fascinating prospect for further exploration because of the afternoon brightening phenomenon long known here.

(8) No tectonic and topographic forms similar to those of Earth have been recognized.

(9) Evidences of both atmosphere/surface effects and topographic effects are observed on the south polar cap. At the cap edge, where the snow is thinnest, strong control by solar heating, as affected by local slopes, is indicated. Crater visibility is greatly enhanced in this area. On the cap itself, intensity variations suggestive of variable snow thickness are seen. These may be caused by wind drifting the snow or by differential solid/vapor exchange and transport, or both. Snow thicknesses here of several grams per square centimeter or several tens of grams per square centimeter are inferred if the snow material is H_2O or CO_2, respectively. The possibility that the material is H_2O seems strongly ruled out for several reasons.

(10) Variable atmosphere and atmosphere/surface effects are seen at high northern latitudes; these effects include the polar hood and bright, diurnally variable circumpolar patches.

(11) Several classical features have been successfully identified with specific topographic forms, primarily craters or crater remnants.

(12) Although findings regarding the question of life on Mars are inconclusive, they support earlier evidence that scarcity of water, past and present, is a serious limiting factor for life on the planet. Nothing in the pictures so far suggests that the dark regions are more favorable for life than other parts of Mars.

REFERENCES

5-1. LEIGHTON, R. B.; MURRAY, B. C.; SHARP, R. P.; ALLEN, J. D.; AND SLOAN, R. K.: Mariner IV Photography of Mars: Initial Results. Science, vol. 149, 1965, pp. 627-630.

5-2. LEIGHTON, R. B.; MURRAY, B. C.; SHARP, R. P.; ALLEN, J. D.; AND SLOAN, R. K.: Mariner IV Pictures of Mars. Tech. Rept. 32-884, Part I, Jet Propulsion Laboratory, 1967.

5-3. LEIGHTON, R. B.; HOROWITZ, N. H.; MURRAY, B. C.; SHARP, R. P.; HERRIMAN, A. G.; YOUNG, A. T.; SMITH, B. A.; DAVIES, M. E.; AND LEOVY, C. B.: Mariner 6 Television Pictures: First Report. Science, vol. 165, 1969, pp. 684-690.

5-4. LEIGHTON, R. B.; HOROWITZ, N. H.; MURRAY, B. C.; SHARP, R. P.; HERRIMAN, A. G.; YOUNG, A. T.; SMITH, B. A.; DAVIES, M. E.; AND LEOVY, C. B.: Mariner 7 Television Pictures: First Report. Science, vol. 165, 1969, pp. 787-795.

5-5. MONTGOMERY, D. G., in preparation.

5-6. DANIELSON, G. E., in preparation.

5-7. SLIPHER, E. C.: An Outstanding Atmospheric Phenomenon on Mars. Publ. Astron. Soc. Pacific, vol. 49, 1937, pp. 137-140.

5-8. POLLACK, J. B.; AND SAGAN, C.: An Analysis of Martian Photometry and Polarimetry. Space Sci. Rev., vol. 9, 1969, pp. 243-299.

5-9. TRASK, N. J.: Size and Spatial Distribution of Craters Estimated From the Ranger Photographs. Progress in the Analysis of the Fine Structure and Geology of the Lunar Surface From the Ranger VIII and IX Photographs. Ranger VIII and IX. Part Two: Experimenters' Analysis and Interpretations. Tech. Rept. 32-800, Jet Propulsion Laboratory, 1966, pp. 252-267.

5-10. FISCHBACHER, G. E.; MARTIN, L. J.; AND BAUM, W. A.: Martian Polar Cap Boundaries, Jet Propulsion Laboratory contract 951547, Lowell Observatory, May 1969.
5-11. BELTON, M. J. S.; AND HUNTON, D. M.: Science, in press.
5-12. HARTMANN, W. K.: Martian Cratering. Icarus, vol. 5, 1966, pp. 565-576.
5-13. ANDERSON, D. L.; AND PHINNEY, R. A.: Early Thermal History of Terrestrial Planets. Mantles of the Earth and Terrestrial Planets, 1967, pp. 113-126.
5-14. ANDERS, E. A.; AND ARNOLD, J. R.: Age of Craters on Mars. Science, vol. 149, 1965, pp. 1494-1496.
5-15. LEIGHTON, R. B.; AND MURRAY, B. C.: Behavior of Carbon Dioxides and Other Volatiles on Mars. Science, vol. 153, 1966, pp. 136-144.
5-16. O'LEARY, B. T.; AND REA, D. G.: Mars: Influence of Topography on Formation of Temporary Bright Patches. Science, vol. 155, 1967, pp. 317-319.
5-17. ENGEL, A. E.; NAGY, B.; ENGEL, C. G.; KREMP, G.; AND DREW, C.: Alga-Like Forms in Onverwacht Series, South Africa: Oldest Recognized Lifelike Forms on Earth. Science, vol. 161, 1968, pp. 1005-1008.
5-18. SCHOPF, J. W.; AND BARGHOORN, E. S.: Alga-Like Fossils From the Early Precambrian of South Africa. Science, vol. 156, 1967, pp. 508-511.
5-19. TRUMPLER, R. J.: Observations of Mars at the Opposition of 1924. Lick Obs. Bull., vol. 13, 1927, pp. 19-45.

ACKNOWLEDGMENTS

We gratefully acknowledge the support and encouragement of the National Aeronautics and Space Administration. An undertaking as complex as that of the Mariner-Mars 1969 Program depends upon a broad base of facilities, technical staff, experience, and management; it requires not only money, but much individual and team effort to bring it to a successful conclusion. Although important roles were played by hundreds of individuals, we are especially appreciative of the support and efforts of H. M. SCHURMEIER and the entire staff of the Mariner-Mars 1969 project.

With respect to the television subsystem, responsibility for the design, assembly, testing, calibration, flight operation, and picture data processing lay with the Jet Propulsion Laboratory. We gratefully acknowledge the contributions of G. M. SMITH, D. G. MONTGOMERY, M. C. CLARY, L. A. ADAMS, F. P. LANDAUER, C. C. LABAW, T. C. RINDFLEISCH, and J. A. DUNNE in these areas. L. MALLING,

J. D. ALLEN, and R. K. SLOAN made important early contributions. We are indebted to V. C. CLARKE, C. E. KOHLHASE, R. MILES, and E. GREENBERG for their help in exploiting the flexibility of the spacecraft to maximize the pictorial data return. We are especially appreciative of the broad and creative efforts of G. E. DANIELSON as experiment representative.

The able collaborative contributions of J. C. ROBINSON, in comparing Mariner pictures with Earth-based photographs, and of L. A. SODERBLOM and J. A. CUTTS, in measuring craters, are gratefully acknowledged.

CHAPTER 6

Infrared Spectroscopy

K. C. Herr and G. C. Pimentel (*Principal Investigator*)

INSTRUMENT DESCRIPTION

The infrared spectrometer (fig. 6–1) carried on Mariners 6 and 7 represents an original application of variable-wedge interference filters and cooled infrared detectors to planetary missions. The instrument telescope has a field of view of 2°; thus, at closest approach (about 3100 km), the geographical area sampled is about 120 by 120 km. A circular variable transmission interference filter provides 0.5 to 1 percent spectral resolution. Every 12th spectrum is recorded through a polystyrene film to provide *in situ* frequency and photometry calibrations.

Spectra that cover a wavelength region of 1.9 to 14.3μ are provided by two

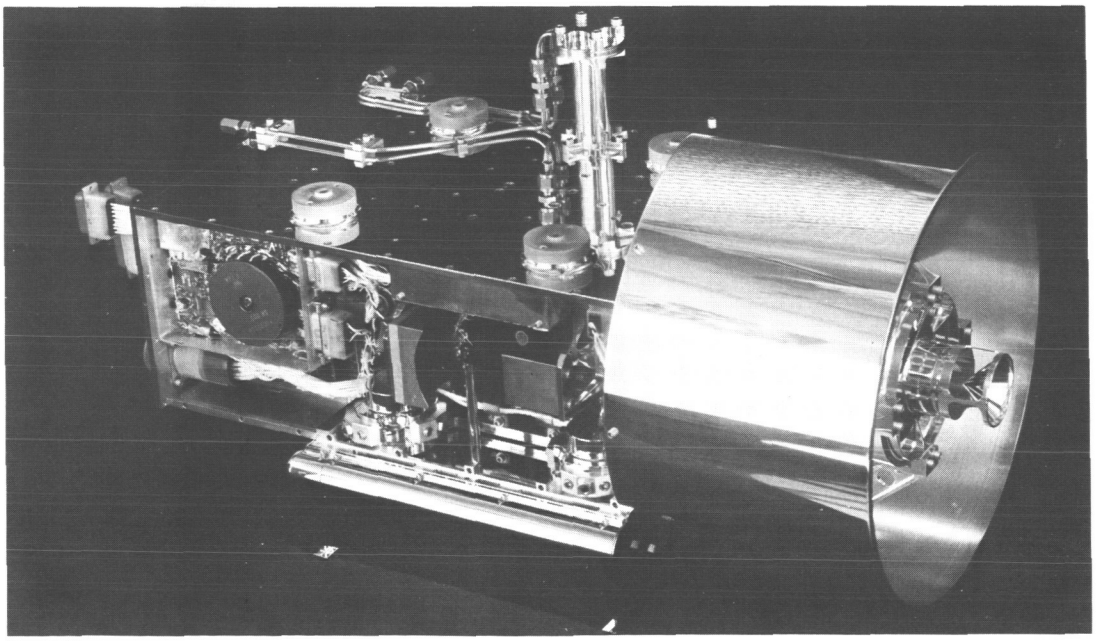

Figure 6–1. — Infrared spectrometer, designed and developed at the University of California, Berkeley, especially for Mariners 6 and 7.

channels: channel 1, which operates on emitted light from the planet and continues to obtain measurements on the dark side of the planet; and channel 2, which operates on solar reflected light. The lead selenide detector in one channel and the chopper blades and aperture of the other channel are cooled to about 165°K by radiation to space. The radiator plate and the other cooled items are supported from the rest of the instrument with low-area contact ball mounts specially designed for the instrument. Interior surfaces are goldplated where necessary to provide radiative isolation. The long-wavelength (mercury-doped germanium) detector is cooled to about 20° K using nitrogen and hydrogen gas.

The radiation is selectively reflected, absorbed, and emitted by the trace and bulk constituents of the atmosphere and surface materials. The spectral features represent signatures of various molecules.

INFRARED ABSORPTIONS NEAR 3μ, RECORDED OVER THE POLAR CAP

Results

A spectrum, typical of those recorded at latitudes near the Martian equator, is shown in figure 6–2. Most of the spectral features are provided by CO_2, the

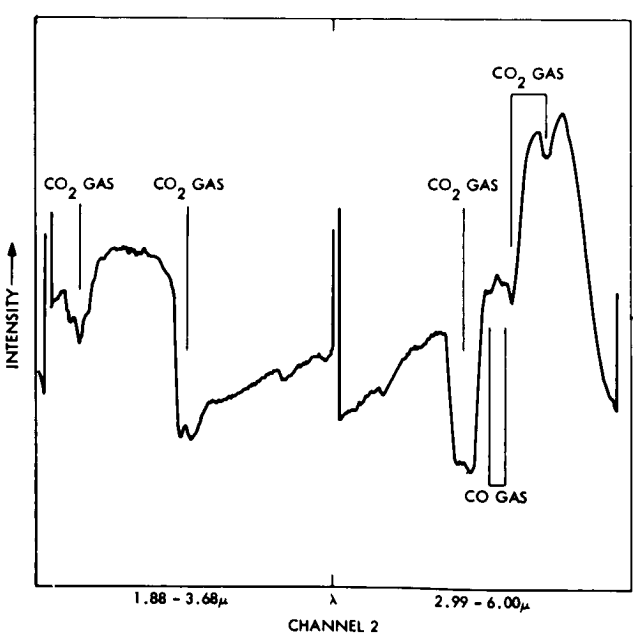

FIGURE 6–2. — Near-infrared spectrum recorded at 0° N latitude, 359° E longitude.

predominant atmospheric constituent. Also visible are two features near 2150 cm^{-1} attributable to the *P* and *R* branches of carbon monoxide and a broad absorption near 3250 cm^{-1} attributable to solid H_2O or, perhaps, to surface hydrates. Part of the 3μ region is recorded twice on either side of the radiometer spike, as shown by the instrumental background absorption at 2980 cm^{-1}. In the low-frequency recording of the 3μ overlap region, spectral resolution is slightly higher.

The infrared spectrometer on Mariner 7 first viewed the planet on August 5 at 04:48:54 G.m.t.[1] at 20° N latitude and 345° E longitude. The instrument field of view swept south to 13° S latitude and 5° E longitude. During this period, 18 spectra were recorded; none showed any evidence of atmospheric absorptions between 2900 and 3100 cm^{-1}.

At 04:51:41 G.m.t., the Mariner 7 scan platform was pointed so that the spectrometer viewed an area at 45° S latitude and 315° E longitude, 15° north of the polar-cap edge. Figure 6–3 shows a sampling of spectra recorded as the scan track passed onto the polar cap, moving toward the Martian south pole. At 62° S latitude and 330° E longitude (04:54:51 G.m.t.), two distinctive spectral changes indicated that the spectrometer field of view was looking at the polar cap. Near 2.7μ, the brightness increased by 60 percent; at 2.0μ, the triplet structure of the gaseous CO_2 absorption was lost, and the peak intensity of the feature more than doubled.

In this spectrum, two new absorptions, *X* and *Y*, are clearly recorded. (The *X* feature is recorded twice on either side of the radiometer spike.) These features are recorded in each of the subsequent 18 spectra. Their intensities seem to grow together, reaching a maximum near 68° S latitude and 341° E longitude (04:56:05 G.m.t.) and then steadily decreasing, becoming almost indiscernible at 78° S latitude, 20° E longitude (04:58:11 G.m.t.). They were detected again as the scan platform slued back to northerly latitudes at a time approximately corresponding to that at which the spectrometer view would pass over the edge of the polar cap. They were not detected in any of the 120 spectra recorded at latitudes more northerly than the polar cap edge. Plainly, the *X* and *Y* absorptions are geographically concentrated near 68° S latitude and localized over the

[1] All times are G.m.t. data receipt times, 5 min and 32 sec later than the data were recorded on Mars. All times, latitudes, and longitudes are based upon postencounter JPL Pegasus calculations made on Aug. 8, 1969. Because Mariner 7 experienced a preencounter orbit anomaly, these latitudes and longitudes are subject to change as postencounter tracking refines the actual orbit.

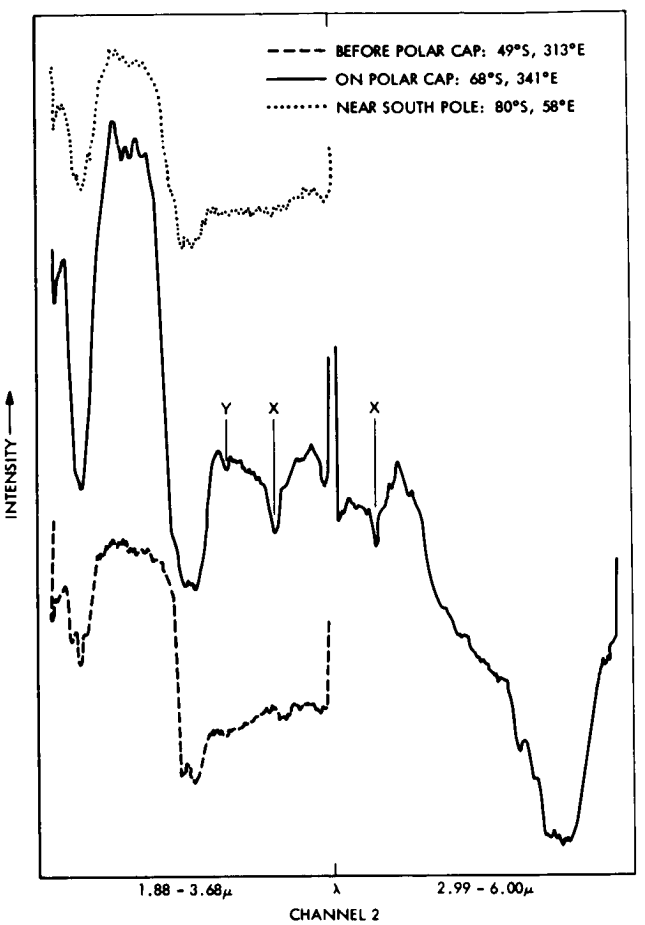

FIGURE 6–3. — Near-infrared spectrum recorded over the southern polar cap.

polar-cap edge, 61° to 80° S. The Martian polar-cap edge at the date of encounter was nearly 60° to 61° S latitude. There was no trace of either of these absorptions in any of the 150 spectra recorded for Mariner 6, which viewed an equatorial region between 13° and 16° N latitude, and between 280° and 95° E longitude.

An initial frequency measurement is provided by the polystyrene calibration spectrum. From prelaunch laboratory spectra, this particular polystyrene film has absorption features centered at 2940 and 3050 cm^{-1}. Linear interpolation gives two independent measurements of the *X* frequency, 3020 and 3027 cm^{-1}. A less accurate estimate of the *Y* frequency can be obtained by extrapolation, 3294 cm^{-1}.

The most accurate *X* and *Y* frequency determination is based upon laboratory reference spectra recorded by the Mariner 7 spectrometer before launch.

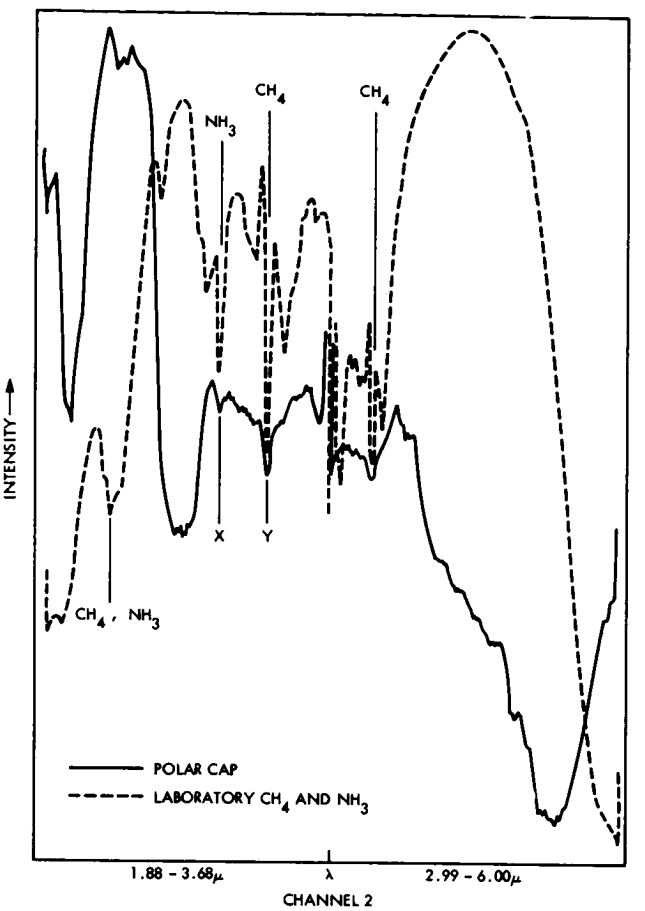

FIGURE 6–4. — Calibration with the laboratory spectrum of gaseous methane and ammonia.

Figure 6–4 shows the superposition of a laboratory spectrum of a gas sample containing about 0.2 m-atm each of methane and ammonia, pressure broadened by 1 atm of air. The Q-branch frequency of the laboratory methane ν_3 band at 3020.3 cm^{-1} matches the X frequency in both left and right spectra within the possible accuracy, which is estimated at ± 15 cm^{-1}. Similarly, the Q-branch frequency of the laboratory ammonia ν_1 band at 3336.7 cm^{-1} matches the Y frequency. The bandwidths at half height are estimated to be about 30 cm^{-1}, to be compared with an expected resolution of 24 cm^{-1}.

Discussion

The identification of these features is of particular interest because of the close frequency match to bands of methane and ammonia, molecules that may

have biological origin. These bands were not associated initially with the spectrum of solid CO_2 for many reasons.

(1) The intensities of the *X* and *Y* features neither correlate uniformly with each other, nor with the intensity of the rather intense solid CO_2 absorption near 4900 cm^{-1}. For example, the ratio of optical density at 4900 cm^{-1} to that at 3020 cm^{-1} varies by as much as a factor of 2, sometimes in successive spectra.

(2) No features had been attributed to solid CO_2 at these frequencies in the spectra reported previously (refs. 6–1 and 6–2).

(3) No features were detected at these frequencies in the laboratory spectra of solid CO_2 recorded before launch with the Mariner instruments or with conventional infrared spectrometers.

(4) These features became quite indistinct during the Mariner 7 scan period while the spectrometer was still viewing the polar cap between 79° and 80° S latitudes.

Nevertheless, we felt it necessary to prove that these features could not be due to solid CO_2, since the spectra recorded near 68° S latitude are so heavily dominated by spectral features obviously attributable to solid CO_2. Accordingly, two types of laboratory studies were performed to test this possibility.

A flight-model spectrometer identical to that of Mariners 6 and 7 was placed in an evacuated environmental chamber with wall temperatures of 77° K. The spectrometer telescope viewed at normal incidence a stainless-steel plate that filled the field of view. The steel plate, which has an emissivity of 0.3 at 3μ, was cooled to 77° K. Gaseous carbon dioxide (Matheson) was condensed upon this plate at a rate of 0.7-mm thickness/hr. The spectrum of the solid was then periodically recorded in the 2 to 4μ region under illumination by a concentric ring of tungsten filaments heated to about 2800° K. At the center of the sample, the angle between the optical path and the direction of illumination could be selected to be 73°, 55°, or 33°. Figure 6–5 shows a typical reflection-absorption spectrum recorded with a sample thickness near 2 to 3 mm. Absorption features that correspond to the *X* and *Y* features are clearly visible in the thickest samples. A mass spectrometric analysis of the carbon dioxide used showed less than 10 ppm CH_4 or NH_3 impurity.

Transmission spectra of thick solid CO_2 samples were recorded using a conventional cold cell (ref. 6–3) and a Beckman IR–7 spectrophotometer. Gaseous CO_2 (Matheson) was deposited at a rate of 0.005 mole/hr onto a cesium iodide salt window held at 77° K. (The temperature was measured with a Au-Co vs

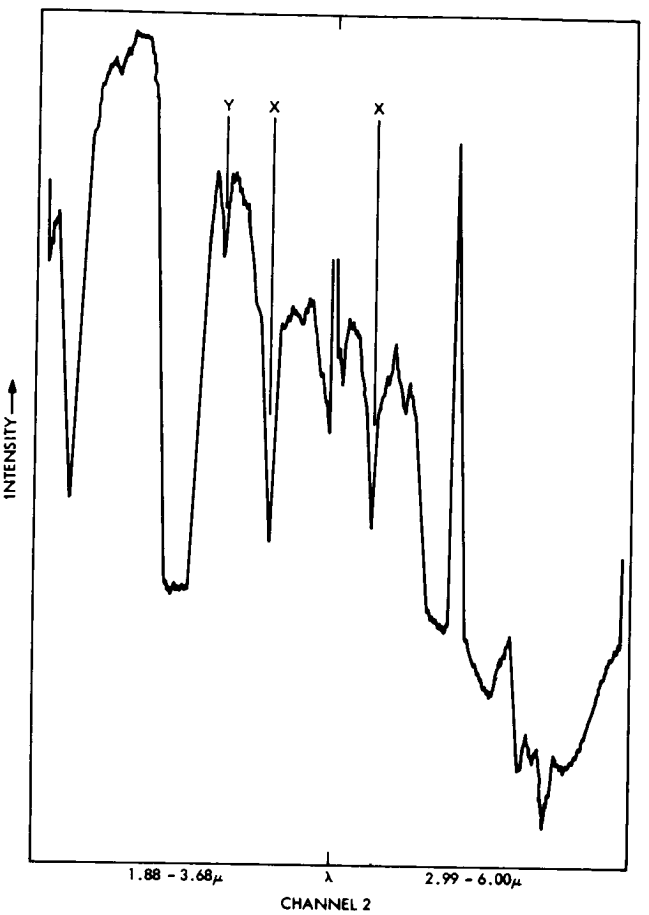

FIGURE 6–5. — Near-infrared reflection-absorption laboratory spectrum of solid CO_2 (77° K).

Cu thermocouple embedded in the window.) The transmission spectrum was recorded with a solid sample, 1.5 mm thick. A distinct absorption at 3013 cm^{-1} was observed; absorption near 3350 cm^{-1} was discernible, though not distinct. This same sample displayed no absorption at 1305 cm^{-1} that could be attributed to methane suspended in solid CO_2. In a separate laboratory study, conducted with Y. M. Huang, CH_4 was trapped in solid CO_2 at 20° K. When the sample was warmed to 77° K, the spectrum of CH_4 became more diffuse and somewhat weaker; plainly, however, most of the methane remained. After the solid was warmed to 100° K, and recooled to 77° K, the methane was approximately halved. The study shows that methane can be trapped in solid CO_2 even at temperatures as high as 100° K, and that, near 3020 cm^{-1}, the spectrum of methane suspended in solid CO_2 is not readily distinguishable from the Mars absorption.

At first consideration, it seems surprising that these absorptions have not been reported earlier. Herzberg (ref. 6–4), for example, does not list them among the 43 transitions observed in the infrared and Raman spectra of gaseous CO_2. Nevertheless, there are possible transitions corresponding to these frequencies. The transitions (0, 0, 0) $\longrightarrow$ (0, 1, 1) and (0, 0, 0) $\longrightarrow$ (1, 3, 0) are calculated to be near 3016 and 3320 cm^{-1}, respectively. The first transition is harmonic oscillator-forbidden (as a binary combination) and it is also selection rule-forbidden ($g \not\longleftrightarrow g$). The second transition is harmonic oscillator-forbidden (as a quaternary combination). Among the 43 transitions listed by Herzberg, there are none that involve odd changes of both quantum numbers v_2 and v_3 as required for the 3016-cm^{-1} transition.

Solid CO_2 has crystal symmetry T_h, and the CO_2 molecules occupy sites of symmetry C_{3i} with four molecules per unit cell (ref. 6–1). The combination of v_2 (symmetry Π_u) and v_3 (symmetry Σ_u^+) gives a state of symmetry Π_g that does not lead to an infrared-active component either in the site group or the factor group analysis. These facts are sufficient to explain the *absence* of the band — we must explain its appearance.

Perhaps there is an analog in the spectrum of solid oxygen (ref. 6–5). Despite a completely forbidden selection rule for this homonuclear diatomic molecule, the fundamental transition at 1549 cm^{-1} can be observed in very thick samples comparable to those used here. In the case of oxygen, the intensity of the forbidden band is sensitively dependent upon deposition conditions; it becomes about four times more intense if the deposition is carried out at 4° K. All evidence indicates that the feature appears because of lattice imperfections, a thesis strongly supported by enhancement of the band through inert-gas impurities deliberately added (ref. 6–6). The evidence suggests that the 3013-cm^{-1} band observed in the laboratory spectra is due to the forbidden (0, 0, 0) $\longrightarrow$ (0, 1, 1) transition of solid CO_2, appearing because of lattice imperfections (surface sites, impurity sites, vacancies, stacking faults, or grain boundaries). We believe that the same explanation is probably applicable to the Martian spectral feature at 3020 cm^{-1}. The appearance and frequency of the feature are also consistent with the spectrum of gaseous methane, but the more mundane explanation seems more likely. Although the band near 3300 cm^{-1} was difficult to obtain in transmission spectra, its presence in the reflection-absorption spectra suggests that it, too, should be attributed to solid CO_2.

No methane absorption was observed at 1305 cm^{-1} in the Martian spectra, but this does not constitute sufficient evidence to eliminate the methane inter-

pretation. Spectra recorded in this spectral region depend upon the temperature difference between the planetary surface, which furnishes the spectral source, and the gaseous absorber. This provides a thermal attenuation factor, which approaches zero as these temperatures approach each other. Thus, a gas near the ground could not be observed at all. Furthermore, the 1305-cm^{-1} feature is weaker than the 3020-cm^{-1} band (under our resolution), and the path length is less than half as great (because the solar light at 3020 cm^{-1} passes through the atmosphere twice).

There remains the need to explain the lack of intensity correlation between the 3020-, 3300-, and 4900-cm^{-1} bands, if all are to be attributed to solid CO_2. Furthermore, the disappearance of these features at the more southerly latitudes must be rationalized if the polar cap near the pole is attributed to solid CO_2. Several possibilities are under investigation. The polar-cap edge could be shrouded by a solid CO_2 cloud (or fog), which, as the spectra suggest, clears at the more southerly latitudes and more easterly longitudes. This would explain both discrepancies, as cloud height, thickness, and coverage could vary during the 10-sec period needed to obtain a spectral record. Such a cloud should, however, be detectable through poorer definition in the television picture near the polar-cap edge, an observation that has not been reported. If the solid CO_2 observed is on the ground, then its spectrum at the polar-cap edge must differ significantly from that nearer the pole. Whether it could differ because of thickness of the layer, particle size, the inclusion of impurities (such as water), or through different growth conditions, is now under study. It could be significant that the southern polar cap may recede only to latitudes near 80° S.

Conclusion

It is clear that continuing studies, directed at laboratory reproductions of the Martian polar-cap spectra, will help to resolve the proper assignment of the two 3μ features. For this preliminary report, the interpretation that they are due to solid CO_2 must be preferred, despite questions that remain for further consideration.

EVIDENCE FOR SOLID CARBON DIOXIDE IN THE UPPER ATMOSPHERE

In both missions, the infrared spectrometer recorded spectra in the 4μ region as the field of view passed through the atmosphere on the bright limb of the planet. There were three opportunities; in each, a reflection spike was recorded

at 2360 ± 15 cm^{-1}, the center of the ν_3 carbon dioxide absorption band. No such reflection was observed in either of two dark-limb crossings. The three bright-limb observations are shown in figure 6–6. Figure 6–7 again shows the second Mariner 6 limb crossing and adds the spectrum recorded 20 sec earlier (off the limb) and that recorded 10 sec later (over the planet). Figure 6–8 shows a laboratory reflection-absorption spectrum of 15μ of annealed solid CO_2 (Matheson) condensed at 77° K on a stainless-steel plate that filled the field of view of a flight-model spectrometer identical to the Mariner instruments. With thicknesses exceeding a few microns, a reflection spike is observed which is due to the index

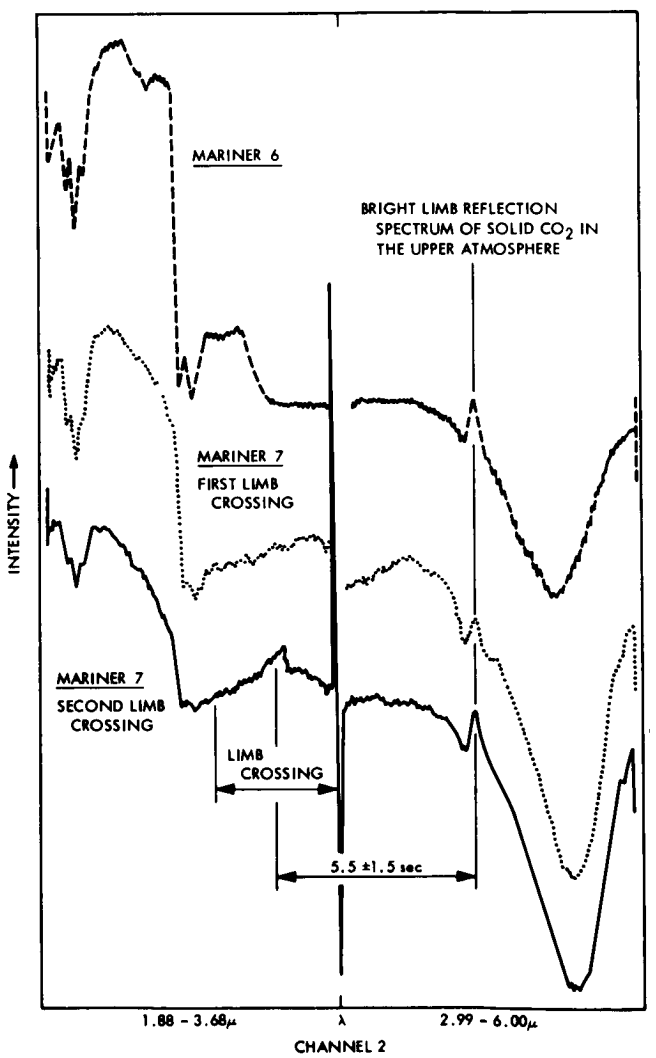

FIGURE 6–6. — Near-infrared spectra recorded through the Martian atmosphere on the bright limb.

of refraction variation through the 4.3μ absorption band of CO_2. Analogous transmission spikes are observed in transmission spectra of molecular solids. They have been observed, for example, for solid carbon monoxide (refs. 6–7 and 6–8).

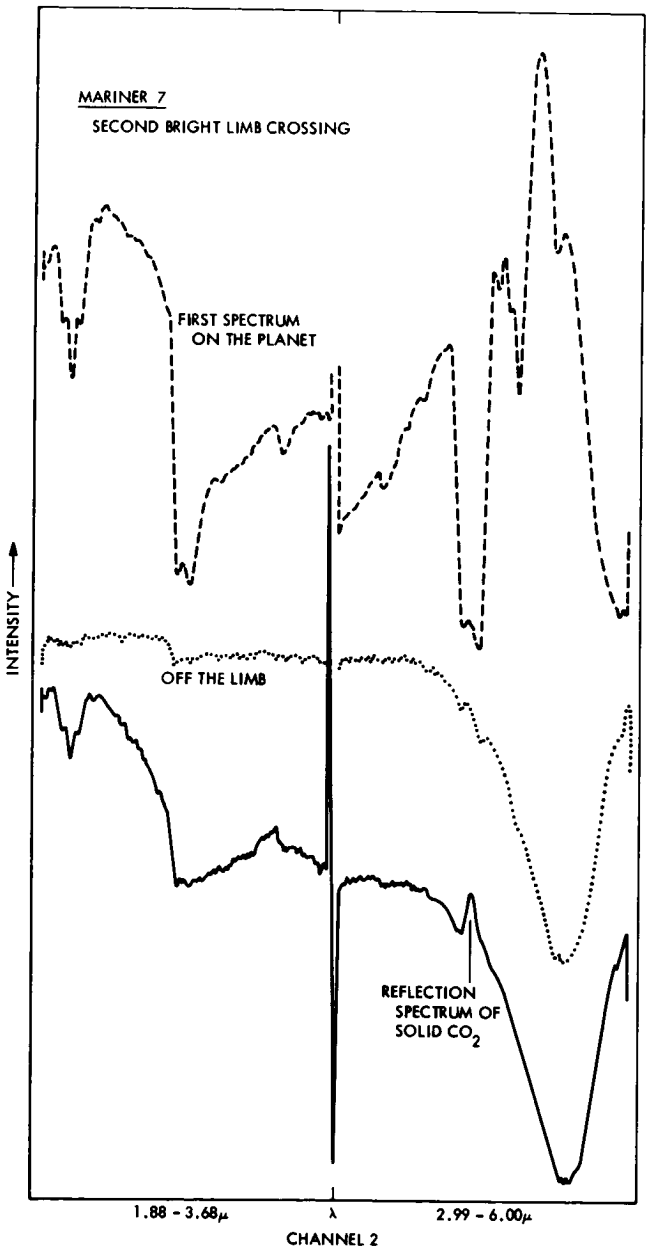

FIGURE 6–7. – Near-infrared spectra recorded just before and after the bright-limb crossing.

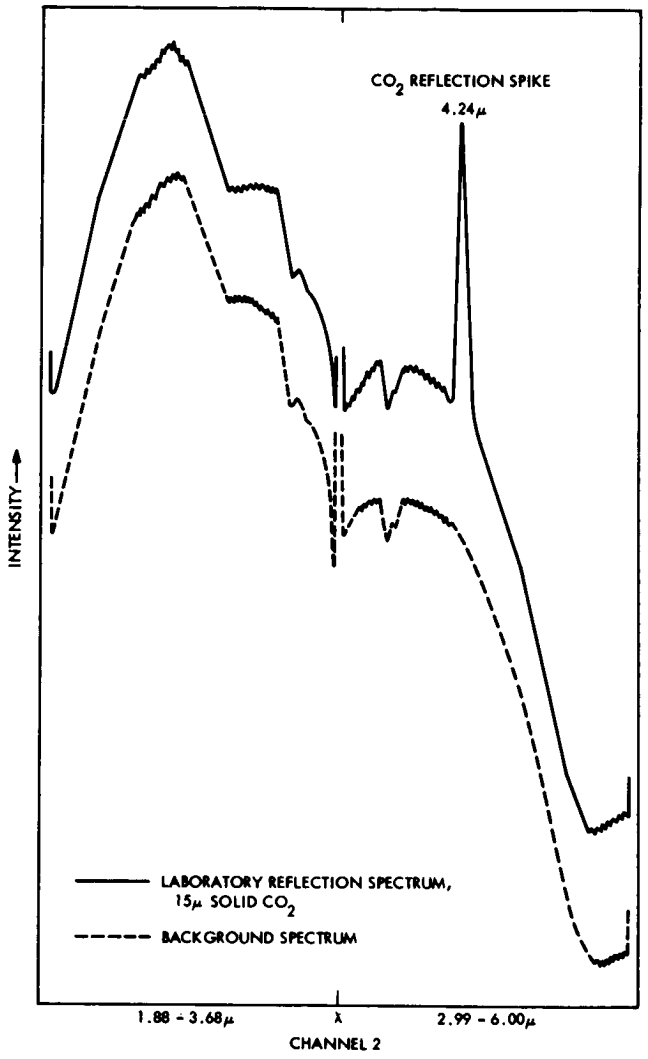

FIGURE 6–8. – Laboratory infrared reflection-absorption spectrum of solid carbon dioxide.

It is clear that the reflection spikes displayed in figure 6–6 are highly characteristic and attributable to solid CO_2. They are not due to solid CO_2 on the planetary surface viewed with stray light from outside the spectrometer's principal field of view. Local surface temperatures at these latitudes exceed 250° K, much too high to permit condensation on the surface. Reflection at 2360 cm^{-1} from the surface would not be observed because the atmosphere is opaque at this frequency. The reflection must be associated with solid CO_2 at such high altitudes that the atmosphere is no longer optically thick.

Table 6–I. — Conditions under which reflection at 2360 cm^{-1} was observed

Parameter	Mariner 6	Mariner 7	Mariner 7
Date, 1969	July 31	August 5	August 5
G.m.t.	05:19:07	04:43:23	04:54:55
Latitude, deg	2.5° S	22° N	3° S
Longitude, deg	300° E	343° E	355° E
Local time	Noon	Late morning	Noon
Surface temperature, °K	—	~250	~275
Slant range, km	8180	9830	6500
Aperture width, km	11	17	11

Trajectory calculations[2] provide geometrical parameters that help to interpret these observations. Table 6–I lists the slant range to the point above which the center of the field of view passes closest to the planet, the latitude and longitude of this point, and the aperture width at this slant range. For the second limb crossing of Mariner 7, it is possible to deduce the time between the reflection spike observation and the limb crossing, 5.5±1.5 sec. This corresponds to an altitude of the optical path at closest approach of 25±7 km.

If it is assumed that this reflection originates over the closest approach point of the field of view, the condensation of CO_2 gives an indication of the temperature at this altitude. The value of T_h so derived, based upon an assumed scale height of 8 km, is 130° K.

There are other infrared absorptions that also may be connected with solid CO_2 in the atmosphere — solid CO_2 absorptions at 3μ observed over the polar-cap edge (see pp. 84–91) and dark-limb absorptions near 12μ. The possible relationships among these observations are under study.

FURTHER INTERPRETATIONS

Literature reports now in preparation will include the following results:

(1) Topography along the track of the field of view.

(2) Temperature along the track, including that near the edge of the polar cap.

Further laboratory work is in progress to permit final interpretation of the following observations:

(3) Solid silica or silicate material was detected on the bright limb, apparently suspended in the atmosphere. Its identity and significance relative to surface composition will be considered.

[2] These trajectory calculations are based upon postencounter JPL Pegasus calculations made for Mariner 6, and for Mariner 7 on Aug. 8, 1969. Because Mariner 7 experienced a preencounter orbit anomaly, altitudes were inferred from the spectra themselves. All times are G.m.t. at the moment of observation at Mars.

(4) Curves of growth will permit determination of the absolute amount of CO_2, CO, and H_2O in the atmosphere.

(5) Curves of growth will establish new upper limits for the several possible polyatomic atmospheric constituents not observed.

REFERENCES

6-1. OSBERG, W. E.; AND HORNING, D. F.: The Vibrational Spectra of Molecules and Complex Ions in Crystals. VI. Carbon Dioxide. J. Chem. Phys., vol. 20, 1952, pp. 1345-1347.

6-2. DOW, D. A.: Torsional Vibrations in CO_2 and N_2O Crystals. Spectrochim. Acta, vol. 13, 1959, pp. 308-310.

6-3. BECKER, E. D.; AND PIMENTEL, G. C.: Stereoscopic Studies of Reactive Molecules by the Matrix Isolation Method. J. Chem. Phys., vol. 25, 1956, pp. 224-228.

6-4. HERZBERG, G.: Infrared and Raman Spectra Polyatomic Molecules. D. Van Nostrand Co., Inc., 1945.

6-5. CAIRNS, B. R.; AND PIMENTEL, G. C.: Infrared Spectra of Solid α- and β-Oxygen. J. Chem. Phys., vol. 43, 1965, pp. 3432-3438.

6-6. CAIRNS, B. R.: Infrared Spectroscopic Studies of Solid Oxygen. Ph. D. Thesis, Univ. of California, Berkeley, 1964.

6-7. EWING, G. E.; AND PIMENTEL, G. C.: The Infrared Spectrum of Solid Carbon Monoxide. J. Chem. Phys., vol. 35, 1961, pp. 925-930.

6-8. EWING, G. E.: Spectroscopic Studies of Substances at Low Temperatures. Ph. D. Thesis, Univ. of California, Berkeley, 1960.

ACKNOWLEDGMENTS

We acknowledge the generous support by NASA for the development of the infrared spectrometers used on Mariners 6 and 7. We acknowledge also the endurance of the JPL project staff and their courage as they activated our instrument when it was considered to be the cause of the spacecraft's flight anomalies and a threat to the Mariner 7 mission. We thank the Chemistry Department Machine Shop and the Space Sciences Laboratory Electronic Shop at Berkeley for their enormous contributions to the fabrication of this instrument. We especially express our indebtedness to the Berkeley group, led by P. B. FORNEY, J. L. HUGHES, D. A. WATSON, R. H. WEITZMANN, and M. A. CARLSON, for their dedicated efforts throughout the project.

CHAPTER 7

Ultraviolet Spectroscopy

C. A. BARTH *(Principal Investigator)*, W. G. FASTIE, C. W. HORD, J. B. PEARCE, K. K. KELLY, A. I. STEWART, G. E. THOMAS, G. P. ANDERSON, AND O. F. RAPER

The ultraviolet spectrometer on Mariners 6 and 7 was designed to measure emissions from the sunlit atmosphere above the limb of Mars. The spectra, obtained at and above the 130-km level in the Martian atmosphere, are comparable in quality to the best spectra obtained by using sounding rocket techniques in this altitude region of the Earth's atmosphere. The success in obtaining spectra of in situ quality from probing distances of about 7500 km was the result of three essential factors:

(1) The instrument design, which utilized a telescope to give a field of view of 0.23° by 2.3° to provide altitude resolution of about one scale height in the upper atmosphere of Mars. In addition to the telescope design, effective off-axis light rejection was achieved by an extensive baffling arrangement. This was necessary to discriminate against the bright disk of Mars, which was 10^5 times as bright as the emissions being measured in the upper atmosphere.

(2) The sophisticated pointing capability of the instrument platform on the spacecraft. This pointing capability was used to choose pointing directions that would cause the projected ultraviolet spectrometer field of view to be alined tangentially to the limb of Mars as the spacecraft motion swept this field of view down through the layers of the Martian atmosphere.

(3) The concurrence of the other Investigator Teams in choosing a platform pointing strategy that allowed this region of the upper atmosphere to be probed twice on each spacecraft.

In this chapter of this preliminary report, the ultraviolet spectrometers are described; the experiment rationale for the spectrometer and the techniques for data analysis are explained. The preliminary results are primarily spectroscopic in nature, representing the identification of ultraviolet emissions occurring in the upper atmosphere of Mars. The more detailed analyses using the techniques described here are in process; the results of these analyses depend not only on the knowledge of the measurement geometries and the photometric properties of the

instrument, but also on the proper assignment of the solar excitation mechanism and the associated cross sections of the molecules. The results of this final analysis will provide the altitude distributions of the observed constituents above 130 km and upper limits on the amounts of constituents that could have been present but were not detected.

INSTRUMENT DESCRIPTION

The instrument used is an Ebert scanning spectrometer with an occulting slit telescope and a baffling system for the elimination of stray light. The optical layout and physical configuration of the instrument are shown in figure 7–1. The short-wavelength detector (1100 to 2150 Å), referred to as the *G*-channel, is a photomultiplier tube with a cesium iodide photocathode and a lithium fluoride window. The long-wavelength detector (1900 to 4300 Å), referred to as the *N*-channel, is a photomultiplier tube with a bialkali photocathode and a sapphire window. The electronics are linear for both channels. The dynamic range necessary to make low-intensity airglow measurements as well as high-intensity bright disk observations on the *N*-channel is achieved by having planet-sensor-induced gain changes. The gain change is accomplished by varying the high voltage applied to the *N*-tube.

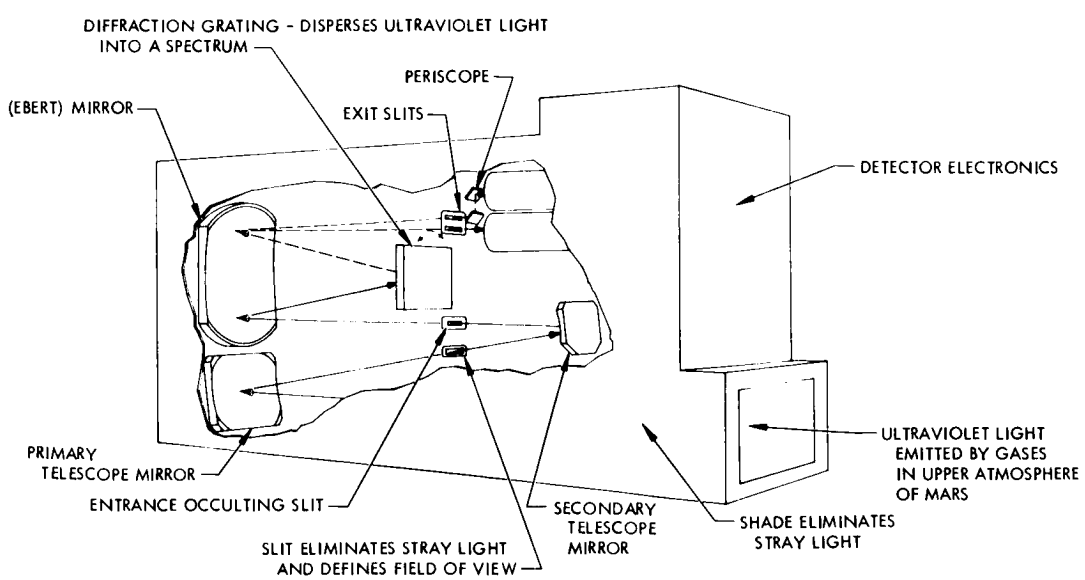

FIGURE 7–1. – Optical layout and physical configuration of the ultraviolet spectrometer used on Mariners 6 and 7.

The Mariner ultraviolet spectrometer scanned its range with a 3-sec period, and gives a spectrum with 20-Å resolution. In addition to taking complete ultraviolet spectra, the design of the electronics subsystem provides sampling at 1216 Å (Lyman-alpha) to utilize a lower data-rate mode. This capability allows Lyman-alpha data to be taken for the time period before the near-encounter mode. Light enters the instrument through a long, baffled light shade and strikes a 250-mm primary telescope mirror. The light is focused through a pre-slit onto a secondary mirror, which focuses it, in turn, on the entrance slit of the spectrometer. The light shade baffling and the pre-slit are used to minimize the amount of off-axis light reaching the spectrometer while the instrument is viewing the limb of the planet. After the light enters the spectrometer, the first half of the Ebert mirror collimates it onto the diffraction grafting. The diffracted light that leaves the grating is focused onto the exit slits by the second half of the Ebert mirror. The short-wavelength light goes through the inner exit slit and directly strikes the short-wavelength photomultiplier tube. After the long-wavelength light goes through the outer exit slit, it is reflected by two mirrors onto the second photomultiplier tube. The mirrors and grating are coated with magnesium fluoride for higher reflectivity in the ultraviolet. The grating is scanned back and forth by a cam system driven by a motor in a sealed bellows. The electronics unit contains high-voltage supplies and low-current amplifiers for the photomultiplier tubes and a power supply for the grating drive system.

EXPERIMENT RATIONALE AND ANALYSIS TECHNIQUE

The ultraviolet spectrometer on Mariners 6 and 7 obtained spectra in the range of 1100 to 4300 Å. The spectral features in this wavelength interval help, in a quantitative way, to characterize the Martian atmosphere. Solar illumination causes the atmosphere to light up or glow in the ultraviolet. Similar measurements in the Earth's upper atmosphere show that the emission spectral features are quite specific and provide unique identification of most atmospheric species. The instrument's projected field of view swept down through the Martian atmosphere toward the bright limb, giving spectra characteristic of the various altitudes from about 25 000 km down. A typical spectrum of the Martian limb is shown in figure 7-2. The variation with altitude of the intensity of a given emission feature gives the altitude distribution of the species causing the emission.

Knowledge of the cross section and solar flux for the particular emission allows absolute number densities to be determined. After the field of view of the

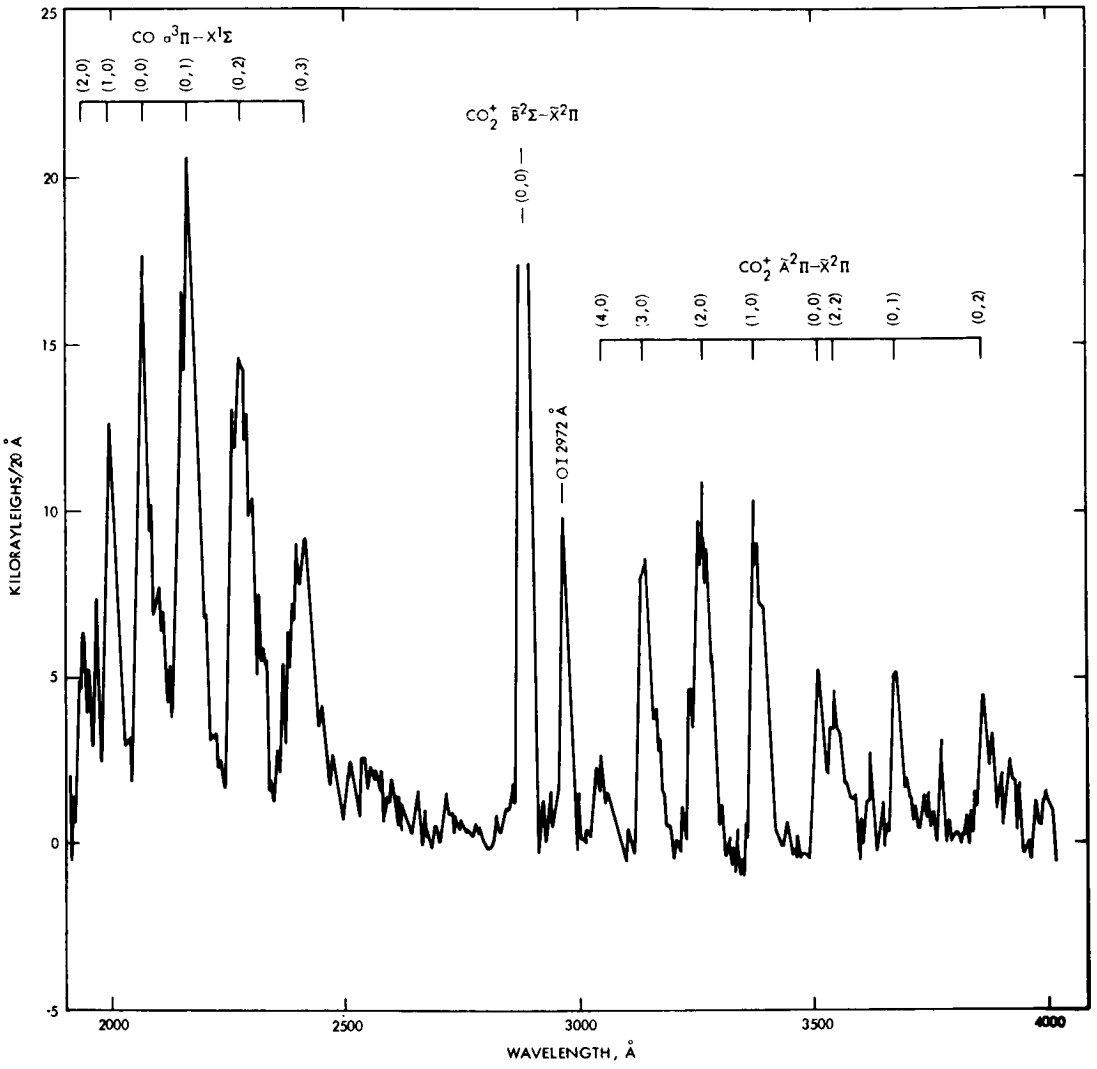

FIGURE 7–2. – Typical spectrum of the Martian limb.

instrument had crossed onto the bright disk of Mars, ultraviolet spectra were obtained at a reduced gain level until the terminator was approached. The gain was increased again to make sensitive measurements on the dark side of the terminator until the projected field of view was about 1000 km above the dark limb of the planet. A typical spectrum of the Martian disk is shown in

figure 7-3. The ultraviolet spectrometer probes an atmosphere down to the altitude where unit optical depth is reached at the particular wavelength that gives rise to the excitation.

The basic analysis technique for understanding the constitution and physics of the upper atmosphere involves the bright limb or flyby geometry, where the atmospheric layer is viewed edgewise instead of vertically.

The response function of the spectrometer must fall rapidly outside the central field of view to allow for effective off-axis light discrimination. The Mariner instrument has an effective baffling arrangement that reduces the sensitivity of the instrument by more than a factor of 10^5 at 1° off axis. The slit function of the Mariner ultraviolet spectrometer falls off almost exponentially outside its central field of view.

Volume emission rate R, i.e., the number of photons given off per unit volume in unit time, is the primary physical quantity of interest. Although the theoretical discussion is centered on the volume emission rate R, the quantity that is observed is the integral of the emission rate along the line of sight. The

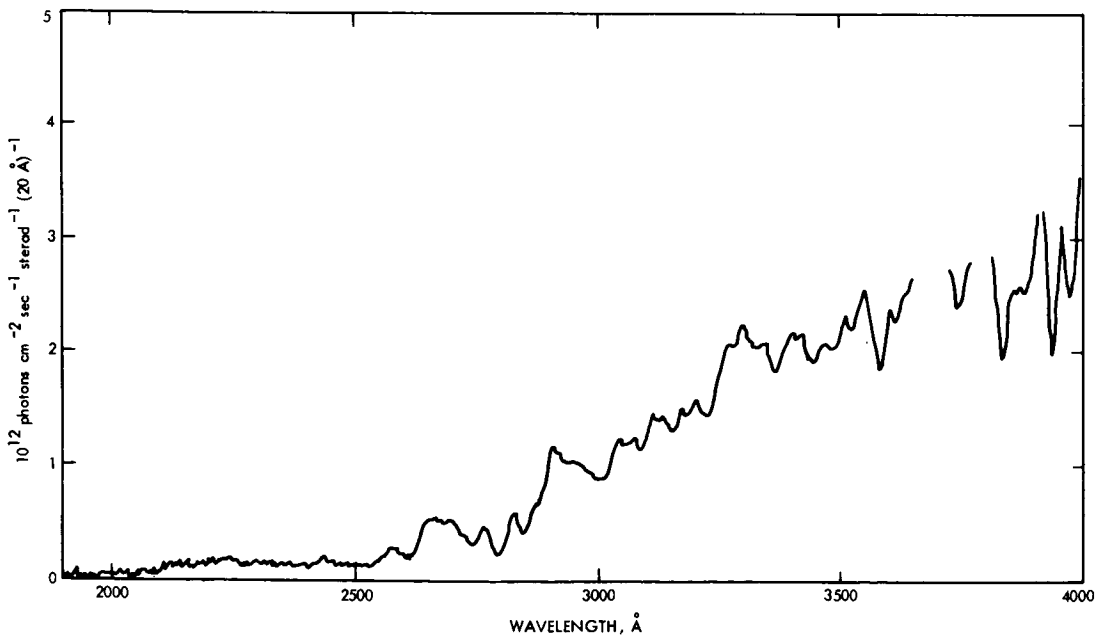

FIGURE 7-3. — Typical spectrum of the Martian disk.

column emission rate $4\pi\mathcal{J}$ in photons cm^{-2} sec^{-1} is related to the volume emission rate by the following integration:

$$4\pi\mathcal{J} = \int_0^\infty R(r)\, ds$$

where ds is the increment of length in the direction of view. The column emission rate is proportional to the volume density of atoms or molecules through the emission rate factor g:

$$4\pi\mathcal{J} = g\int_0^\infty n(r)\, ds$$

The volume density in planetary atmosphere may be a function of only the planetocentric distance, while the line of sight of the observation may be in a different direction s. The column density of atoms in the direction of view may be related to the vertical column density by an integration using the Van Rhijn function:

$$\int_0^\infty n(r)\, ds = \int_{r_0}^\infty n(r)\, V(\chi, r)\, dr$$

where

$$V(\chi, r) = \left[1 - \frac{r_0^2}{r}\sin^2\chi\right]^{-1/2}$$

where χ is the angle between the direction of observation and the planet vertical, and r_0 is the planetocentric distance of the point of observation. The ratio of the column density in the direction of view to the vertical column density is defined as the Chapman function, $\mathrm{Ch}(\chi)$, which is a function of χ and the atom density distribution, $n(r)$. The column emission rate along the direction of observation is related to the volume density by

$$4\pi\mathcal{J} = g\mathrm{Ch}(\chi)\int_{r_0}^\infty n(r)\, dr$$
$$= gN_0\mathrm{Ch}(\chi)$$

where N is the vertical column density of atoms or molecules. For an isothermal atmosphere, the Chapman function is approximated by

$$\mathrm{Ch}(\chi, r_0/\mathrm{H}) = \left(\frac{\pi r_0}{2\mathrm{H}}\right)^{1/2} \exp\left(\frac{r_0}{2\mathrm{H}}\cos^2\chi\right) \mathrm{erfc}\left(\frac{r_0}{2\mathrm{H}}\cos^2\chi\right)^{1/2}$$

where erfc (x) is the complementary error function. This is the appropriate equation to use with observations of the illuminated planetary disk. For the limb observations, where the instrument's field of view is outside the atmosphere, the appropriate function to use is twice the value of the Chapman function at

$$\chi=90°,\ 2\left(\frac{\pi}{2}\frac{r_0}{H}\right)^{1/2},\ \text{or}\ (2\pi r_0/H)^{1/2}$$

In an extended planetary exosphere, the atom density distribution may be approximated by a power law

$$n(r)=n(r_0)\left(\frac{r_0}{r}\right)^k$$

For observations made from outside the exosphere, the observed column emission rate is related to the atom density by the use of the equation

$$4\pi J = gn(r_0)r_0\frac{2(\pi)^{1/2}}{(k-1)}\frac{\Gamma\left(\frac{k+1}{2}\right)}{\Gamma\left(\frac{k}{2}\right)}$$

where $\Gamma(x)$ is the complete gamma function.

PRELIMINARY RESULTS

Initial analyses of the Mariner 6 and 7 ultraviolet atmospheric emissions indicate the presence of a hydrogen corona extending to about 25 000 km above the Martian surface. This is the altitude at which the Lyman-alpha signal from the hydrogen associated with Mars becomes comparable with the galactic intensity. The origin of this hydrogen is presumed to be the photodissociation of H_2O vapor in the Martian atmosphere. Below an altitude of 300 km, the 1304-Å emission of atomic oxygen is visible. The small magnitude of the intensity indicates that, compared with the upper atmosphere of Earth, a very small amount of atomic oxygen is present. Preliminary analyses of the altitude distribution of the upper atmospheric emissions show the temperature of the Martian exosphere to be less than that of the Earth's by more than a factor of 2. Based upon these data, the final value for the temperature of the exosphere involves a radiative transfer solution that includes the effects of multiple scattering.

Observed emissions in the 1900- to 4300-Å wavelength range are associated with ionized carbon dioxide and carbon monoxide. These emissions are the Fox-Duffendack-Barker bands, the prominent ionized CO_2 spectral peak at 2890 Å,

and the Cameron bands. The altitude variations of these emissions indicate that the upper atmosphere of Mars is dominated by CO_2 with a CO_2^+ ionosphere. The scale height of the neutral CO_2 above the ionospheric peak is about 23 km.

When the Mariner spectral data of Mars in the 1900- to 4300-Å wavelength range are compared with similar spectral data taken in the Earth's upper atmosphere, the most striking observation is that only one spectral feature, the 2972-Å line of atomic oxygen, is common to both planets. This is particularly significant as all of the major constituents in the Earth's upper atmosphere, with the exception of helium, have spectroscopic signatures in this wavelength range. Notably missing from the upper atmosphere of Mars are the emission features of atomic, molecular, and ionized molecular nitrogen. The absence of these emissions indicates that molecular nitrogen cannot make up as much as 1 percent of the total Martian atmosphere. The gamma bands of nitric oxide, strong emission features in the Earth's atmosphere, are also absent from the spectra of Mars.

CHAPTER 8

Infrared Radiometry

G. NEUGEBAUER (*Principal Investigator*), G. MÜNCH, S. C. CHASE, JR., H. HATZENBELER, E. MINER, AND D. SCHOFIELD

The infrared radiometer (ref. 8–1) carried on Mariners 6 and 7 was specifically designed to measure the energy emitted in two broad wavelength bands of the spectrum of Mars. The instrument was mounted on the scan platform of the spacecraft and was boresighted with the narrow-angle television camera (refs. 8–2 and 8–3). The radiometer consisted of two 2.5-cm (1-in.) refracting telescopes, each with an uncooled bimetallic thermopile detector. The optical train of the radiometer included a rotatable plane mirror that reflected the incident energy into the detector telescopes. Once each 63 sec, the mirror was rotated to view empty space, thus providing a zero energy reference for absolute radiometric measurements. The planet was viewed by rotating the mirror 90°; observations were made for 56.7 sec at 2.1-sec intervals. In a third orthogonal mirror position, the instrument measured the thermal energy of a plate, whose temperature was monitored directly by a thermistor each 63 sec.

The radiometer had a dynamic range of 120° to 330° K. To cover this range, there were two spectral channels, located in atmospheric windows. Channel 1 emphasized the upper temperatures of this range; channel 2, the lower temperatures. The output over this temperature range was linear in energy and was digitized into 1024 levels. In practice, the detector noise was dominated by the size of the digitization steps. The passbands of channel 1 (8.5 to 12.4μ) and channel 2 (18 to 25μ) were defined by interference filters to exclude atmospheric gaseous absorption; consequently, radiation from the surface was measured.

Data were obtained both in the far-encounter mode, when the spacecraft was at distances exceeding 100 000 km, and during near encounter. Although the radiometers were affected by stray light to an extent greater than anticipated from laboratory tests, the radiometric sensitivity of the units during flight remained essentially the same as that established during laboratory calibrations.

Energies measured in the near-encounter mode are shown in figures 8–1 and 8–2; the corresponding brightness temperatures have been derived assuming

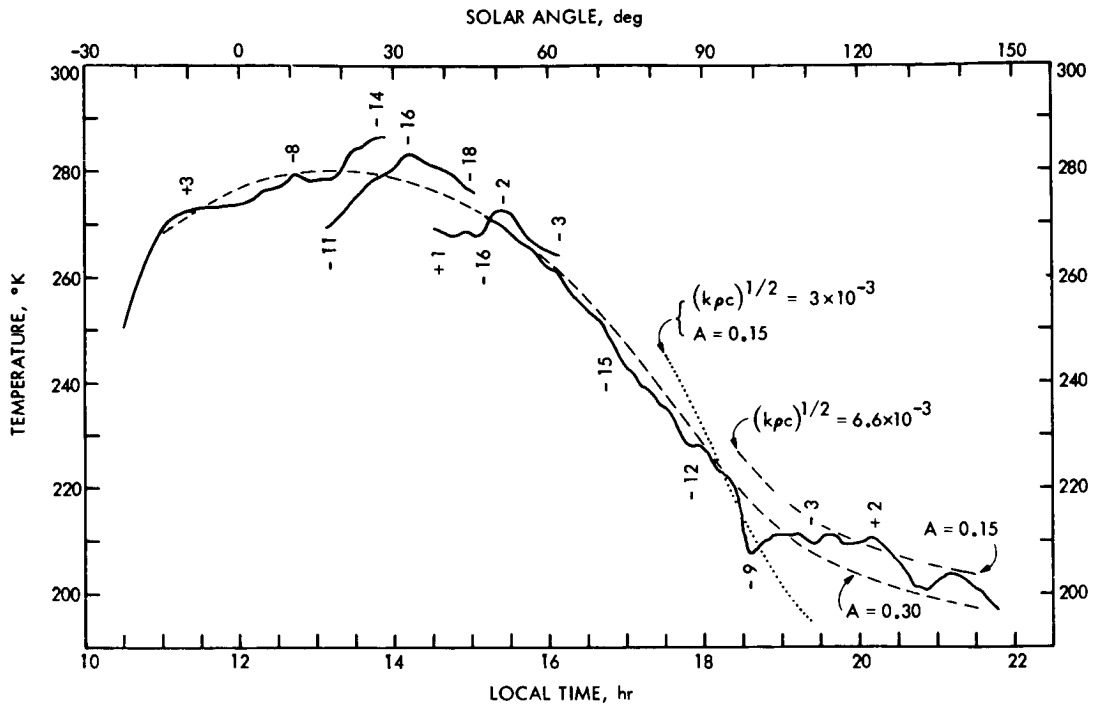

FIGURE 8–1. — Temperatures measured in channel 1 (8.5 to 12.4μ) of the Mariner 6 infrared radiometer during near encounter (solid curves), as a function of local time. The curve is not continuous because of the various platform slues. Planetocentric latitudes (in deg) along the tracks swept by the center of the field of view are indicated. The dashed and dotted lines represent cooling curves of homogeneous solids with thermal inertias $(k\rho c)^{1/2}$ (cgs units) and albedos A as indicated, for a latitude of $-10°$ and local times corresponding to the observed points.

unit emissivity of the planet's surface. In this preliminary report, emphasis has been placed on the data that relate to the temperature of the southern polar cap and to the scale of the temperature variations over the surface.

The track of Mariner 7 was chosen to sweep over the south polar cap (ref. 8–2). As shown in figure 8–1, the temperature decreased to 225° K when the platform was slued to latitudes near, but not on, the polar cap. As the track continued south, the temperature decreased slowly; however, around −61° S latitude, when the radiometer crossed the boundary of the polar cap, the temperature suddenly dropped below 160° K. As the field of view swept over the

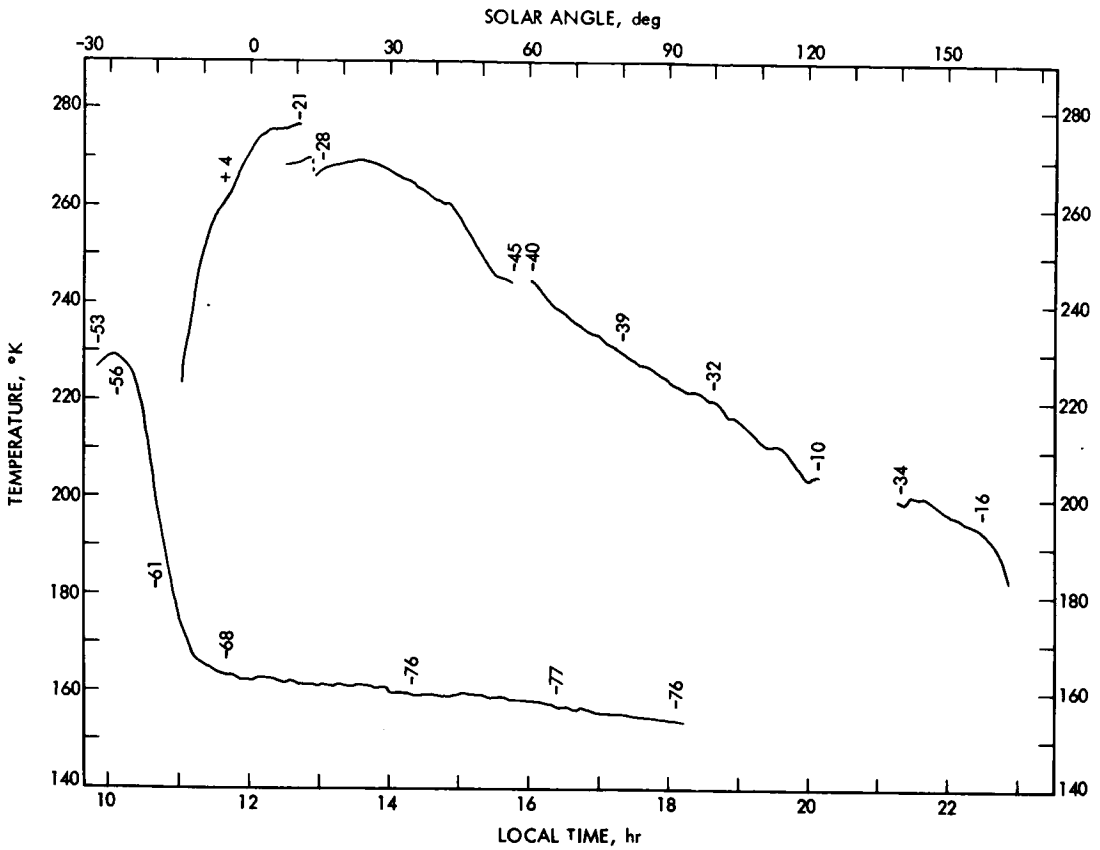

FIGURE 8-2. – Temperatures measured in channel 2 (18 to 25μ) of the Mariner 7 infrared radiometer during encounter, as a function of local time. Planetocentric latitudes (in deg) along the various swaths described by the center of the field of view are indicated.

polar cap, the temperature decreased to at least 153° K near the terminator just before the platform was slued north.

The frost temperature of CO_2 is 148° K at a vapor pressure of 6.5 mb. We interpret agreement between this value and the observed temperatures, as well as the large change in temperature at the onset of the cap to provide evidence for frozen CO_2 to be the major constituent of the polar cap. This hypothesis has been discussed in detail by Leighton and Murray (ref. 8-4).

Temperatures obtained under the assumption of unit emissivity need not be equal to the actual surface temperature of the polar cap. The television pic-

tures of Leighton et al. (ref. 8–2) show bare surface that is not covered by frost within the cap. If only 5 percent of the field of view in the polar cap were filled by sources with a brightness temperature of 200° K, the resulting measured brightness temperatures would be raised by 4° K.

Although a discussion of possible instrumental systematic errors in the measurements is not included in this report, it is important to note that the radiometers responded significantly to off-axis sources. For example, the response of channel 2 of the Mariner 7 radiometer, to a point source at a distance of 12° off axis, was only 0.3 percent of that for the same source on axis. Because of the large solid angles subtended, however, the extended wings beyond a central area 1° in diameter contributed 27 percent of the total response of a measurement of the energy radiated by an isothermal source filling the entire object space. The correction to the minimum temperature measured by Mariner 7 is about −3° K, because of the extended response of channel 2 and based on a model temperature distribution over the surface of the planet. At low temperatures, the correction for off-axis radiation was greater for channel 1 than for channel 2. A more refined analysis is being performed on the systematic effects, based on data obtained before near encounter and during passage across the limb. All known systematic errors show that the observed temperatures are higher than the true value.

Mariners 6 and 7 provided the opportunity to measure temperatures on an areal scale about 10 times finer than that obtainable from Earth. Although transsitions between dark (maria) and light (desert) areas are well defined in the data, there appear to be no sharp temperature changes that exceeded 1° K in contiguous fields of view (50 km at closest approach). The only sharp temperature fluctuation that does not seem to be associated with any feature in the classical maps of Mars was recorded in both channels of Mariner 6 at −3.5° S latitude and 307.0° E longitude, identified in figure 8–1. The television pictures of this area show a chaotic terrain structure that may be related to this temperature anomaly.

Because the track of Mariner 6 was nearly equatorial (ref. 8–3) and extended well beyond the terminator, it is particularly suited for a determination of the parameters characterizing the gross thermophysical properties of the Martian surface. Although obvious departures that represent both variations in albedo and/or in thermal inertia may be seen in figure 8–1, the temperatures can be fit by assuming a homogeneous solid and values of thermal inertia that are consistent with the values derived by Sinton and Strong (ref. 8–5) from measurements with the 200-in. telescope.

It is emphasized that the temperatures presented in this report are derived from the raw measurements, on the basis of laboratory calibrations. Accordingly, inferences drawn from them at the present time should be considered tentative. A definite discussion will be published when the corrections for off-axis radiation are completed.

REFERENCES

8-1. CHASE, S. C., JR.: Infrared Radiometer for the 1969 Mariner Mission to Mars. Applied Optics, vol. 8, Mar. 1969, pp. 639–643.

8-2. LEIGHTON, R. B.; HOROWITZ, N. H.; MURRAY, B. C.; SHARP, R. P.; HERRIMAN, A. G.; YOUNG, A. T.; SMITH, B. A.; DAVIES, M. E.; AND LEOVY, C. B.: Mariner 7 Television Pictures: First Report. Science, vol. 165, Aug. 1969, pp. 788–795.

8-3. LEIGHTON, R. B.; HOROWITZ, N. H.; MURRAY, B. C.; SHARP, R. P.; HERRIMAN, A. G.; YOUNG, A. T.; SMITH, B. A.; DAVIES, M. E.; AND LEOVY, C. B.: Mariner 6 Television Pictures: First Report. Science, vol. 165, Aug. 1969, pp. 685–690.

8-4. LEIGHTON, R. B.; AND MURRAY, B. C.: Behavior of Carbon Dioxide and Other Volatiles on Mars. Science, vol. 153, 1966, pp. 136–144.

8-5. SINTON, W. M.; AND STRONG, J.: Radiometric Observations of Mars. Astrophys. J., vol. 131, 1960, pp. 459–469.

ACKNOWLEDGMENTS

Many persons within the Mariner-Mars 1969 project contributed to the success of the infrared radiometry experiment, but our special thanks are extended to H. SCHURMEIER, J. STALLKAMP, and C. KOHLHASE for their support of our efforts. We acknowledge also J. BENNETT and D. GRIFFITH for their help in the data acquisition and reduction.

We are indebted to R. B. LEIGHTON and the Mariner-Mars 1969 television team for permitting us to see the television pictures before publication and for giving us their valuable comments.

CHAPTER 9

S-Band Occultation

A. KLIORE *(Principal Investigator)*, G. FJELDBO,
B. SEIDEL, AND S. I. RASOOL

Mariner 4 was the first spacecraft to make radio occultation measurements of a planetary atmosphere by utilizing a radio signal. These measurements indicated an unexpectedly low surface pressure, ranging from about 5 mb at the point of entry into occultation to about 9 mb at the point of exit. Mariners 6 and 7 provided opportunities for four more occultation measurements of the atmosphere, ionosphere, and surface configuration of Mars, thus increasing the amount of occultation data obtained by more than 200 percent.

Mariner 6 made its closest approach to Mars on July 31, 1969, at 05:19:07 G.m.t. About 20 min later, it disappeared from the view of the Earth, and its radio beam was interrupted by the Martian surface at a point near Meridiani Sinus (4° N latitude, 355° E longitude). The local time at this point was about 15:40, and the solar zenith angle was about 57°. At the moment of occultation, the spacecraft was about 9800 km from the limb. After remaining in occultation for about 20 min, the spacecraft emerged in the vicinity of the North Pole (79° N latitude, 84° E longitude). The local time at that point was about 21:40, and the solar zenith angle was about 107°. At that time, the spacecraft was about 17 400 km from the limb.

Mariner 7 made its closest approach on August 5 at 05:00:49 G.m.t. About 19 min later, its S-band radio beam was cut by the Martian surface in the area of Hellespontus (58° S latitude, 30° E longitude). The local time was about 14:20, and the solar zenith angle was about 56°. At the moment of occultation, the spacecraft was about 9050 km from the limb. About 30 min later, the spacecraft's radio signal emerged from behind Mars in the vicinity of Amazonis and Arcadia (38° N latitude, 212° E longitude). The local time was 03:00, and the solar zenith angle was about 130°. At that time, the spacecraft was about 20 180 km from the limb.

DATA ACQUISITION

During each entry and exit of the radio beam through the Martian atmosphere, the frequency and amplitude of the signal received on Earth were changed by effects of refraction on the propagation of the radio signal. (These effects are discussed in detail in refs. 9–1 through 9–3.) A simplified diagram of the data acquisition procedure is presented as figure 9–1.

Entry into occultation was performed in a two-way mode of operation in which a frequency referenced to a rubidium standard at the tracking station is transmitted to the spacecraft where it is coherently retransmitted. Exit data were obtained in the one-way mode of operation in which the spacecraft's transmitter is referenced to its onboard crystal oscillator. The received signal was passed through the standard phase-locked-loop receiver and the record of nondestructively counted Doppler data was recorded. This procedure provides the closed-loop data. Simultaneously, the signal was passed through a special open-loop receiver, with an audio passband of about 5 kHz. It produced a

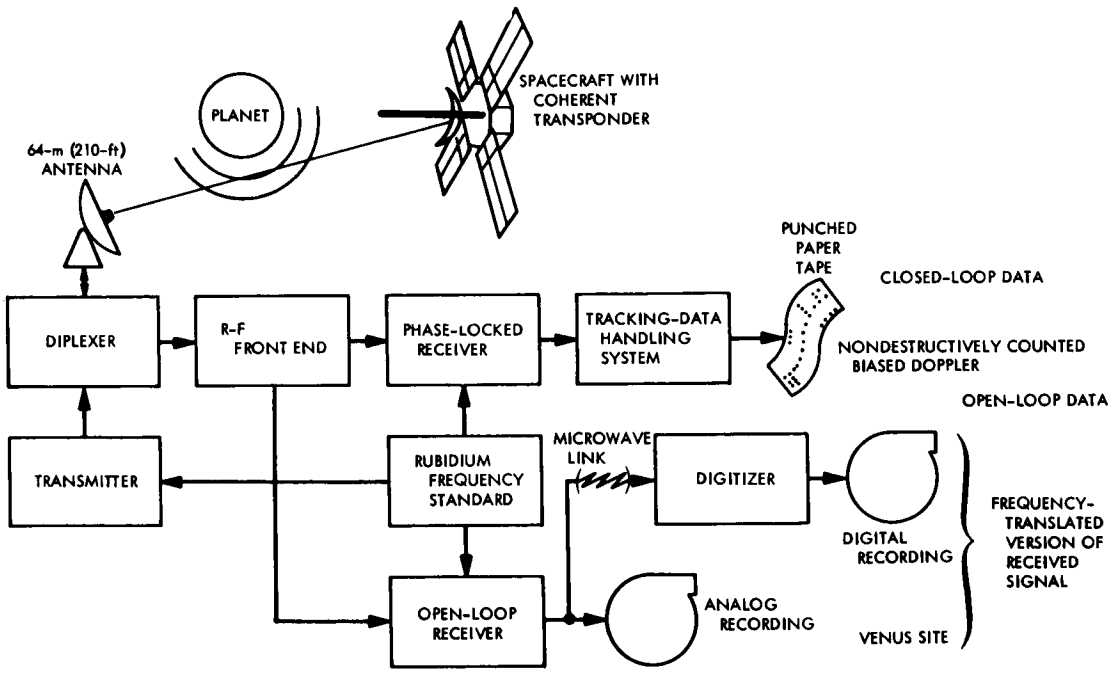

FIGURE 9–1. — Simplified schematic of data acquisition procedure for S-band occultation experiment on Mariners 6 and 7.

frequency-translated version of the received signal which was recorded on an analog tape recorder, as well as digitized in real time and recorded on digital magnetic tape. This procedure provides the open-loop data.

For the S-band occultation experiment on Mariners 6 and 7, the Mars and Echo sites of the Goldstone tracking station were instrumented with open-loop receivers, and the open-loop data from the Mars site were transmitted over a microwave link to the Venus site (Goldstone), where they were digitized in real time and recorded. Closed-loop Doppler data also were taken at the Mars and Echo sites and at the tracking station in Woomera, Australia. The open-loop receiver is necessary to insure instantaneous reception of the data as the spacecraft reemerges from behind the planet. (This is difficult to accomplish with the phase-locked-loop receiver because of its finite lockup time.)

Another purpose of the open-loop receiver is to obtain amplitude data that cannot be obtained from the phase-locked-loop receiver because of the long time constant of its automatic gain control circuit. The bandwidth of the open-loop receiver was selected on the basis of the projected Doppler frequency rates caused by the motion of the spacecraft. These rates, together with the fact that it was undesirable to retune the receiver within 3 min of occultation, led to an open-loop passband selection of about 5 kHz.

To insure precise tuning of the open-loop receivers, as well as to preserve their frequency-translation integrity, all local oscillator frequencies were synthesized from a rubidium standard. An audio phase-locked-loop receiver, a spectrum analyzer, and other test equipment were provided in the open-loop system to give a real-time indication of the signal received and recorded. This test equipment could be switched between the output of the open-loop receiver and the various reproducing units of the analog tape recorders. A 20-kHz test tone referenced to a rubidium standard was added to the data channel before recording to insure that the frequency recorded by the analog recorders was not distorted by more than a fraction of 1 kHz. Later, this test tone was used as a time base for keying the digitizers sampling the data. The analog recordings were used primarily as backups to the real-time digital recordings, which, because of system constraints, had to be obtained over a microwave link.

Digital open-loop data are passed through the Decimation and Spectral Analysis Programs and the Digital Phase-Lock Receiver Program, which produces a record of the frequency and amplitude of the received signal sampled at arbitrary intervals of time. The frequency is then compared with predictions based

on the orbit of the spacecraft; the differences in frequency constitute the open-loop residuals. The closed-loop data, consisting of the biased Doppler counts, are processed by the Orbit Determination Program, which compares the counts to predictions based on an orbit; the differences constitute the closed-loop residuals. Because of system limitations, the maximum sampling frequency is 1 sample/sec. The residuals are then passed through a Data Preparation Program, which removes any bias or drift that may be present, and integrates to obtain a record of the total phase path change due to refraction effects in the ionosphere and atmosphere. From there the data go to the Inversion Program, which utilizes the trajectory data provided by the Double Precision Trajectory Program and performs integral inversion (ref. 9–4) of the data to obtain the refractivity profile. This profile is used to compute the electron density in the ionosphere and the pressure, temperature, and other parameters of the lower atmosphere. The profile of refractivity, as obtained by inversion, can be directly

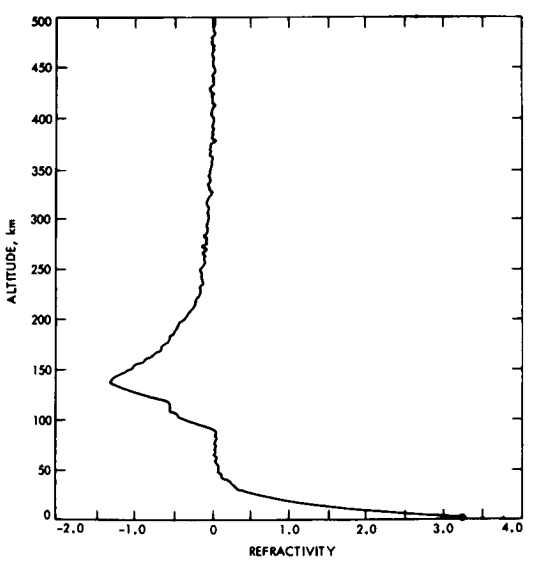

FIGURE 9–2. — Atmospheric refractivity profile obtained near Meridiani Sinus at 4° N latitude, 355° E longitude, at 15:40 (local time) in early fall. Data were obtained from two-way tracking during the Mariner 6 immersion. No filtering was used in the data analysis.

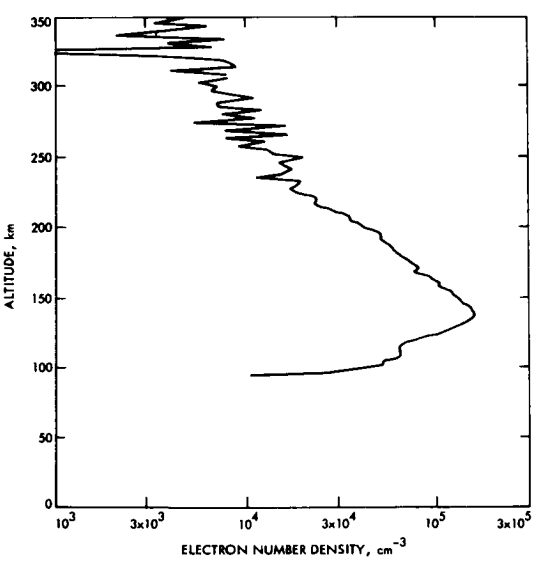

FIGURE 9–3. — Ionospheric electron number density distribution derived from figure 9–2. The measurements were made near Meridiani Sinus at 4° N latitude, 355° E longitude, at 15:40 (local time) in early fall. The solar zenith angle was about 57°.

interpreted in terms of the electron density in the upper atmosphere. (See figs. 9–2 and 9–3.) However, to obtain profiles of density, pressure, and temperature in the lower atmosphere, an assumption of the composition must be made.

RESULTS

It is generally accepted that CO_2 is the major constituent of the Martian atmosphere; however, estimates on the exact amount of concentration range from 60 to 100 percent. This poses an interesting question regarding the identity of the other constituents, a question that has bearings on the origin of the Martian atmosphere. It has been argued that if the present atmosphere of Mars is a remnant of a primordial atmosphere, which once had a solar composition, then after the escape of H_2 and He, the atmosphere should contain 60 percent CO_2, 25 percent Ne, and about 15 percent N (refs. 9–5 and 9–6). However, if the present atmosphere of Mars is the result of outgassing from the interior, as is the case on Earth, then by analogy with Earth, Ne should be completely absent and the atmosphere should contain about 95 percent CO_2, 2 to 3 percent N, and traces of Ar, depending on the extent of outgassing. The presence or absence of Ne in the atmosphere of Mars is therefore an important datum for the understanding of the origin of the Martian atmosphere.

In deriving the results presented here, CO_2 was assumed to be the major constituent in the Martian atmosphere. This assumption is based on results from Earth-based spectroscopy and on the results of other experiments on Mariners 6 and 7. (See chs. 6 and 7 of this report.) The temperatures and pressure profiles shown in figures 9–4 through 9–7 were obtained for a composition of 90 percent CO_2 and 10 percent Ar. They are valid as long as CO_2 remains the major constituent in the atmosphere. If it became necessary, however, to revise the estimate of CO_2 downward and to fill the remaining portion with some less refractive gas, the results would be substantially changed. For example, if the composition should change to 80 percent CO_2 and 20 percent Ne, the temperatures at all altitudes would decrease by about 10 percent. Confirmation of this composition or a more reliable composition will emerge when data analysis from Mariners 6 and 7 is completed.

Figure 9–4 shows the profiles of pressure as a function of the distance of the radio beam from the center of Mars for all four of the occultation measurements. The error limits on the pressure measurements are based on an assumption of a 0.05 N-unit uncertainty in the refractivity. (These error limits do not

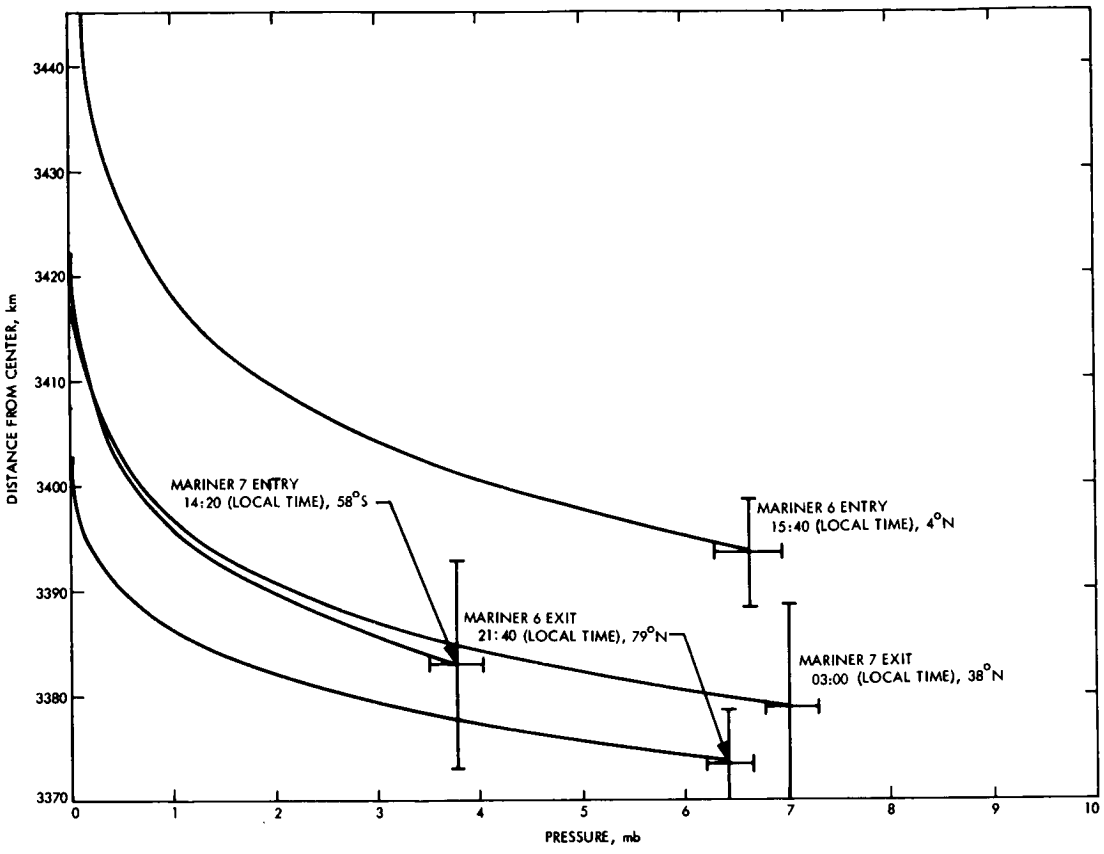

FIGURE 9-4. – Pressure as a function of distance of the radio beam from the center of the planet, derived from Mariners 6 and 7.

include the possible effects of an incorrectly assumed composition.) The uncertainties in the vertical scales depend on the accuracy of the knowledge of the orbital paths of Mariners 6 and 7. When these results were computed, the uncertainties in the orbits produced a ±5-km uncertainty for Mariner 6 in the knowledge of the position of the radio beam with respect to the center of Mars and ±10-km uncertainty for Mariner 7. These uncertainties probably will be reduced to about ±1 km when the orbit determination is more precise. For an atmosphere in hydrostatic equilibrium, the pressure should be approximately equal on a gravitational equipotential surface. Figure 9-5 shows the derived pressure profiles plotted as a function of altitude above a mean reference ellipsoid with an equatorial radius of 3394 km and an ellipticity of 0.0052. This corre-

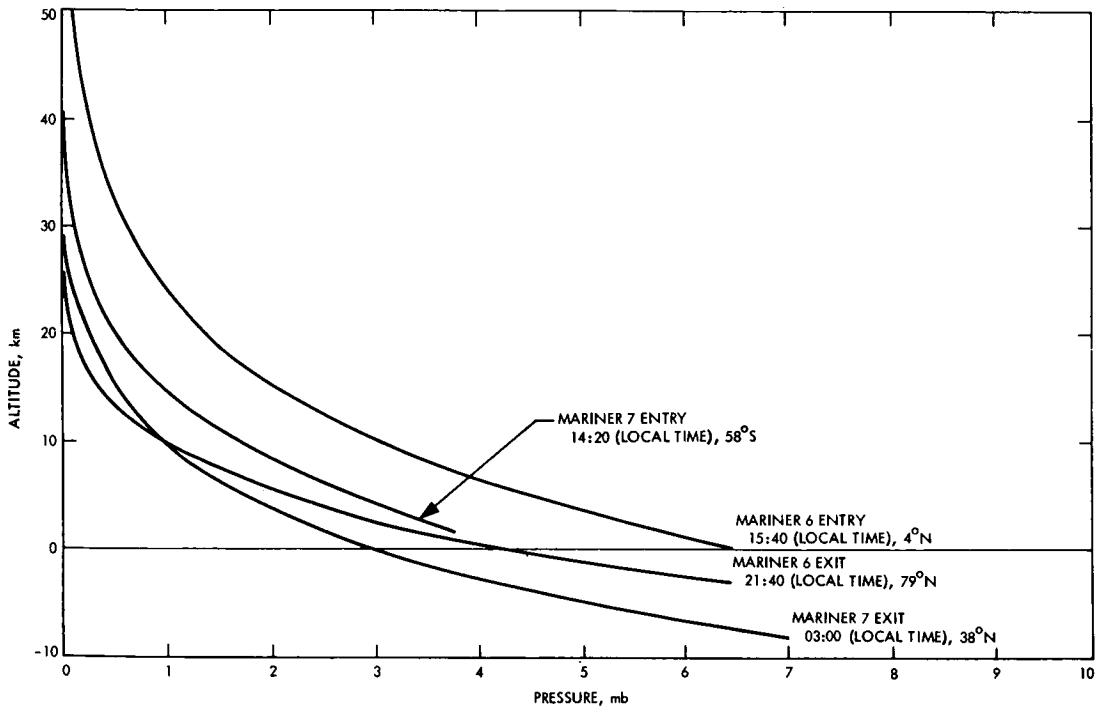

FIGURE 9-5. — Pressure as a function of altitude, referred to an ellipsoid with $a = 3394$ km and $e=0.0052$.

sponds to a figure of Mars inferred from dynamical measurements of oblateness. If the reference ellipsoid were correct and if the radial distance scales of the original pressure profiles were correct, the profiles would lie very close to one another. The evident disagreement in the profiles of figure 9-5 indicates that this is not yet the case. However, when the radial distance coordinates are established to a greater degree of precision, it will be possible to use these measurements to compute the reference equipotential gravitational surface of Mars.

It is evident from figures 9-4 and 9-5 that three of the four measurements of pressure at the surface fall between 6.4 and 7 mb. Thus, these measurements, taken over diverse latitudes and longitudes, seem to lie close to a common equipotential surface. The fourth measurement, however, taken in the region of Hellespontus (58° S), yields a pressure of only 3.8 mb, indicating that the surface feature which interrupted the radio signal at that point lies some 5 to 6 km above the mean ellipsoid in the vicinity of the other three occultation observations. For Mariner 6, the radius measured at 4° N differs by about 20 km

from that measured at 79° N. Because the pressures measured at these two points are almost equal, it can be assumed that one is measuring the shape of the gravitational equipotential surface, and thus conclude that the physical surface of Mars has a shape similar to that of the gravitational equipotential surface predicted by the dynamical oblateness of Mars, as opposed to the optically observed flattening.

The profiles of temperature as a function of distance from the center of Mars for all four measurements are shown in figure 9–6. The uncertainty boundaries again have been established assuming an uncertainty of 0.05 N-units in the refractivity, and do not reflect possible errors in the assumed composition. Pressure and temperature profiles are crossplotted in figure 9–7.

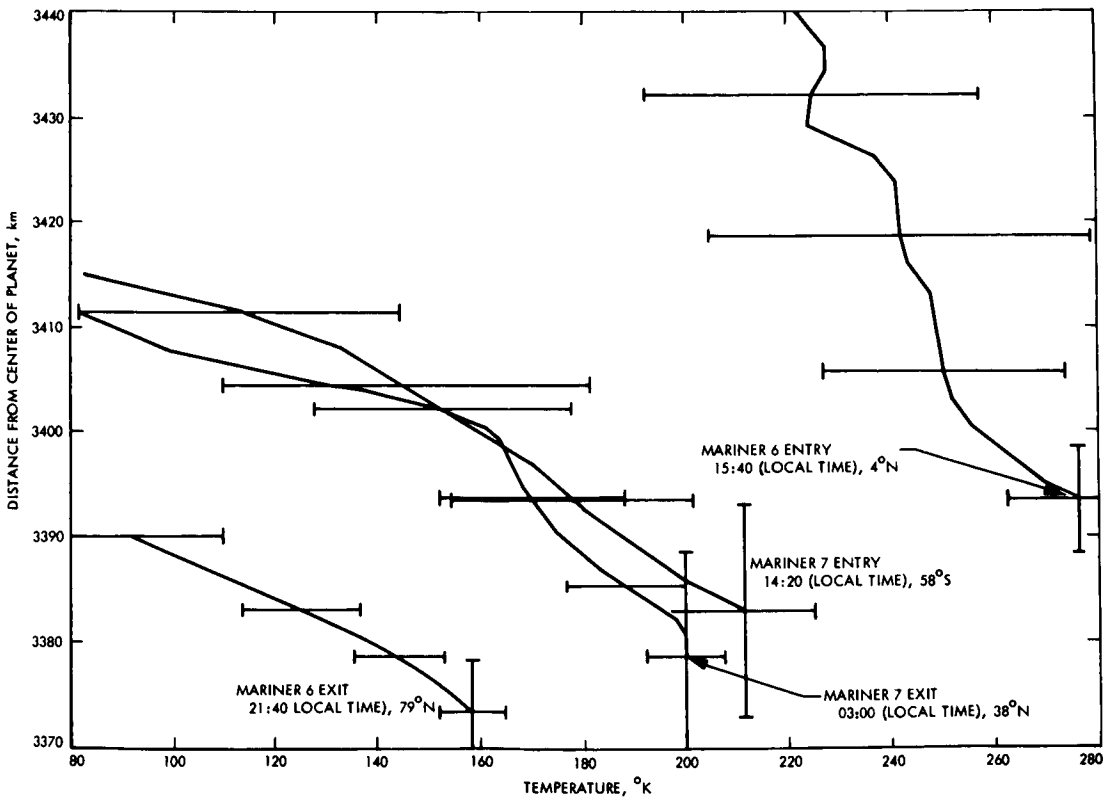

FIGURE 9–6. — Temperature as a function of distance from the center of the planet. The uncertainty boundaries include only the effect of estimated uncertainty in the determination of refractivity.

The vertical distributions of temperature in the Martian atmosphere, as shown in figures 9–6 and 9–7, have been derived assuming that the atmosphere is in hydrostatic equilibrium, and that the ideal gas law is valid. The thermodynamics of atmospheric condensation has not been considered. For this reason, in three of the four cases shown in figure 9–7, especially that of the Mariner 6 exit, the atmospheric temperatures are substantially lower than the condensation temperatures of CO_2, implying that the atmosphere at these levels is supersaturated. In reality, if suitable condensation nuclei are present, condensation should occur, releasing latent heat and, therefore, raising the atmospheric temperatures. If it is assumed that radiational cooling is balanced by transport

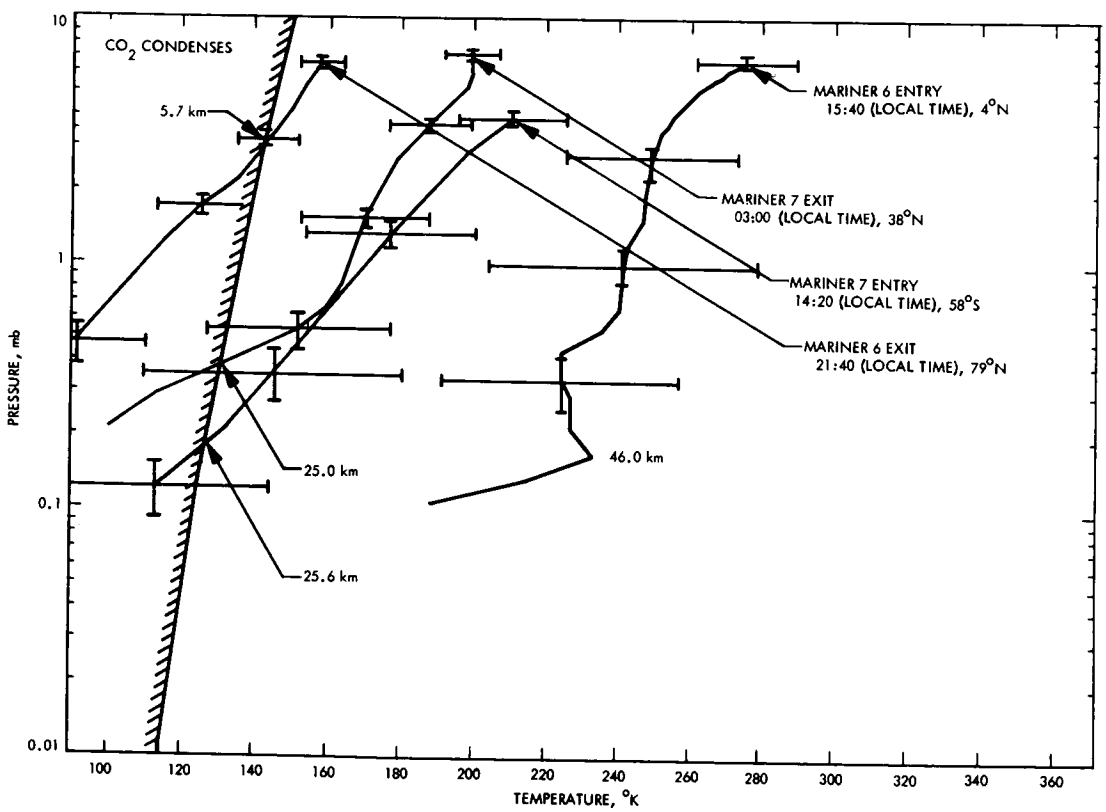

FIGURE 9–7. – Pressure as a function of temperature for all profiles, derived from Mariner 6 and 7 measurements. The region to the left of the shaded boundary is favorable for the condensation of CO_2. The numbers referred to the boundary denote the approximate altitude at which the boundary is reached.

of energy by circulation, then the atmospheric temperatures should follow closely the saturation temperature curve shown in figure 9–7. As this may be the case, particularly in the polar night on Mars, it seems more appropriate that, when the derived temperatures fall below the condensation curve temperature of CO_2, the saturation law, rather than ideal gas relation, be used to derive the temperature and pressure profiles. When the refractivity data are reduced in this way, the atmospheric temperatures are never lower than the saturation temperatures of CO_2 and have the effect of raising the surface pressure by a few percent.

The results of this analysis are shown in figures 9–8 through 9–11. Each of these figures shows two profiles: one for 100 percent CO_2, the other for 90 percent CO_2 and 10 percent Ne.

In the interpretation of the refractivity data in terms of atmospheric number density, it is the presence of Ne that makes a substantial difference in the temperature profiles that result. The addition of only 10 percent Ne in the atmosphere makes the derived temperatures substantially lower than those of 100 percent CO_2, because the refractivity of Ne is about six times smaller than that of CO_2.

The variety and range of the temperature profiles shown in figures 9–8 through 9–11 reveal several important and unexpected aspects of Martian meteorology. In the following discussion, the salient features of these results

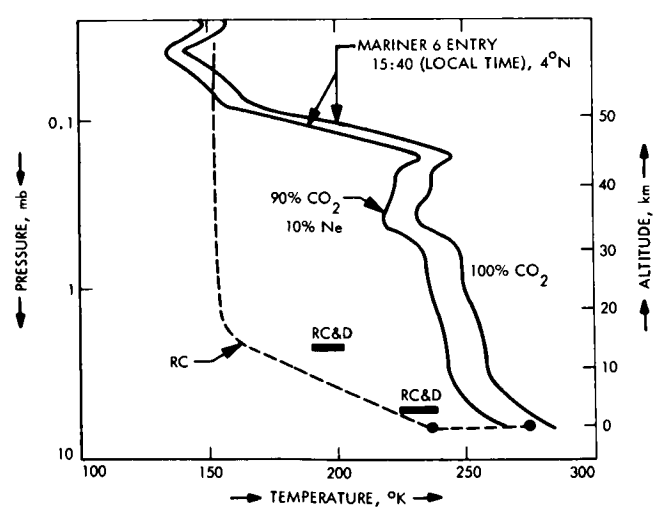

FIGURE 9–8.–Temperature as a function of pressure in the Martian atmosphere at the entry point of Mariner 6 (heavy line) for two assumed compositions. The dashed line represents the temperature distribution calculated for radiative-convective equilibrium (RC) by Gierasch and Goody (ref. 9–7), also for the Mariner 6 entry point. The horizontal bars marked RC&D are the temperature values estimated for two pressure levels when atmospheric dynamics is considered (refs. 9–9 and 9–10).

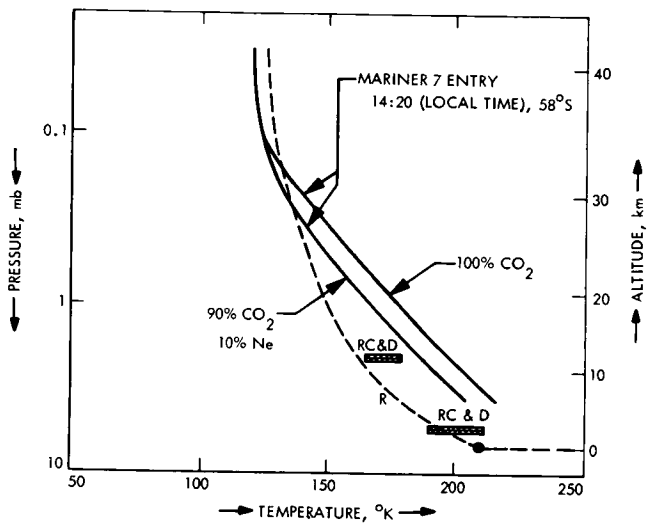

FIGURE 9-9. – Temperature as a function of pressure in the Martian atmosphere at the entry point of Mariner 7 (heavy line) for two assumed compositions. The dashed line is the radiation (R) curve adapted from Ohring and Mariano. (See ref. 9-12.)

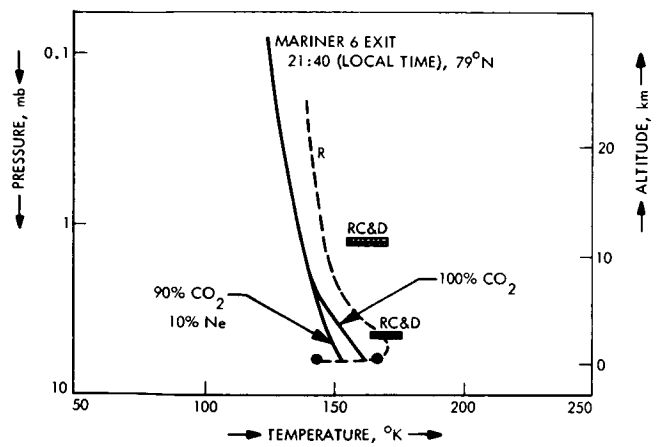

FIGURE 9-10. – Same as figure 9-8, but for exit of Mariner 6. The radiation curve is after Gierasch and Goody (ref. 9-7).

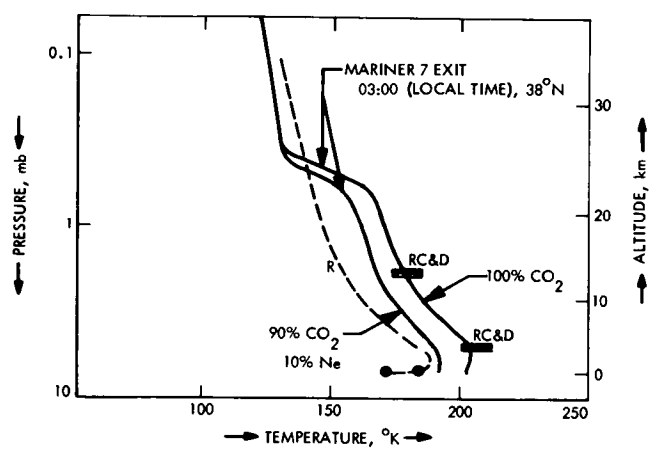

FIGURE 9-11. – Same as figure 9-9, but for exit of Mariner 7. The radiation curve is adapted from Ohring and Mariano. (See ref. 9-12.)

are emphasized by comparing each of the observed temperature profiles with the atmospheric temperature profiles predicted by existing theoretical models of the Martian atmosphere.

The thermal structure of the atmosphere has been the object of several comprehensive studies during the last few years. Notably, it has been argued that because CO_2 is the major constituent of the atmosphere and because the total surface pressure is only about 10 mb, radiative heat exchange should dominate over convective and advective energy transport (refs. 9–7 and 9–8). Consequently, the Martian atmosphere should be radiatively coupled to the surface more strongly than is the terrestrial atmosphere, and the temperature distribution in the atmosphere above a given point on the Martian surface should be determined essentially by local radiative-convective balance. Because the atmosphere is optically thin, one may expect a sharp temperature discontinuity of as large as 70° K at midday and −50° K at night (see refs. 9–7 and 9–8) between the atmosphere near the surface and the surface itself.

In actuality, however, atmospheric circulation on a planetary scale would modify such a thermal structure to some extent. Detailed numerical computations by Leovy and Mintz (refs. 9–9 and 9–10) indicate that the overall effect of advection is to decrease the magnitude of the temperature discontinuity at the ground, and to raise the atmospheric temperatures so that the lapse rate becomes subadiabatic at the equator and close to zero at the poles.

In figures 9–8 and 9–11, the measured temperature distributions are compared with temperature profiles calculated for similar conditions, considering radiation (R) transfer alone, and both radiation and convection (RC) exchange. Also indicated are the temperatures anticipated at two different levels in the atmosphere if all three processes, radiation, convection, and dynamics (RC&D), are considered.

Figures 9–8 and 9–9 correspond to daytime; figures 9–10 and 9–11 correspond to nighttime on Mars. Comparison of the observed temperature structures with the theoretical models for the four different locations indicates the following significant features:

(1) The atmospheric temperatures observed at the equator in midafternoon are significantly higher than the predicted temperature up to an altitude of 40 km. The gradient observed in the lower atmosphere is subadiabatic, and suggests the presence of a tropopause at an altitude of 9 km. The temperature

found in the equatorial stratosphere is 100° K higher than had been predicted by radiative transfer alone. The observations also indicate a sudden decrease of temperature at a pressure level of 0.2 mb with the temperature gradient becoming superadiabatic. However, this is the least certain feature of the temperature profile.

(2) The temperature distributions in midafternoon near the south polar cap (fig. 9–9) and in the subtropics in the early morning hours (fig. 9–10) seem to be quite close to the profiles predicted when atmospheric dynamics were considered.

(3) At 79° N latitude, where the polar night is just beginning, the observed temperature profile, if interpreted with the assumption of saturation and condensation of CO_2 in the atmosphere, suggests that condensation of CO_2 is occurring at almost all heights in the atmosphere.

The tropical atmosphere in daytime (fig. 9–8) is the most interesting. At the equator, the atmosphere is much warmer than expected. For 100 percent CO_2, the atmospheric temperature near the surface is about 283° K. However, the actual surface temperature measured by the infrared radiometer near the point of occultation is about 275° K (see ref. 9–11), indicating an inconsistent negative temperature discontinuity of 8° K. For the case with 10 percent Ne, the atmospheric temperature near the ground is 268° K, and the temperature discontinuity is only 7° K, differing markedly from the predicted value of Gierasch and Goody. (See ref. 9–7.) The remaining problem consists of the fact that the atmosphere is substantially warmer than suggested from the theoretical calculations. Either the opacity of the atmosphere is much higher than estimated by the various CO_2 absorption-band models or a significant amount of solar radiation is deposited in the middle atmosphere by absorption in the near-infrared bands of CO_2, or a combination of both.

Refractivity measurements in the upper atmosphere of Mars, as derived from Mariners 6 and 7, yielded results similar to those obtained from Mariner 4 (ref. 9–1). On the dayside, the main layer was now located near 135-km altitude, and had a peak density of about 1.7×10^5 electrons/cc. The minor layer was observed near 110-km altitude. The topside plasma temperature was 400° to 500° K, assuming CO_2^+ as the principal ion. No ionization was detected on the dark side of the planet.

Figures 9–12 and 9–13 show the density and temperature profiles derived from the high latitude dayside measurements from Mariners 4 and 7. The

atmospheric models shown in these figures are based on the asssumption that the main ionization layer is an F_1 region produced by solar extreme ultraviolet. Solid curves represent results derived from the refractivity data. Dashed curves indicate interpolation between the measurements made in the ionosphere and in the neutral atmosphere. The figures show that the upper and the lower atmospheres are warmer now than they were in 1965. The temperature increases presumably are due to seasonal changes, increased solar activity, and a 10-percent reduction in the distance to the Sun.

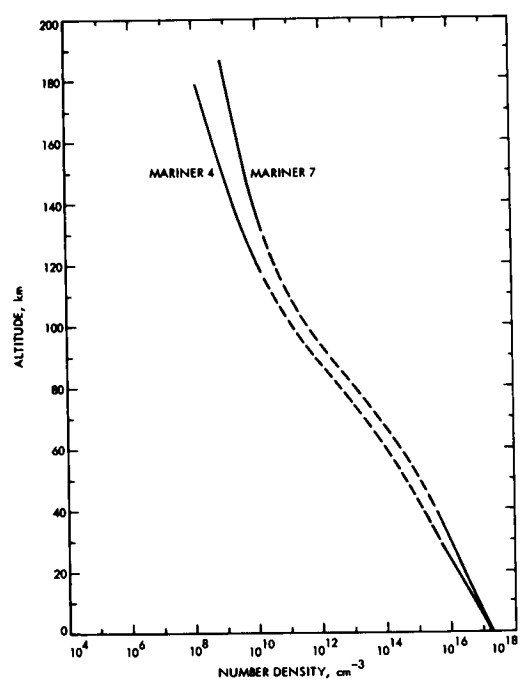

FIGURE 9-12.—Number density vs altitude. The Mariner 4 (1965) data were obtained near 50° S latitude at 13:00 (local time) in late winter. The solar zenith angle was 67°. The Mariner 7 (1969) data were obtained near 58° S latitude at 14:30 (local time) in early spring. The solar zenith angle was about 56°.

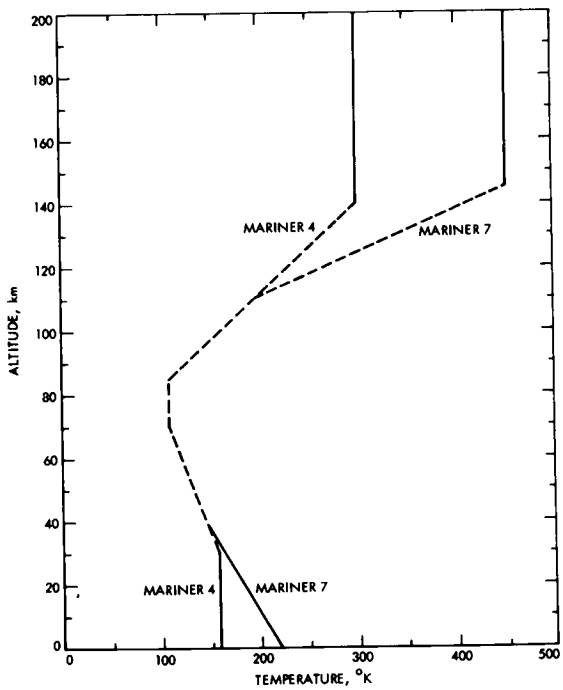

FIGURE 9-13.—Temperatures vs altitude for Mariners 4 and 7.

REFERENCES

9-1. KLIORE, A.; CAIN, D. L.; LEVY, G. S.; ESHLEMAN, V. R.; FJELDBO, G.; AND DRAKE, F. D.: Occultation Experiment: Results of the First Direct Measurements of Mars' Atmosphere and Ionosphere. Science, vol. 149, 1965, pp. 1243–1248.

9-2. KLIORE, A.; CAIN, D. L.; AND LEVY, G. S.: Radio Occultation Measurements of the Martian Atmosphere Over Two Regions by the Mariner IV Space Probe. Space Research VI, Moon and Planets, North-Holland Pub. Co. (Amsterdam), 1967, pp. 226–239.

9-3. FJELDBO, G.; AND ESHLEMAN, V. R.: The Atmosphere of Mars Analyzed by Integral Inversion of the Mariner IV Occultation Data. Planetary Space Sci., vol. 16, 1968, pp. 1035–1059.

9-4. FJELDBO, G.; AND ESHLEMAN, V. R.: The Bistatic Radar-Occultation Method for the Study of Planetary Atmospheres. J. Geophys. Res., vol. 70, 1965, pp. 3217–3225.

9-5. RASOOL, S. I.; GROSS, S.; AND MCGOVERN, W. E.: The Atmosphere of Mercury. Space Sci. Rev., vol. 5, 1966, pp. 565–584.

9-6. GROSS, S. H.; MCGOVERN, W. E.; AND RASOOL, S. I.: Mars: Upper Atmosphere. Science, vol. 151, 1966, pp. 1216–1221.

9-7. GIERASCH, P. J.; AND GOODY, R. M.: A Study of the Thermal and Dynamical Structure of the Martian Lower Atmosphere. Planetary Space Sci., vol. 16, 1968, pp. 615–646.

9-8. GOODY R.: Vol. 1 of Comments on Astrophysics and Space Physics, 1969, pp. 128–133.

9-9. LEOVY C.; AND MINTZ, Y.: A Numerical General Circulation Experiment for the Atmosphere of Mars. RM-5110-NASA, Rand Corp., Dec. 1966.

9-10. LEOVY, C.; AND MINTZ, Y.: J. Atmospheric Sci. (in press).

9-11. NEUGEBAUER, G.; MÜNCH, G.; CHASE, S. C., JR.; HATZENBELER, H.; MINER, E.; AND SCHOFIELD, D.: Mariner 1969: Preliminary Results of the Infrared Radiometer Experiment. Science, vol. 166, 1969, pp. 98–99.

9-12. OHRING, G.; AND MARIANO, J.: Seasonal and Latitudinal Variations of the Average Surface Temperature and Vertical Temperature Profile on Mars. J. Atmospheric Sci., vol. 25, 1968, pp. 673–681.

ACKNOWLEDGMENTS

We thank the staff of the Mariner-Mars 1969 project and the personnel of the Deep Space Network who, through their competence, guaranteed the flawless

acquisition of S-band occultation data. We especially thank D. NIXON for his help in data acquisition, and M. P. MILANE, JOAN JORDAN, and NANCY HAMATA for their assistance in data reduction. Special thanks are extended to P. J. GIERASCH, C. LEOVY, and R. STEWART for discussions helpful to the interpretation of our results.

CHAPTER 10

Celestial Mechanics

J. D. ANDERSON (*Principal Investigator*), L. EFRON, AND S. K. WONG

The use of two-way, phase-coherent range and Doppler tracking data from the NASA/JPL Deep Space Network was required for the accurate navigation of Mariners 6 and 7 to the vicinity of Mars. Because of the importance of these data to the field of celestial mechanics, tracking coverage of Mariners 6 and 7 from launch to Mars encounter and beyond was scheduled in such a way that new information could be obtained on the Earth/Moon mass ratio, the gravity field of Mars (in particular the mass of the planet), and the ephemerides of Mars and Earth. It was recognized that these data complemented earlier Doppler data from Mariner 4 (range measurements were not obtained from that spacecraft), and that a combination of data from the three flyby trajectories and from direct radar range measurements to the planet itself during the 1969 opposition would result in significant improvements in the ephemeris of Mars. Because of these improvements, exploration of the size, shape, and gross topography of Mars would be permitted by using the radar range measurements to its surface. In this regard, it was realized that the times of immersion and emersion as the spacecraft were occulted by Mars would provide important calibration points for the size of the planet. (See ch. 9 of this report.)

Meaningful analysis of the tracking data from Mariners 6 and 7 and the radar range measurements to Mars, which are still being obtained, will require many months to complete. Therefore, this chapter contains a discussion of only the tracking data to determine the Earth/Moon mass ratio and the mass of Mars.

EARTH/MOON MASS RATIO

The Earth revolves about the center of mass of the Earth/Moon system at a distance of about 4671 km and a speed of 12.4 m/sec. It impresses a sinusoidal curve on range and Doppler tracking data with a frequency equal to the sidereal mean motion of the Moon and with an amplitude inversely proportional to $(1+\mu^{-1})$, where μ^{-1} is the ratio of the masses of the Earth and the Moon and is approximately equal to 81.3. The principle involved in the determination of μ^{-1}

is that a value can be found that eliminates the monthly cycle in the tracking data residuals in a least-squares sense. The determination of μ^{-1} is direct and reliable; no other unknown parameter in the representation of the tracking data has a frequency anywhere near that of the Moon's orbit. The lunar ephemeris is good to seven or eight figures and does not introduce any noticeable error into μ^{-1}, which, by comparison, can be determined to the order of 10 to 20 ppm. When searching for possible sources of systematic error in the data, it is very difficult to think of anything significant with a monthly cycle, although a sufficiently great S-band propagation effect correlated with the rotation of the Sun would be close enough to cause difficulty. Periodic variations in the interplanetary medium, the only reasonable possibility, must be very small for Mariners 6 and 7, however, even if present.

For the Mariner Earth-to-Mars trajectories, the total delay for an inverse square distribution of electrons with a density of 6/cc at the Earth's distance is a maximum of only 4 m. Melbourne (ref. 10–1) has suggested that a 28-day sinusoidal solar flux variation of 0.1 percent with the appropriate phase could produce an error of about 0.001 in μ^{-1} because of a similar variation in the solar radiation pressure on the spacecraft. The agreement of the several interplanetary spacecraft, however, seems to indicate that this sort of systematic error is not present unless the phase of the flux variation is the same for each mission, which does not seem likely. Data derived from the spacecraft's temperature control flux monitor, which measures relative variations in solar flux to a better than 0.1 percent accuracy, should determine whether a variation is present that could significantly bias the solutions for μ^{-1}.

Table 10-I shows the results on the Earth/Moon mass ratio, as determined from 12 weeks of Mariner 6 Doppler data[1] and about 11 weeks of Mariner 7 Doppler data.[2] Results from Mariner 2 (ref. 10–2), Mariner 4 (ref. 10–3), Mariner 5 (ref. 10–4), and Pioneers 6 and 7 (ref. 10–5) are also given. The deviations $\mu^{-1}-\bar{\mu}^{-1}$ from the arithmetic mean $\bar{\mu}^{-1}$ of the Mariner and Pioneer values are tabulated for each spacecraft.

A solution obtained by combining data from Rangers 6 through 9 (ref. 10–6) is also shown, although the gravitational constant G_M for the Moon was determined directly by the Ranger impact trajectories; μ^{-1} must be computed with an assumed value for the geometric gravitational constant G_E, which is

[1] From May 4 to July 28, 1969.
[2] From May 8 to July 22, 1969.

Table 10–I.—Determinations of Earth/Moon mass ratio μ^{-1}, as determined from Mariner, Pioneer, and Ranger tracking data

Spacecraft	μ^{-1}	$\mu^{-1}-\bar{\mu}^{-1}$
Mariner 2 (Venus)	81.3001±0.0013	−0.0007
Mariner 4 (Mars)	81.3015± .0017	.0007
Mariner 5 (Venus)	81.3006± .0008	−.0002
Mariner 6 (Mars)	81.3011± .0015	.0003
Mariner 7 (Mars)	81.2997± .0015	−.0011
Pioneer 6	81.3005± .0007	−.0003
Pioneer 7	81.3021± .0004	.0013
Combined Rangers	81.3035± .0012	.0027

defined by $\mu^{-1}=G_E/G_M$. The error in G_E, however, is about 1 ppm; therefore, the percentage error in the value of μ^{-1} determined from Ranger is almost equal to the percentage error in G_M. The fundamentally different method of determining μ^{-1} from Ranger impact trajectories, as opposed to using interplanetary trajectories such as those of Mariner and Pioneer, is reflected in a significant difference in the values. An arithmetic mean of the seven Mariner and Pioneer values results in $\mu^{-1}=81.3008$, with an rms deviation from the mean of 0.0008. The Ranger value, however, differs from this mean value by 0.0027. There is no reason to suspect that the direct determination of μ^{-1} from Mariner and Pioneer spacecraft is subject to systematic errors of a size that would adjust the value to that provided by Ranger.

The Mariner data have been processed with two computer programs: one in single precision (about 8 figures) and the other in double precision (about 16 figures), with both heliocentric and geocentric formulations of the equations of condition in the method of weighted least squares. The value of μ^{-1} is essentially the same in all cases; therefore, in the authors' opinions, it is necessary to perform new reductions of data from the lunar spacecraft. Since the Ranger solution for μ^{-1} was obtained, about 2½ yr ago, several conditions have changed. First, knowledge of the gravity field and ephemeris of the Moon has increased significantly through analyses of Lunar Orbiter data (ref. 10–7). In addition, it is now possible to perform the necessary computations in double precision; those of 2½ yr ago were performed only in single precision. In any case, the reconciliation of the μ^{-1} values derived from lunar and interplanetary spacecraft is receiving increased attention because of the results of Mariners 6 and 7, which argue for a μ^{-1} value closer to 81.300 or 81.301 than to 81.303 or 81.304, as suggested by the combined Ranger data.

MASS DETERMINATION

For both Mariners 6 and 7, the determination of the mass of Mars is complicated by nongravitational forces acting on the spacecraft. One channel of the infrared spectrometer (IRS), for example, operates in a cryogenic environment produced by expelling hydrogen and nitrogen gases from a pressure-regulated system. This gas expulsion imparts a force of 100 dyn or more to the spacecraft and produces a velocity change in its trajectory on the order of 0.1 m/sec. In normal operation, the system starts jetting about 35 min before encounter (the closest approach to Mars) and continues at a constant pressure through encounter for a period of about 80 min. After this period, the gas is allowed to escape into space without pressure regulation; about 5 hr are required for the gas to decay to an insignificant level at approximately an exponential rate.

On Mariner 6, the system did not operate normally; as a result, the force on the spacecraft acted over a period of 4 or 5 days after encounter instead of over the intended period of a few hours. The system seems to have operated normally on Mariner 7. However, this spacecraft was affected 6 days before encounter by an unknown event, which imparted a velocity increment to the trajectory on the order of 1 m/sec, or a change of 4×10^7 g cm/sec in momentum. It is possible that the spacecraft was hit by a meteoroid; whatever the reason, however, the spacecraft attitude was disrupted. Beyond this point, it is not clear whether additional unknown forces were also acting on the spacecraft; one possibility is that the spacecraft battery, which gave indication of a malfunction following the time of the event, was punctured by the impact and that the leaking electrolyte imparted a low-thrust force over a period of about 1 day. Because of uncertainties regarding the event and the resulting forces on the spacecraft in the few days before encounter, no results from Mariner 7 are available at this time.

Mariner 6 did not experience an event of the same type as Mariner 7. Therefore, data acquired before the initiation of the IRS cryogenic system blowdown can be used to obtain a value for the mass of Mars (fig. 10–1). However, data from about 35 min before encounter and beyond will be analyzed when, similar to Mariner 7, engineering telemetry data can be combined with the tracking data in an analysis of the nongravitational forces acting on the spacecraft.

To obtain the mass of Mars, we fit 670 Doppler points from July 26, 5 days before encounter, to July 31, at 04:39:57 G.m.t., about 7 min before initiation of IRS cooling. The parameters in the least-squares solution were the position

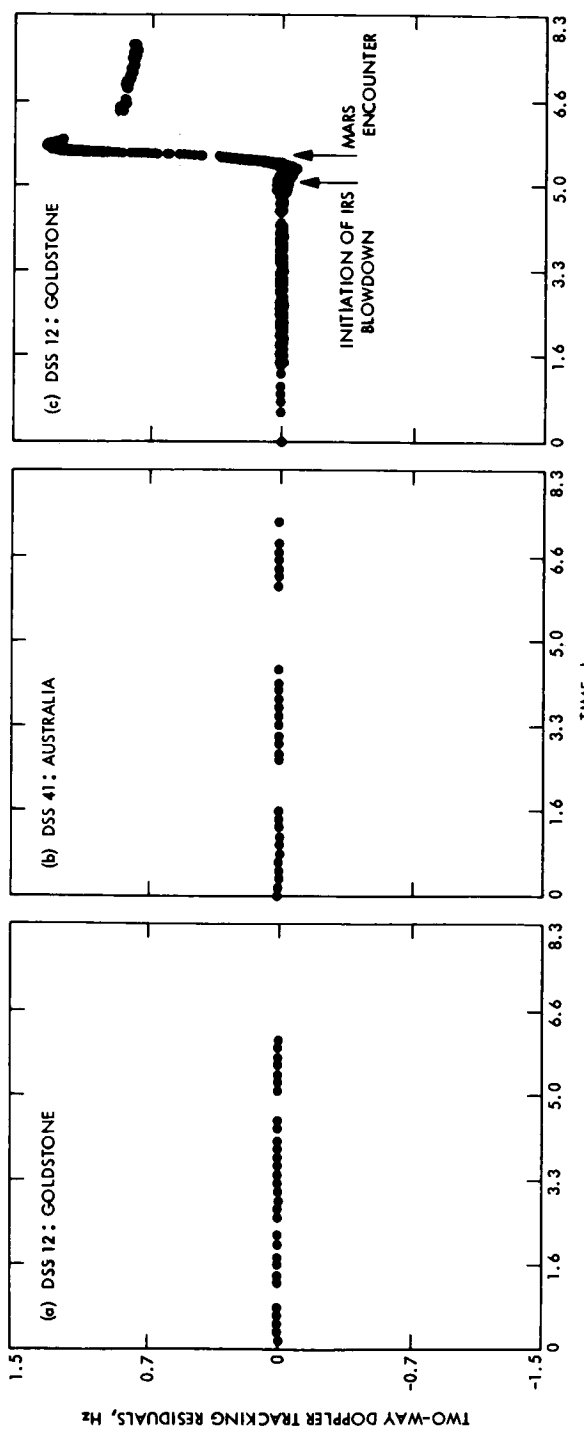

FIGURE 10–1. — Mariner 6 two-way Doppler tracking residuals. Doppler and range data used in the fit cover the period from 5 days before encounter to a few minutes before initiation of IRS gas blowdown. The three plots show the precision with which the orbit was known until the perturbation was introduced by the jetting gas. The Doppler count time C_c was 600 sec until 01:00 G.m.t. on July 31 and then 60 sec until 04:35 G.m.t., at which time T_c became 10 sec. At 06:17 G.m.t., T_c again became 60 sec. The noise on the residuals is proportional to $T_c^{1/2}$. The abscissa is given as time in hours as shown below. (a) From July 29, 1969, 23:48 G.m.t. (b) From July 30, 1969, 08:22 G.m.t. (c) From July 30, 1969, 23:44 G.m.t.

and velocity of the spacecraft at the epoch, the gravitational constant for Mars $G_{M\delta}$, the distance off the Earth's axis of rotation, and the longitude of each of the five tracking stations for which data were available. The statistical properties of the fit are summarized in table 10–II. The solution for $G_{M\delta}$ is 42828.22±1.83 km^3/sec^2.

A second solution was performed in which the Doppler data were fit along with nine range measurements taken on July 27 from DSS 14 at Goldstone, Calif., with the experimental ranging system installed for Mariner 5. The changes to the statistical properties of the Doppler fit are shown in table 10–III, and the nine range residuals are shown in table 10–IV. As shown in table 10–III, the Doppler fit is not changed significantly by the introduction of range data. The value of $G_{M\delta}$ for the range and Doppler fit is 42828.48±1.38 km^3/sec^2, which is not significantly different from the Doppler-only value, either in size or in estimated standard error. This estimate was computed with a standard error of 62×10^{-9} sec on each range point and 0.05 Hz on Doppler data sampled at 1-min intervals.

Although the introduction of range data into the fit does not affect appreciably the solution for the mass of Mars, it does help to determine the orbit of Mariner. This has important implications to other experiments, such as the

Table 10–II.—Statistical properties of fit to preencounter Doppler data

Deep Space Station	Number of points	Data interval, G.m.t.	Residuals, Hz[a]	
			Mean	rms
41 (Australia)	200	July 26, 06:49 to July 30, 15:41	0.000006	0.0028
51 (South Africa)	26	July 27, 16:28 to July 27, 23:02	.000164	.0019
62 (Spain)	80	July 26, 17:29 to July 30, 22:31	—.000086	.0025
12 (California)	311	July 26, 01:33 to July 31, 04:40	—.000105	.0043
14 (California)	53	July 26, 00:35 to July 30, 06:38	—.000098	.0024

[a] Units are Hz at S-band and can be converted approximately to millimeters per second by multiplying by 67.

Table 10–III.—Statistical properties of fit to preencounter range and Doppler data

Deep Space Station	Number of points	Data interval, G.m.t.	Residuals, Hz	
			Mean	rms
41 (Australia)	200	July 26, 06:49 to July 30, 15:41	0.000008	0.0028
51 (South Africa)	26	July 27, 16:28 to July 27, 23:02	.000164	.0019
62 (Spain)	80	July 26, 17:29 to July 30, 22:31	—.000088	.0025
12 (California)	311	July 26, 01:33 to July 31, 04:40	.000127	.0042
14 (California)	53	July 26, 00:35 to July 30, 06:38	.000090	.0024

Table 10–IV.—Range residuals from fit to preencounter range and Doppler data

Reception on July 27, 1969, G.m.t.	Residual, 10^{-9} sec [a]
01:12:02	−42.1
01:59:02	62.7
02:29:02	5.9
02:59:02	6.2
03:29:02	2.9
03:59:02	−16.2
04:29:02	5.5
06:06:02	−8.2
06:36:02	−19.5

[a] Units can be converted to meters in one-way range by multiplying by 0.15. The mean residual is −0.30 and the rms of the 9 residuals is 26.9 or 4.0 m.

S-band occultation and the ultraviolet spectroscopy, both of which will require good orbital data to complete a final analysis. Precise knowledge of the orbit is important in obtaining information on the ephemeris of Mars and will play a major role in later analyses of the tracking data when the nongravitational forces on Mariners 6 and 7 are understood better. We believe, at present, that the Mars-centered orbit for Mariner 6 from the fit to range and Doppler data can predict events along the trajectory to better than 1 sec in time or to better than 8 km along the flightpath. For example, the best estimate of the time of closest approach to Mars is on July 31, 1969, 05:19:06 G.m.t.; it is estimated that this value should be good to ±1 sec.

The only source for an accurate determination of the mass of Mars, other than Mariners 6 and 7, is from Mariner 4. A recent analysis (ref. 10–8) of Doppler data taken over a 10-day interval centered about closest approach has yielded a value for $G_{M\delta}$ of 42828.32±0.13 km^3/sec^2. The masses determined from Mariners 4 and 6 are, therefore, in agreement, and there is good reason to accept the spacecraft-determined value when performing analyses with other planetary data.

REFERENCES

10–1. MELBOURNE, W. G.: The Determination of Planetary Masses from Radio Tracking of Space Probes and Planetary Radar. Paper presented at 12th Planetary Meeting, COSPAR, Symposium C: Space Probes — Part I (Prague, Czechoslovakia), May 11–24, 1969.

10–2. ANDERSON, J. D.: Determination of the Masses of the Moon and Venus and the Astronomical Unit from Radio Tracking Data of the Mariner II

Spacecraft. Ph. D. dissertation in astronomy, UCLA. Also, Tech. Rept. 32-816, Jet Propulsion Laboratory, Pasadena, Calif., July 1967.

10-3. NULL, G. W.; GORDON, H. J.; AND TITO, D. A.: The Mariner IV Flight Path and Its Determination from Tracking Data. Tech. Rept. 32-1108, Jet Propulsion Laboratory, Pasadena, Calif., Aug. 1967.

10-4. PEASE, G. E.: Part 1. Orbit Determination from DSIF Tracking Data. The Mariner V Flight Path and Its Determination From Tracking Data. Tech. Rept. 32-1363, Jet Propulsion Laboratory, Pasadena, Calif., July 1969, pp. 1-26.

10-5. ANDERSON, J. D.; AND HILT, D. E.: Improvement of Astronomical Constants and Ephemerides from Pioneer Radio-Tracking Data. AIAA, vol. 7, June 1969, pp. 1048-1054.

10-6. VEGOS, C. J.; AND TRASK, D. W.: Range Combined Analysis. Part II: Determination of the Masses of the Earth and Moon from Radio-Tracking Data. The Deep Space Network. Space Programs Summary 37-44, vol. III, Jet Propulsion Laboratory, Pasadena, Calif., Apr. 1967, pp. 11-28.

10-7. LORELL, J.: Lunar Orbiter Gravity Analysis. Tech. Rept. 32-1387, Jet Propulsion Laboratory, Pasadena, Calif., June 1969.

10-8. NULL, G. W.: A Solution for the Mass and Dynamical Oblateness of Mars Using Mariner IV Doppler Data. Paper presented at the 130th Meeting the AAS (Albany, N.Y.), Aug. 12, 1969.

ACKNOWLEDGMENTS

We acknowledge the able assistance and support given to the Mariner-Mars 1969 celestial mechanics experiment by H. GORDON, D. CURKENDALL, W. ZIELENBACH, M. SYKES, S. REINBOLD, N. THOMAS, and many others in the JPL Flight Path Analysis and Command Team and the JPL Precision Navigation Project.

APPENDIX A

Preliminary Portraits

A sampling of partially processed pictures obtained in the television experiment on Mariners 6 and 7 was promptly released for publication. The six shown here indicate the details discernible in even raw prints. Further processing is expected to increase the value of these pictures in quantitative studies of Martian phenomena.

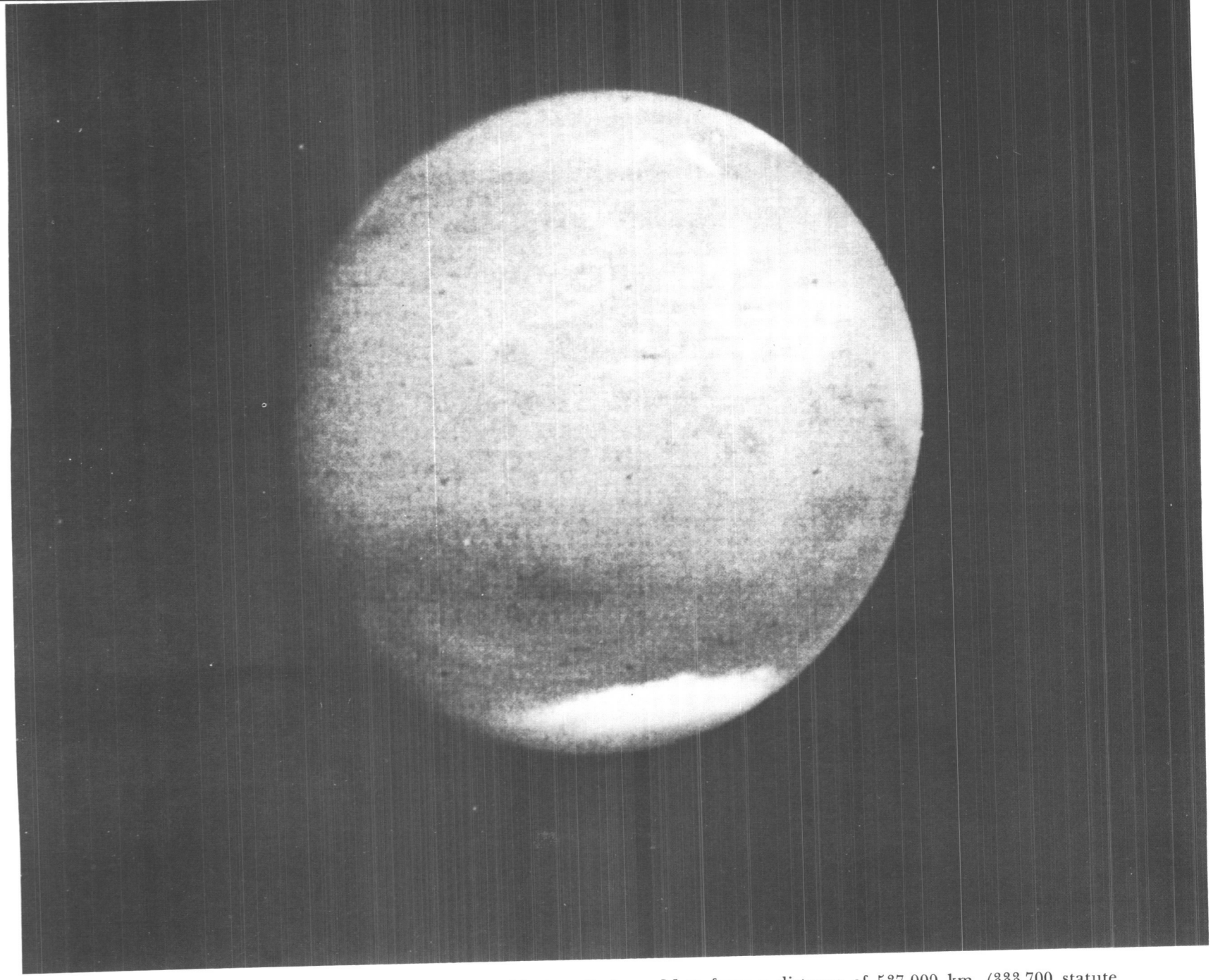

FIGURE A-1. — A far-encounter picture from Mariner 6 shows Mars from a distance of 537 000 km (333 700 statute miles) with the morning terminator at the left. The white rim with a central spot slightly above center has been

FIGURE A–2. — This Mariner 7 far-encounter picture was taken 861 850 km (535 650 statute miles) from Mars. In the upper right is a bright ring; this is the area known as Elysium. Toward the bottom the irregularity of the border around the south polar cap, which was slowly shrinking, can be seen.

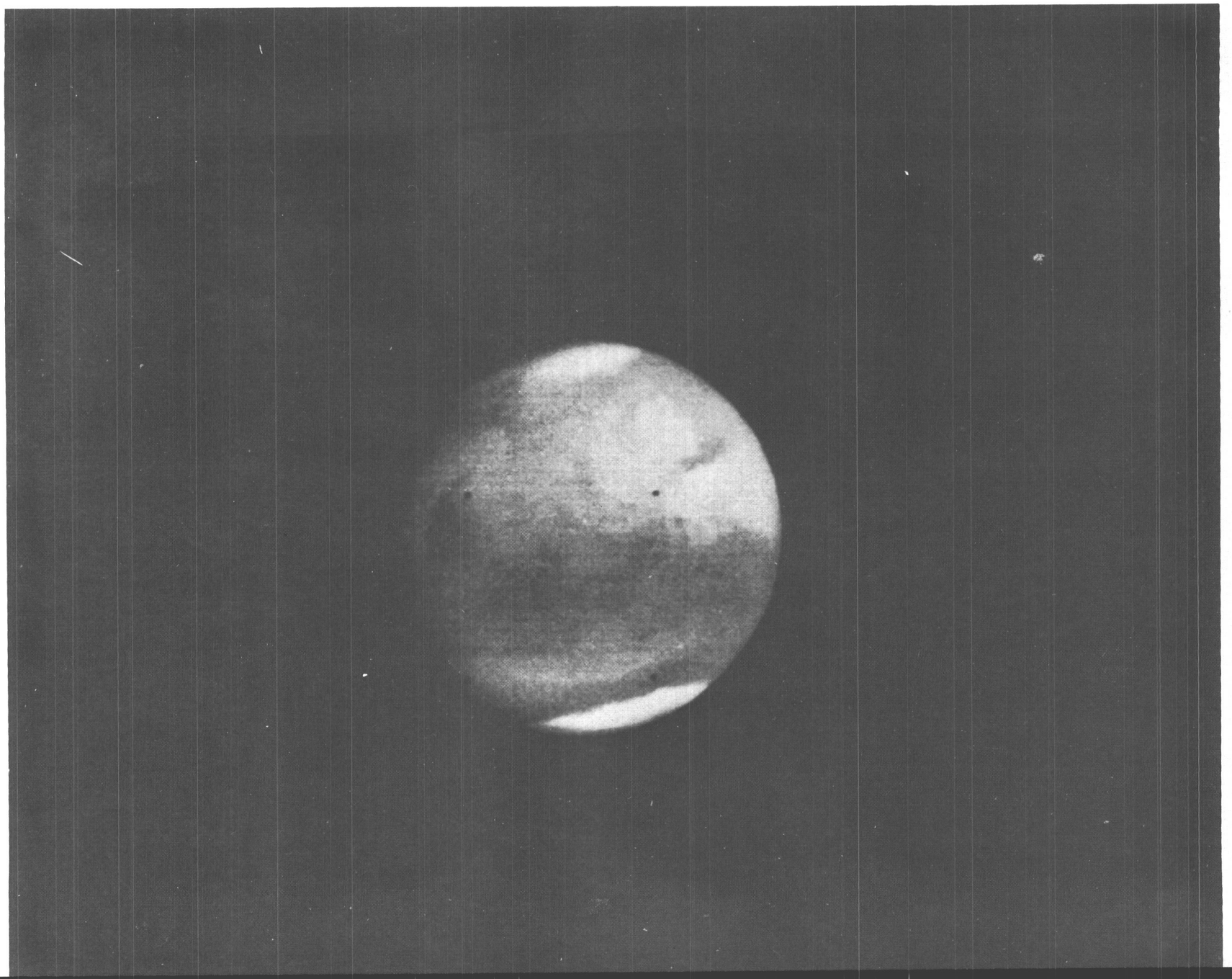

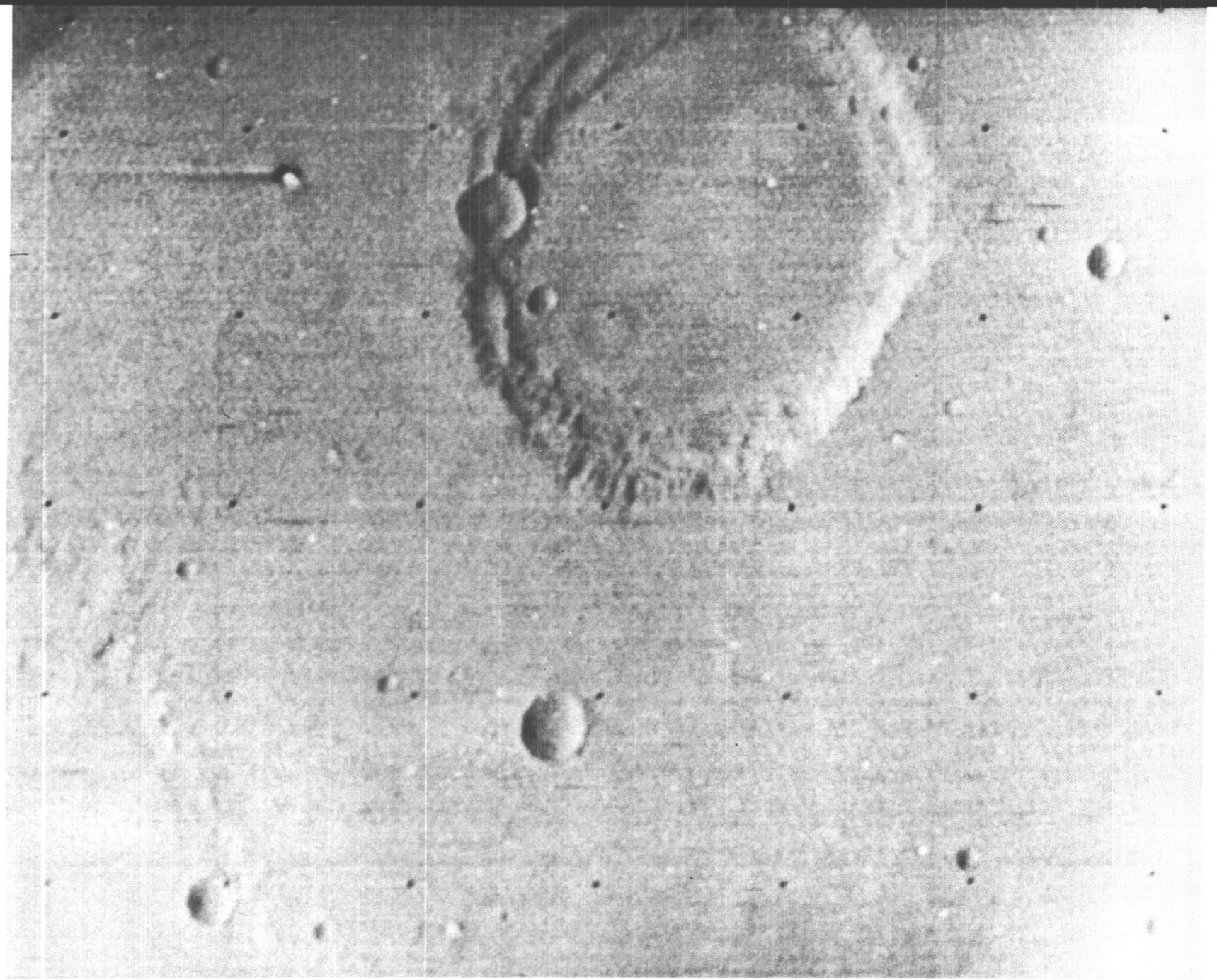

FIGURE A–3. – Mariner 6's narrow-angle camera took this near-encounter picture of a 63- by 48-mile area from a distance of 2300 miles. It shows features similar to findings on the Moon. The large crater is 24 miles wide. *On*

FIGURE A–4. — Mariner 6's wide-angle camera took this picture of a 560- by 430-mile area of Mars from a distance of 2150 miles. The regularly spaced black dots are reference points. At least 100 craters, including some with crudely polygonal outlines, are recorded here.

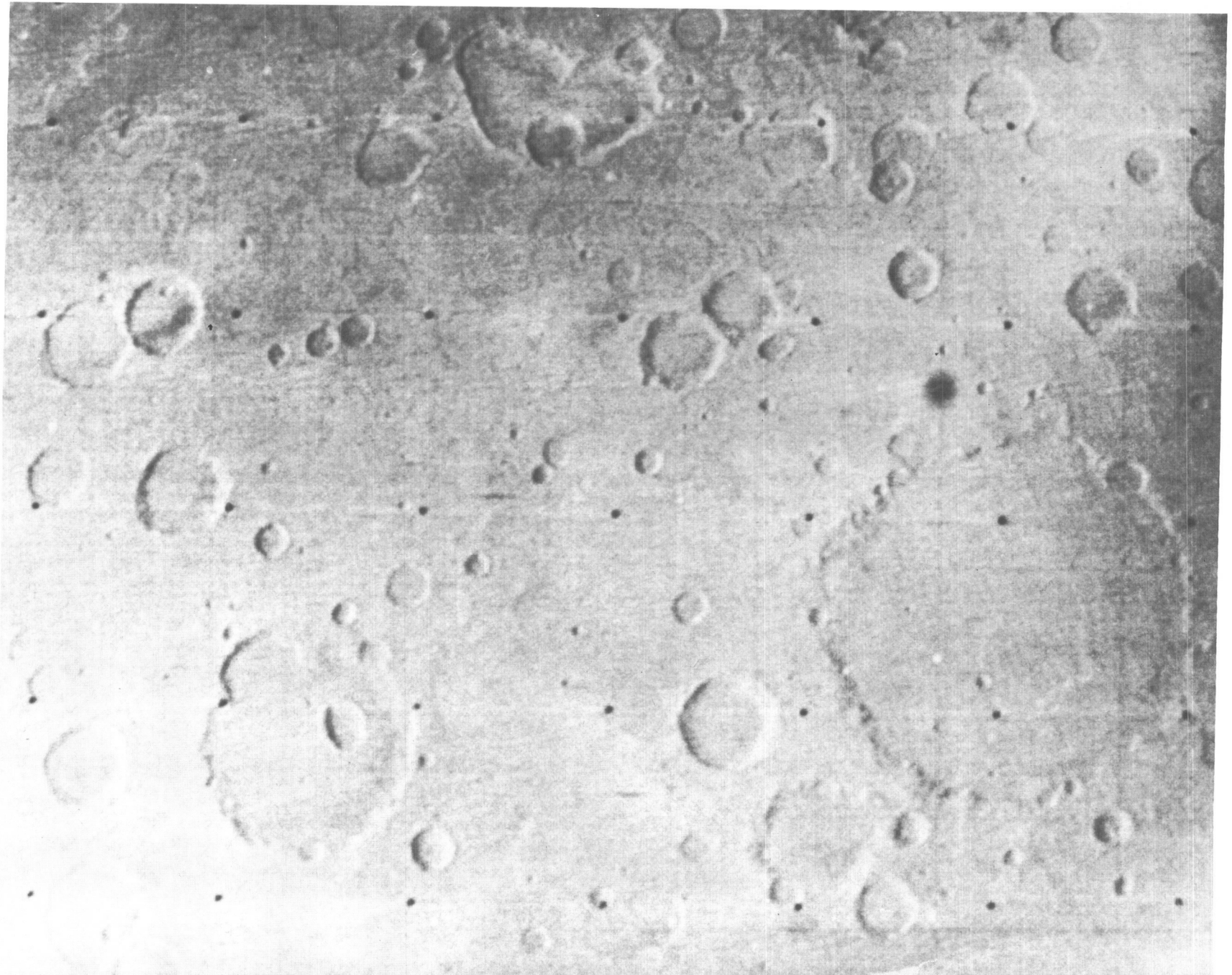

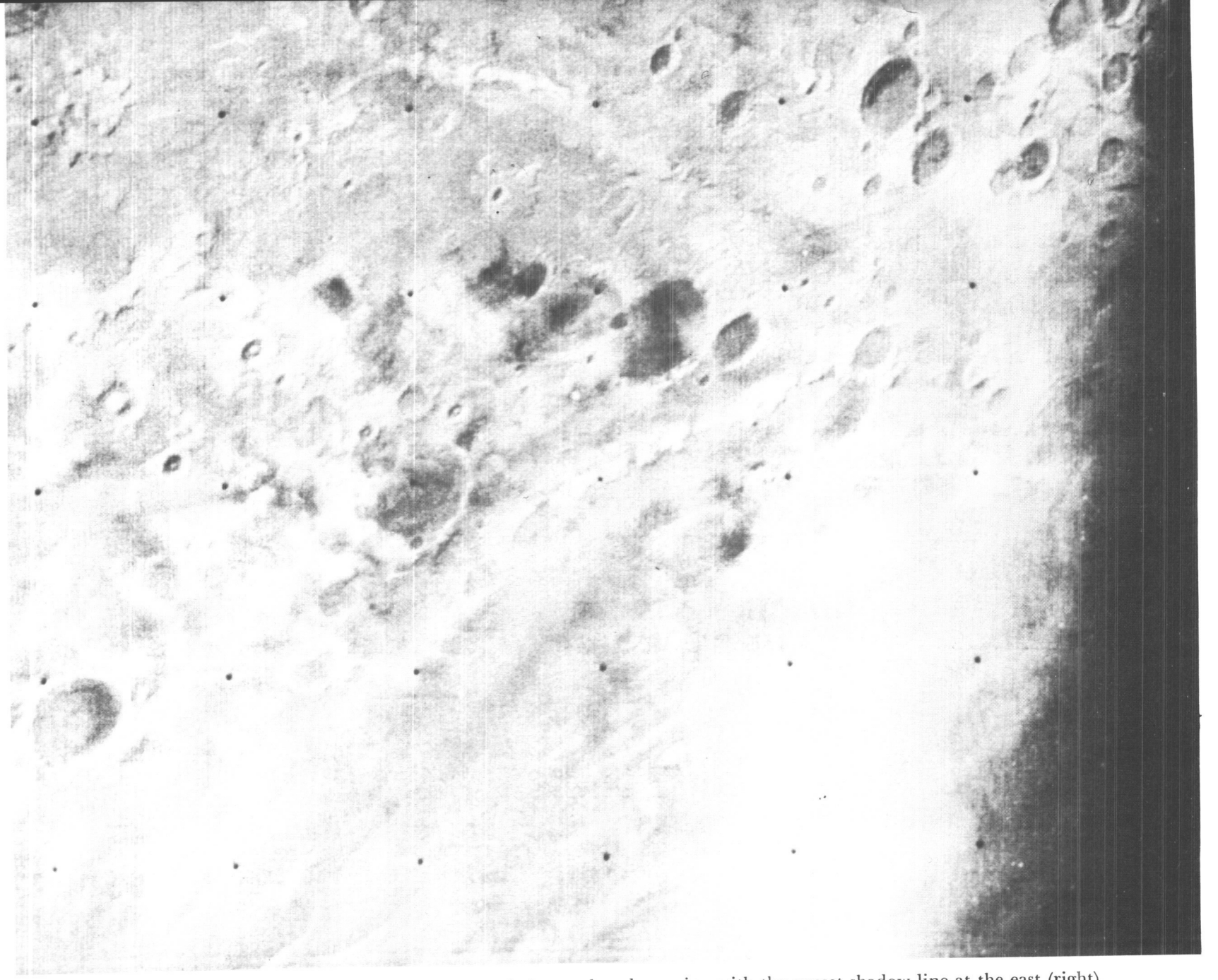

FIGURE A–5. – Mariner 7 sent back this view of the south polar region with the sunset shadow line at the east (right). It includes craters of various sizes and shapes, as well as linear and blotchy features. Two craters in the right

FIGURE A–6. — Mariner 7 also obtained this oblique, high-resolution picture of the craters forming the "giant footprint." The Sun was 8° above the local horizon off to the northwest (upper left). The area shown, about 75° south latitude, is about 85 by 200 miles.

APPENDIX B

Investigator Teams for Mariner-Mars 1969 Mission

VISUAL IMAGING

Robert B. Leighton, Principal investigator	California Institute of Technology
Bruce C. Murray	California Institute of Technology
Robert P. Sharp	California Institute of Technology
Norman H. Horowitz	California Institute of Technology
Richard K. Sloan	Jet Propulsion Laboratory
Alan G. Herriman	Jet Propulsion Laboratory
Merton E. Davies	RAND Corporation
Conway B. Leovy	University of Washington
Andrew T. Young	Jet Propulsion Laboratory
Bradford A. Smith	New Mexico State University

INFRARED SPECTROMETRY

George C. Pimentel, Principal investigator	University of California, Berkeley
Kenneth C. Herr	University of California, Berkeley

INFRARED RADIOMETRY

Gerry Neugebauer, Principal investigator	California Institute of Technology
Guido Münch	California Institute of Technology
Stillman C. Chase	Santa Barbara Research Corporation

ULTRAVIOLET SPECTROMETRY

Charles Barth, Principal investigator	University of Colorado
William G. Fastie	Johns Hopkins University
Fred C. Wilshusen	University of Colorado
Kermit Gause	University of Colorado
Edward F. Mackey	Packard-Bell Electronics
Ken K. Kelly	University of Colorado
Ray Ruehle	University of Colorado
Jeffrey B. Pearce	University of Colorado
Charles W. Hord	University of Colorado
Gary E. Thomas	University of Colorado
A. Ian Stewart	University of Colorado

S-BAND OCCULTATION

Arvydas J. Kliore, Principal investigator	Jet Propulsion Laboratory
Gunnar Fjeldbo	Jet Propulsion Laboratory
S. I. Rasool	Goddard Institute for Space Studies
Boris Seidel	Jet Propulsion Laboratory

CELESTIAL MECHANICS

John D. Anderson, Principal investigator	Jet Propulsion Laboratory
Warren L. Martin	Jet Propulsion Laboratory

APPENDIX C

Mariner-Mars 1969 Management Organization

NATIONAL AERONAUTICS AND SPACE ADMINISTRATION

J. E. Naugle	Associate Administrator, OSSA
O. W. Nicks	Deputy Associate Administrator, OSSA
D. P. Hearth	Director, Planetary Programs
D. G. Rea	Deputy Director, Planetary Programs
N. W. Cunningham	Manager, Mariner-Mars 1969
R. A. Kennedy	Program Engineer
R. F. Fellows	Program Scientist
D. P. Easter	Staff Scientist

JET PROPULSION LABORATORY

W. H. Pickering	Director
R. J. Parks	Assistant Laboratory Director for Flight Projects
H. M. Schurmeier	Project Manager
H. W. Norris	Spacecraft System Manager
W. R. Dunbar (LeRC)	Launch Vehicle System Manager
M. S. Johnson	Mission OPS System Manager
N. A. Renzetti	Tracking and Data System Manager

NASA-Langley, 1970 —— 31

"The aeronautical and space activities of the United States shall be conducted so as to contribute . . . to the expansion of human knowledge of phenomena in the atmosphere and space. The Administration shall provide for the widest practicable and appropriate dissemination of information concerning its activities and the results thereof."

— NATIONAL AERONAUTICS AND SPACE ACT OF 1958

NASA SCIENTIFIC AND TECHNICAL PUBLICATIONS

TECHNICAL REPORTS: Scientific and technical information considered important, complete, and a lasting contribution to existing knowledge.

TECHNICAL NOTES: Information less broad in scope but nevertheless of importance as a contribution to existing knowledge.

TECHNICAL MEMORANDUMS: Information receiving limited distribution because of preliminary data, security classification, or other reasons.

CONTRACTOR REPORTS: Scientific and technical information generated under a NASA contract or grant and considered an important contribution to existing knowledge.

TECHNICAL TRANSLATIONS: Information published in a foreign language considered to merit NASA distribution in English.

SPECIAL PUBLICATIONS: Information derived from or of value to NASA activities. Publications include conference proceedings, monographs, data compilations, handbooks, sourcebooks, and special bibliographies.

TECHNOLOGY UTILIZATION PUBLICATIONS: Information on technology used by NASA that may be of particular interest in commercial and other non-aerospace applications. Publications include Tech Briefs, Technology Utilization Reports and Technology Surveys.

Details on the availability of these publications may be obtained from:

SCIENTIFIC AND TECHNICAL INFORMATION DIVISION

NATIONAL AERONAUTICS AND SPACE ADMINISTRATION

Washington, D.C. 20546